

POLITECNICO DI TORINO

Collegio di Ingegneria Meccanica, Aerospaziale, dell'Autoveicolo e della Produzione

**Corso di Laurea Magistrale
in Automotive Engineering (Ingegneria dell'Autoveicolo)**

Tesi di Laurea Magistrale

Analysis of the effect of tire inflation pressure on vehicle dynamics and control strategies



Relatori

Prof. Stefano d'Ambrosio
Prof. Nicola Amati

Candidato

Carlo Di Pasquale

Novembre/Dicembre 2018

Introduction

Tires, being the interface between the vehicle on the road have a huge influence on vehicle performance: through the tires the vehicle is able to exert traction, braking and cornering forces. A key parameter in particular that affects tire capabilities is inflation pressure.

According to the National Highway Traffic Safety Administration (NHTSA) more than a quarter of automobiles travel with underinflated tires in the U.S. [1], while a study by Michelin and Kwik Fit evidenced a percentage of the 40% in the U.K. [2].

An under-inflation creates not only safety issues, affecting the handling of the vehicle, but results also in an increased tire wear and fuel consumption (due to a bigger rolling resistance): a reduction of 0,5 bar from the recommended inflation pressure brings to a growth of rolling resistance of about the 10% bringing to an increase of consumptions of the 1-2% [3].

The ATCP (Active Tire Pressure Control) team has the goal to develop a system capable to monitor and maintain a desired pressure, that can be regulated according to the working conditions of the vehicle. The opportunities of a pressure control are several: from an optimization of consumptions (and consequently CO₂ emissions) to a control of the cornering and braking behaviour of the vehicle.

In this thesis, the effect of pressure on the main tire parameters is analysed using Pacejka's MF 5.2 model. Then the analysis focus on the vehicle dynamics, ensuring a safe operation of the vehicle throughout the range of pressure considered and checking configurations that optimize the braking and cornering performance of the vehicle. Different manoeuvre simulations were performed on the software Adams Car for a passenger car (Fiat Grande Punto) and a light duty vehicle (Iveco Daily). Experimental tests performed on track permitted to tune and validate the Grande Punto model. Finally, an overview of the interaction between different strategies of pressure control was made.

Index

| | |
|----------------------------------------------------------------------------------------|-----------|
| 1 An active tire pressure control..... | 1 |
| 1.1 The ATPC team..... | 1 |
| 1.2 Rolling Resistance..... | 2 |
| 1.3 Contact Patch..... | 4 |
| 1.4 Tire wear..... | 5 |
| 2 Preliminary theory concepts..... | 8 |
| 2.1 Tires..... | 8 |
| 2.1.1 Structure and characteristics..... | 8 |
| 2.1.2 Wheel's reference system and forces acting on the tire..... | 11 |
| 2.1.3 Pacejka's Magic Formula MF 5.2..... | 15 |
| 2.1.4 Improved Magic Formula to take in account inflation pressure changes MF 6.2..... | 17 |
| 2.2 Longitudinal dynamics..... | 18 |
| 2.2.1 Load distribution..... | 18 |
| 2.2.2 Braking in ideal conditions..... | 20 |
| 2.3 Lateral dynamics..... | 20 |
| 2.3.1 Low speed or kinematic steering..... | 21 |
| 2.3.2 Ideal steering | 22 |
| 2.3.3 Simplified approach for high speed cornering | 25 |
| 2.3.4 High speed cornering 282.3.5 Definition of understeer and oversteer..... | 32 |
| 3 The effect of inflation pressure on tire performance..... | 35 |
| 3.1 Tire 185/65 R 15 | 35 |
| 3.1.1 Longitudinal analysis..... | 35 |
| 3.1.2 Lateral analysis..... | 37 |
| 3.1.3 Self aligning moment..... | 38 |

| | |
|----------------------------------------------------------------|-----------|
| 3.1.4 Summary table of the results..... | 39 |
| 3.2 Tire 225/65 R 16 | 40 |
| 3.2.1 Longitudinal analysis..... | 40 |
| 3.2.2 Lateral analysis..... | 41 |
| 3.2.3 Self aligning moment | 43 |
| 3.2.4 Summary table of the results..... | 44 |
| 3.3 Tire 195/75 R 16..... | 44 |
| 3.3.1 Longitudinal analysis | 44 |
| 3.3.2 Lateral analysis..... | 46 |
| 3.3.3 Self aligning moment..... | 48 |
| 3.3.4 Summary table of the results..... | 49 |
| 4 Effect of inflation pressure on vehicle dynamics..... | 50 |
| 4.1 Fiat Grande Punto..... | 50 |
| 4.1.1 Braking..... | 50 |
| 4.1.2 Analysis of braking results and literature overview..... | 53 |
| 4.1.3 Lateral Dynamics..... | 54 |
| 4.1.3.1 Step Steer..... | 55 |
| 4.1.3.2 Steering Pad..... | 58 |
| 4.1.4 Analysis of lateral dynamics results..... | 60 |
| 4.2 Iveco Daily..... | 60 |
| 4.2.1 Braking (225/65 R16)..... | 60 |
| 4.2.2 Braking (195/75 R16)..... | 63 |
| 4.2.3 Analysis of braking results and literature overview..... | 65 |
| 4.2.4 Lateral dynamics (225/65 R16)..... | 66 |
| 4.2.4.1 Step Steer..... | 66 |
| 4.2.4.2 Steering Pad..... | 69 |
| 4.2.5 Lateral dynamics (195/75 R16)..... | 70 |
| 4.2.5.1 Step Steer..... | 70 |
| 4.2.5.2 Steering Pad..... | 73 |

| | |
|-------------------------------------------------------------------------|-----------|
| 4.2.6 Analysis of lateral dynamics results and literature overview..... | 73 |
| 5 Vehicle Dynamics Strategies..... | 75 |
| 5.1 Passenger Car (Grande Punto)..... | 75 |
| 5.1.1 Longitudinal dynamics..... | 75 |
| 5.1.2 Lateral dynamics..... | 77 |
| 5.1.3 Interaction between strategies..... | 79 |
| 5.2 Light duty vehicle with 225/65 R16 tires (Daily)..... | 81 |
| 5.2.1 Longitudinal dynamics..... | 81 |
| 5.2.2 Lateral dynamics..... | 82 |
| 5.2.3 Interaction between strategies..... | 83 |
| 5.3 Light duty vehicle with 195/75 R16 tires (Daily)..... | 85 |
| 5.3.1 Longitudinal dynamics..... | 85 |
| 5.3.2 Lateral dynamics..... | 86 |
| 5.3.3 Interaction between strategies..... | 87 |
| 6 Conclusions..... | 90 |
| 7 Bibliography..... | 91 |
| 8 List of figures..... | 92 |
| 9 List of tables..... | 99 |

1 An active tire pressure control

In this chapter is made an overview of the ATPC team targets and field of operation.

1.1 The ATPC team

The ATPC (Active Tire Pressure Control) team, born in 2013 has the aim to develop an active system to manage the tire inflation pressure under specific vehicle working conditions. The use of a pressure control system allows better performances in the warm up of the tires, fuel consumption, safety and driveability [3].

The management is performed through an automatic, electro-pneumatic central tire inflation system: a schematic layout is presented in Figure 1.1 [3].

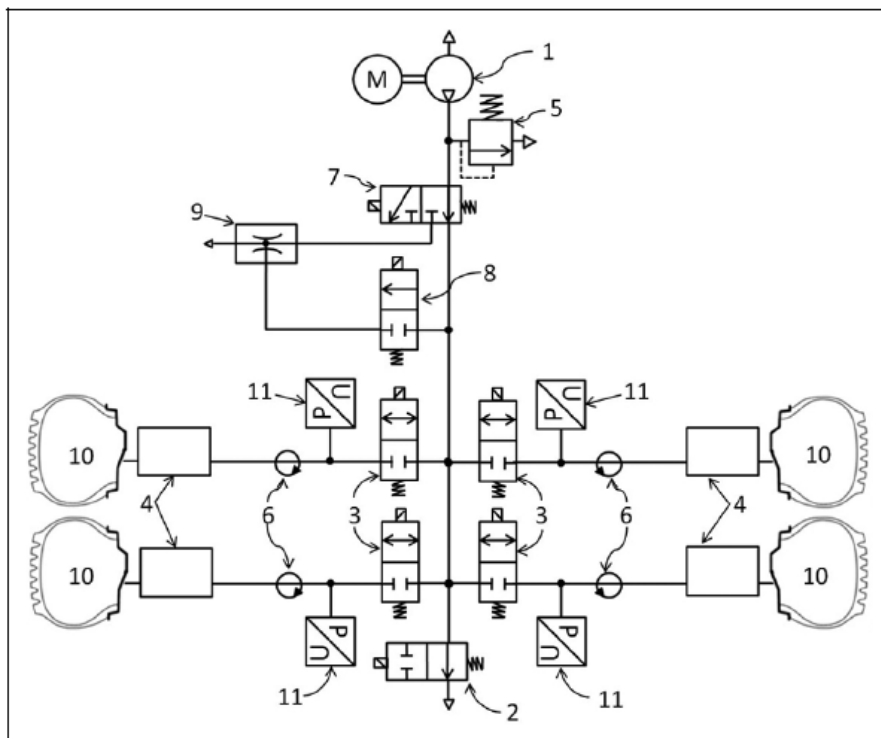


FIGURE 1.1. Electro-pneumatic layout of the ATPC system with air compressor (1); ejector (9); central electro-valves: one on the compressor line (7) and one on the vacuum line (8); vent valve (2); four pipelines for the connection of the tires to the central part (10), including a solenoid valve (3), pressure transducer (11), rotating pneumatic joint (6), and an on-wheel valve or valve unit (4).

The inflation pressure has in fact influence on the adherence and on the wear of the tire (changing size and shape of the contact patch) but also on rolling resistance (that has a great contribution to the resistance to motion). Several strategies can be implemented to improve performance and consumptions.

In the following chapters the effect of inflation pressure on the main tire parameters affecting vehicle dynamics will be investigated with the aim of:

- Ensuring that fuel economy strategies don't affect in a dangerous way the dynamic of the vehicle
- Developing strategies to improve the performance of the vehicle or to maintain constant the vehicle dynamic with the change of its load condition
- Check a possible compatibility between the different strategies

1.2 Rolling Resistance

The tire and the ground are not rigid, so deformations occur in the contact zone. During tire motion new material is continuously entering in this zone, deforming and springing back. The energy expended for this process is not completely recovered because of the internal damping of the material [4].

These dissipations are the main causes for rolling resistance and in the case of a pneumatic tire rolling on tarmac or concrete are localized mainly in the tire itself [4].

The distribution of the contact pressure of the wheel on the ground, that in standstill is symmetric with respect to the centre of the contact zone, is asymmetric in rolling (Fig 1.2b) and the resultant of the vertical force F_z moves forward, producing a torque opposed to the wheel rotation $M_z = F_z \Delta x$ [4].

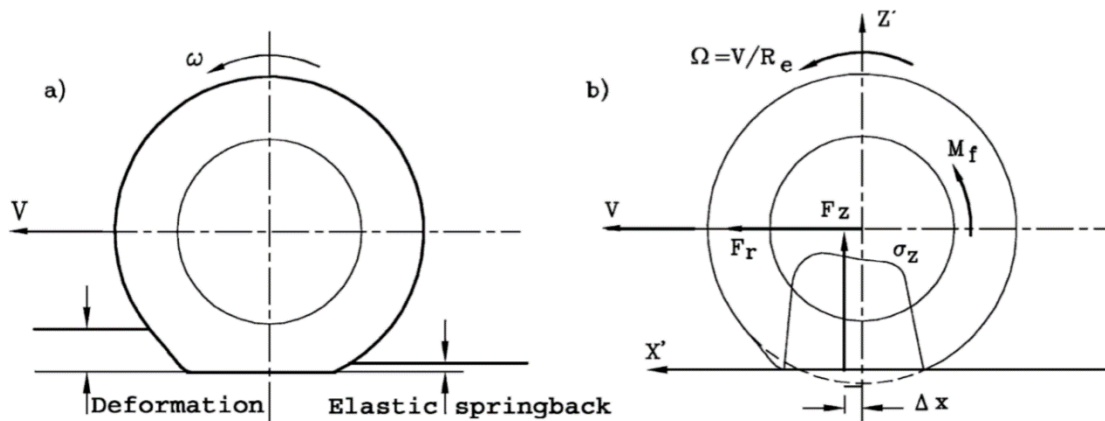


FIGURE 1.2. (a) Rolling tire on a deformable surface: ground deformation and spring back. (b) Forces F_z and F_r and contact pressure σ_z in a rolling tire

The entity of the deformations and so the rolling resistance, increase with the load and decrease with the inflation pressure. Consequently, a heavier load should be compensated by a higher inflation pressure [4].

On Fig 1.3 is plotted the effect of pressure and load on the rolling resistance of a tire.

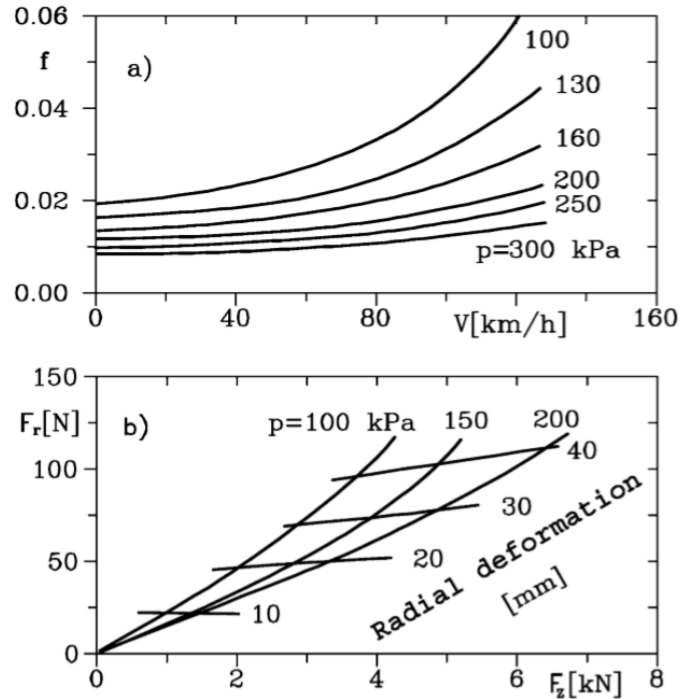


FIGURE 1.3. (a) Effect of inflation pressure on $f(V)$. (b) Rolling resistance for different values of load and pressure

To study the effect of inflation pressure on reducing rolling resistance, the team performed several simulations for four different homologation driving cycles: *NEDC* (New European Driving Cycle EU), *FTP75* (Federal Test Procedure USA), *US06* (Integrating FTP75 with more aggressive cycles) and the *HWFET* (Highway Fuel Economy Test for highway driving). The tests were performed on a B segment Vehicle (Fiat Grande Punto 1.3 MultiJet 75 cv) that saw an improvement on fuel consumption up to 1% (Fig 2) for a +25% increase of pressure. Decreasing inflation pressure of the same quantity caused instead an increase of consumptions of the 1-2% (the results are presented in Fig 1.4.). Even greater advantages can be obtained for highway driving [3].

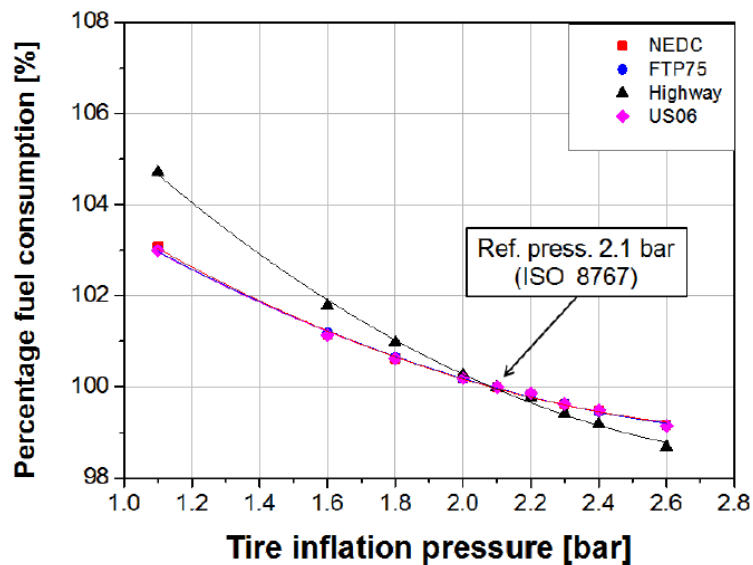


FIGURE 1.4 Percentage of fuel consumption referring to the reference pressure of the tire for the different driving cycles.

Other simulations were made for different loads and inflation pressures. A comparison was made for two cases:

- A baseline case in which the load increased but the pressure was kept constant and equal to the nominal
- A variable pressure case in which the pressure was adapted to the different load conditions to maintain constant the contact patch.

The variable pressure case brings to a decrease of consumptions of the 1.6% for NEDC and 2.4% for HWFET respect to the baseline case [3] (Fig 1.5).

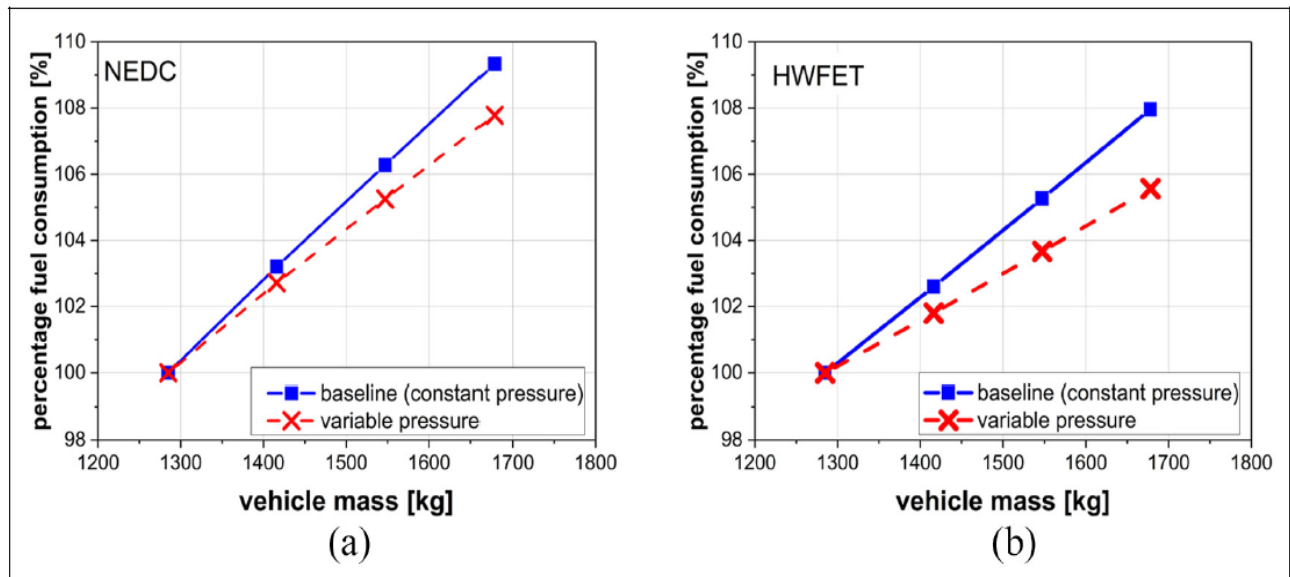


FIGURE 1.5 Percentage of fuel consumption for baseline and variable pressure strategy changing the load of the vehicle.

1.3 Contact Patch

The contact patch is the zone in which the tire exchange forces with the ground: the area is big enough to generate a pressure-area product equal to the vertical force [4]. The size of the contact area depends on the tire cross section, its shape and structure but also on inflation pressure and load.

A bigger vertical load causes an increase of the contact patch, while it decreases increasing pressure [5].

The size of the contact patch is strictly related to the forces that the tire can exert; on the other hand, the size of the contact area can be increased decreasing pressure only till a certain point, because the growth of length is then followed by a decrease of width and the forces concentrate only in the edge tire ribs (Fig 1.6) [6].

Also for high inflation pressure the force distribution becomes uneven, concentrating on the central part and on the edge ribs (Fig 1.6) [6].

Both extreme conditions then cause an increase of tire wear and lower performance, narrowing the convenient range of action of a pressure control with the aim of maximize adherence. However, a pressure control system allows to compensate the effect of a bigger load on the vehicle maintaining a more constant and even force distribution.

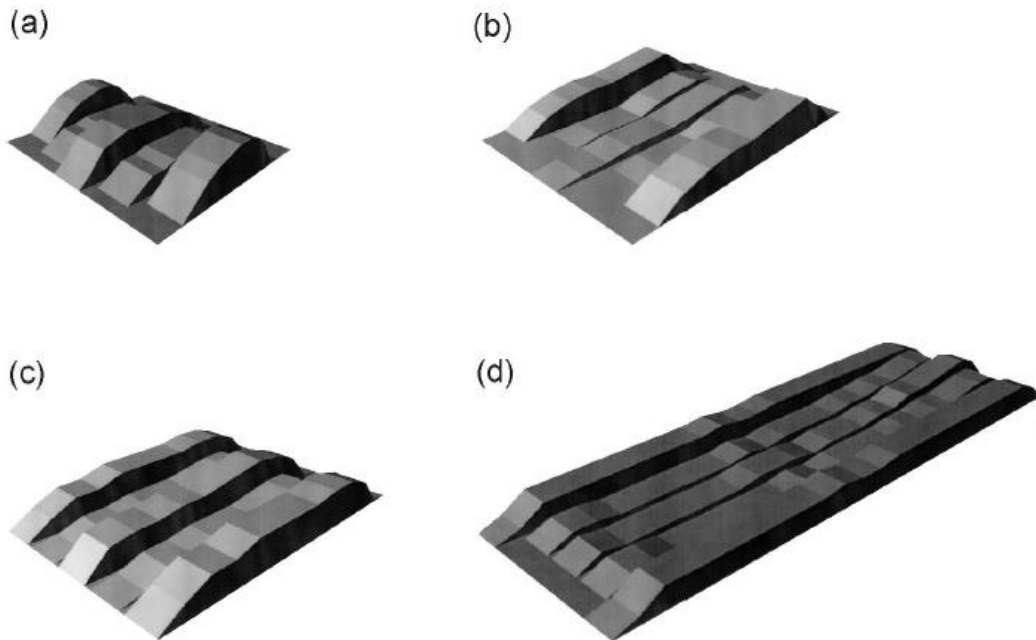


FIGURE 1.6. Three-dimensional vertical contact load plots for (a) 4.6 kN tire load, inflation pressure 690 kN/m²; (b) 4.6 kN tire load, inflation pressure 100 kN/m²; (c) 19.6 kN tire load, inflation pressure 690 kN/m²; and (d) 19.6 kN tire load, inflation pressure 100 kN/m².

1.4 Tire wear

As already said, the wear depends on the contact patch and on the load distribution on ground, the tire pressure cannot be too high (causing uneven distribution and highly concentrated loads) nor too low (abnormal deflection, overheating). On Fig 1.7 provided by Michelin in its truck tire service manual is showed the impact of inflation pressure on tire life: an over-inflation of 20% causes a reduction of tire mileage about the 10% while an equal under-inflation brings to a reduction of life that is almost double.

Tire wear contributes also to the generation of particles due to the shear forces between the tread of the tire and the ground. A study by P. Pant and R.M. Harrison [7] studied this effect, evidencing the presence of predominantly coarse (PM_{2,5} PM₁₀) and volatilization particles. Tire tread contains not only natural rubber copolymers but also zinc (to facilitate the process of vulcanization) [7], making tire wear a significant source of Zn in emissions [8].

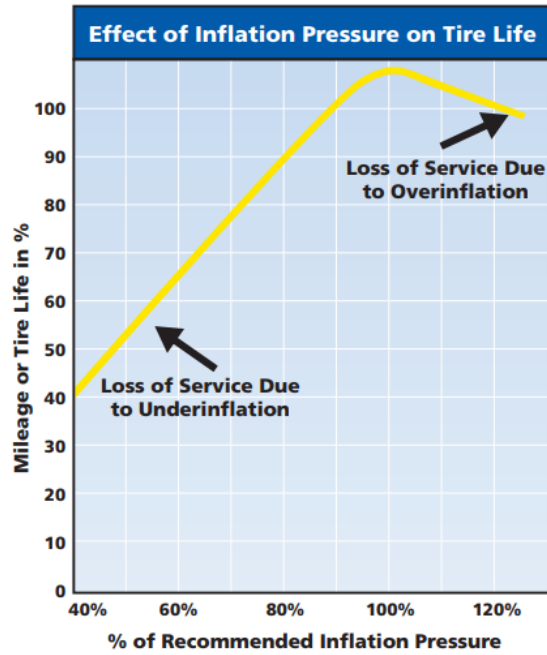


FIGURE 1.7 Effect of inflation pressure on tire life (©2011 Michelin North America Inc.)

Even if tread wear increases adherence at high speed (Fig 1.8) it also reduces the ability to displace water from the contact zone on a wet surface: this causes a reduction of the contact zone, lower adherence and brings to a higher probability of the phenomenon of aquaplaning (Fig 1.9) [4].

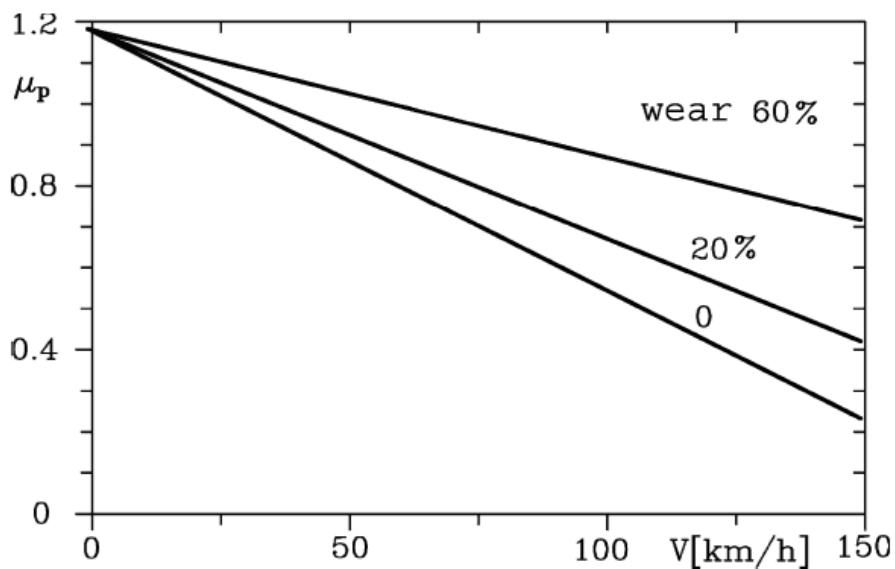


FIGURE 1.8 Effect of tread wear on peak longitudinal adherence

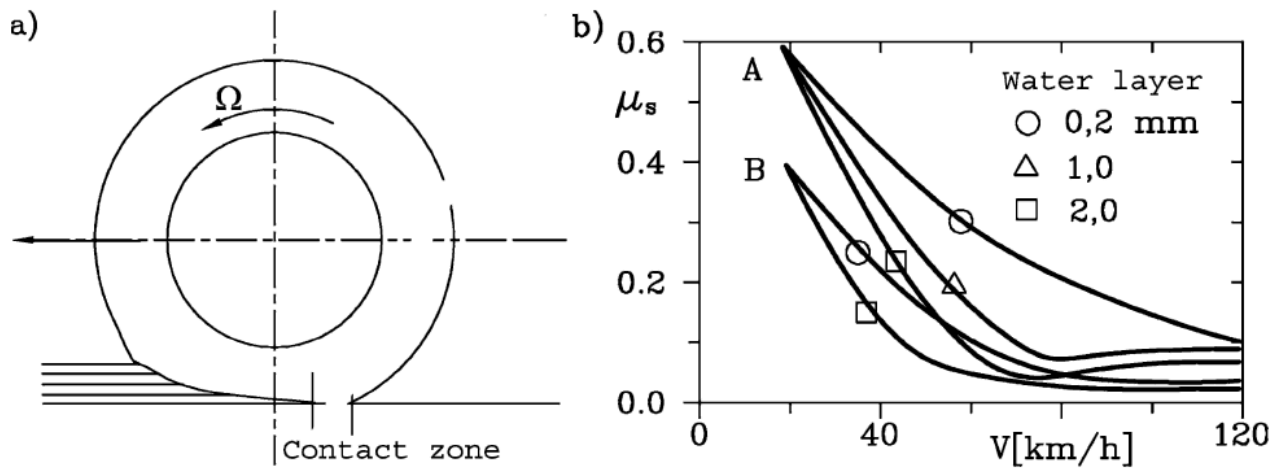


FIGURE 1.9 (a) Hydrodynamic lift of the wheel (aquaplaning) (b) adherence in function of speed on a wet road for a tire with tread (curve A) and without tread (curve B).

2 Preliminary theory concepts

In this section some theoretical concepts will be addressed to better comprehend the work done with the team.

2.1 Tires

The main functions of vehicle wheels are to support its weight exchanging vertical forces with the road and to make possible the vehicle movement, exchanging longitudinal and lateral forces [4].

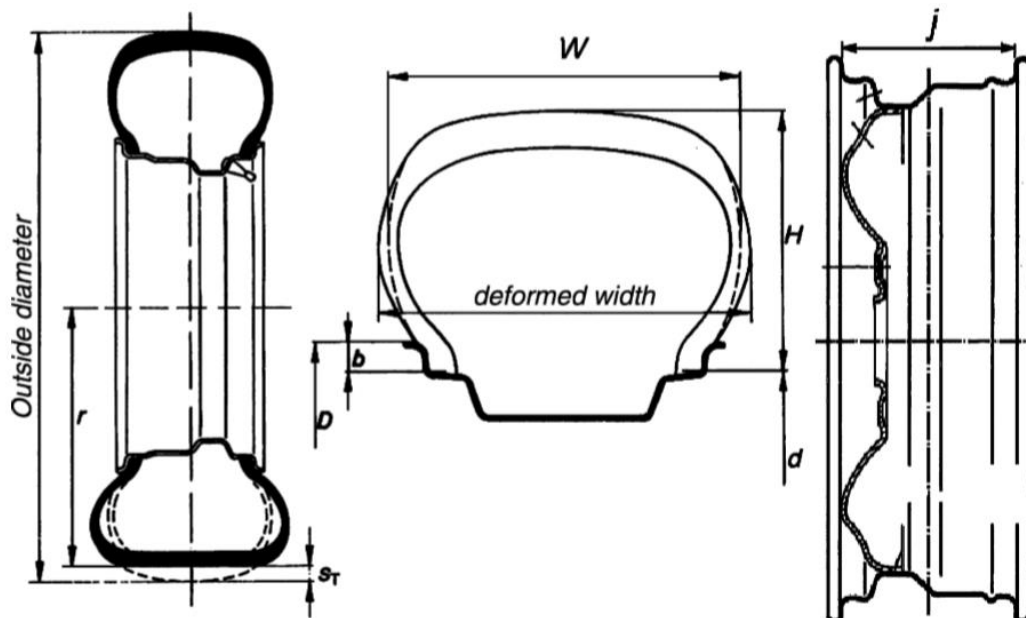


FIGURE 2.1. Section of a wheel including rim and tire and their main dimensions.

2.1.1 Structure and characteristics

Wheels include two elements: the rim and the tire (Fig 2.1). The tire is the actual interface with the ground and it's made of several layers of rubberized fabric (*plies*) with reinforcement cords. The *crown angle* is the angle between the direction of the cords and the circumferential direction of the tires [4].

Cross ply tires have a crown angle of 35-40 deg, *radial ply* instead have plies that are perpendicular to the circumferential direction and are surrounded by other belt plies with smaller angles (Fig 2.2). Radial tires are more vulnerable in the flanks respect to cross ply, but stiffer in the belt region: this arrangement give them superior cornering and comfort characteristics [4]. For this reason, cross ply tires are no longer used with the exception of few applications [9].

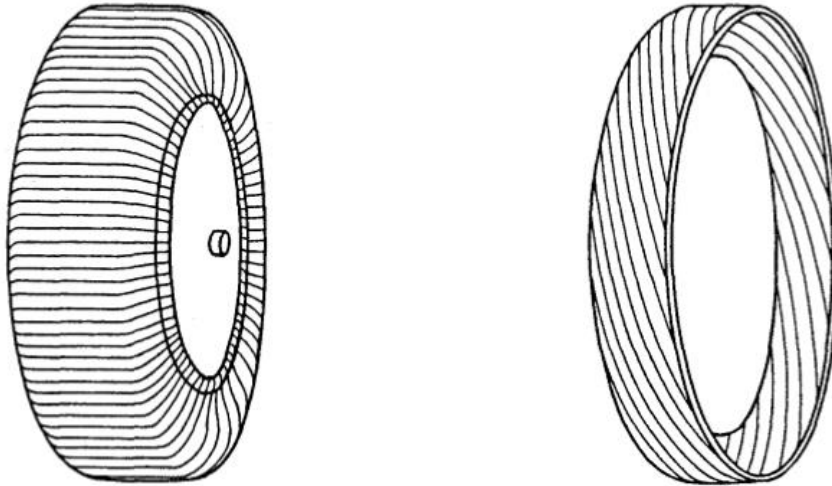


FIGURE 2.2. Left: substructure of a radial tire, right: substructure of a cross ply.

A radial tire (Fig 2.3) is constituted of two bead cores joined radially by the carcass. The necessary stiffness is provided by the cords. In the external part of the tyre there are the tread, the sidewall and the interior of the inner lining, which ensures the tyre proper sealing [9].

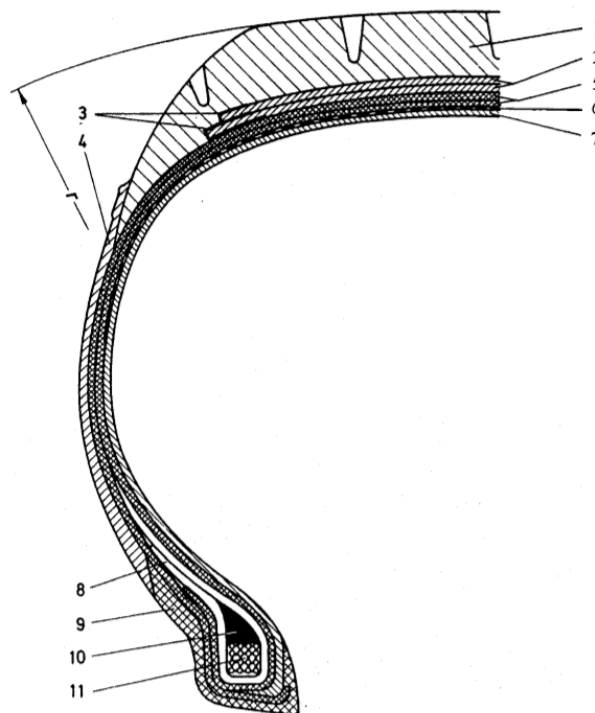


FIGURE 2.3. Radial tire structure: 1 running tread; 2 steel belt; 3 edge protection for the belt, in rayon or nylon; 4 sidewall; 5 two layers substructure; 6 cap; 7 inner lining; 8 flipper; 9 bead profile; 10 core profile; 11 bead core.

The tread is made of vulcanized filled rubber, it's the contact surface to the ground and so determines friction [4].

To permit exchangeability, tires are standardized by *ERTO (European Tyre and Rim Technical Organization)* [9] and are designated by a series of numbers and letters as in the following example:

195/75 R16 107R

Where:

- The first digit (195) is the width *W* (Fig 2.1) in mm. The measure is referred to an undeformed situation with no load applied and with nominal inflation pressure.
- The second (75) is the *aspect ratio* equal to the ratio H/W between the radial height of the tire and the width. The ratio is expressed in percentage: in this example $H = 0.75 \cdot 195 = 146.25 \text{ mm}$.
- The letter *R* indicates that the tire is radial ply, the designation is otherwise omitted.
- The third digit (16) is the rim diameter in inches.
- The fourth figure is the *load factor* that indicates the maximum allowed load at an assigned inflation pressure. It refers to a standardization table (Fig 2.4) and has no physical meaning.
- The final letter is the speed class of the tire and refers to Fig. 2.5 It indicates the maximum speed allowed by the tire.

| Load index | Wheel load capacity in kg with tyre pressure measured in bars | | | | | | | | | | |
|------------|------------------------------------------------------------------|-----|-----|-----|-----|-----|-----|-----|-----|-----|-----|
| | 1.5 | 1.6 | 1.7 | 1.8 | 1.9 | 2.0 | 2.1 | 2.2 | 2.3 | 2.4 | 2.5 |
| 69 | 215 | 225 | 240 | 250 | 260 | 270 | 285 | 295 | 305 | 315 | 325 |
| 70 | 225 | 235 | 245 | 260 | 270 | 280 | 290 | 300 | 315 | 325 | 335 |
| 71 | 230 | 240 | 255 | 265 | 275 | 290 | 300 | 310 | 325 | 335 | 345 |
| 72 | 235 | 250 | 260 | 275 | 285 | 295 | 310 | 320 | 330 | 345 | 355 |
| 73 | 245 | 255 | 270 | 280 | 295 | 305 | 315 | 330 | 340 | 355 | 365 |
| 74 | 250 | 260 | 275 | 290 | 300 | 315 | 325 | 340 | 350 | 365 | 375 |
| 75 | 255 | 270 | 285 | 300 | 310 | 325 | 335 | 350 | 360 | 375 | 387 |
| 76 | 265 | 280 | 295 | 310 | 320 | 335 | 350 | 360 | 375 | 385 | 400 |
| 77 | 275 | 290 | 305 | 315 | 330 | 345 | 360 | 370 | 385 | 400 | 412 |
| 78 | 280 | 295 | 310 | 325 | 340 | 355 | 370 | 385 | 400 | 410 | 425 |
| 79 | 290 | 305 | 320 | 335 | 350 | 365 | 380 | 395 | 410 | 425 | 437 |
| 80 | 300 | 315 | 330 | 345 | 360 | 375 | 390 | 405 | 420 | 435 | 450 |
| 81 | 305 | 325 | 340 | 355 | 370 | 385 | 400 | 415 | 430 | 445 | 462 |
| 82 | 315 | 330 | 350 | 365 | 380 | 395 | 415 | 430 | 445 | 460 | 475 |
| 83 | 325 | 340 | 360 | 375 | 390 | 405 | 425 | 440 | 455 | 470 | 487 |
| 84 | 330 | 350 | 365 | 385 | 400 | 420 | 435 | 450 | 470 | 485 | 500 |
| 85 | 340 | 360 | 380 | 395 | 415 | 430 | 450 | 465 | 480 | 500 | 515 |
| 86 | 350 | 370 | 390 | 410 | 425 | 445 | 460 | 480 | 495 | 515 | 530 |
| 87 | 360 | 380 | 400 | 420 | 440 | 455 | 475 | 490 | 510 | 525 | 545 |
| 88 | 370 | 390 | 410 | 430 | 450 | 470 | 485 | 505 | 525 | 540 | 560 |
| 89 | 385 | 405 | 425 | 445 | 465 | 485 | 505 | 525 | 545 | 560 | 580 |
| 90 | 400 | 420 | 440 | 460 | 480 | 500 | 520 | 540 | 560 | 580 | 600 |
| 91 | 410 | 430 | 450 | 475 | 495 | 515 | 535 | 555 | 575 | 595 | 615 |
| 92 | 420 | 440 | 465 | 485 | 505 | 525 | 550 | 570 | 590 | 610 | 630 |
| 93 | 430 | 455 | 475 | 500 | 520 | 545 | 565 | 585 | 610 | 630 | 650 |
| 94 | 445 | 470 | 490 | 515 | 540 | 560 | 585 | 605 | 625 | 650 | 670 |
| 95 | 460 | 485 | 505 | 530 | 555 | 575 | 600 | 625 | 645 | 670 | 690 |
| 96 | 470 | 495 | 520 | 545 | 570 | 595 | 620 | 640 | 665 | 685 | 710 |
| 97 | 485 | 510 | 535 | 560 | 585 | 610 | 635 | 660 | 685 | 705 | 730 |
| 98 | 500 | 525 | 550 | 575 | 600 | 625 | 650 | 675 | 700 | 725 | 750 |
| 99 | 515 | 540 | 570 | 595 | 620 | 650 | 675 | 700 | 725 | 750 | 775 |
| 100 | 530 | 560 | 590 | 615 | 640 | 670 | 695 | 720 | 750 | 775 | 800 |

FIGURE 2.4. Standardized table for load index

| v_{max} in km/h^{-1} | Speed symbol | Identification |
|--------------------------|--------------|-----------------|
| 80 | F | |
| 130 | M | |
| 150 | P | |
| 160 | Q | |
| 170 | R | |
| 180 | S | |
| 190 | T | |
| 210 | H | |
| 240 | V | |
| 270 | W | |
| 300 | y | |
| over 210 | | VR |
| over 240 | | ZR (old system) |

FIGURE 2.5. Standardized table for speed class

2.1.2 Wheel's reference system and forces acting on the tire

Is useful to define the wheel reference system $X'Y'Z'$ in Fig. 2.6 to study the forces between tire and ground. The origin is set at the center of the contact patch in the theoretical contact point between ground and the undeformed equatorial plane; the X' axis has the same direction of vehicle speed and lies in the intersection between the equatorial plane and the ground; the Z' axis is perpendicular to the ground and consequently the Y' is on the ground and points left [4].

The total force is supposed to be applied in the origin and can be decomposed along the axes as: *longitudinal force* F_x , *lateral force* F_y , and *vertical force* F_z . In the same way also the moments can be broken down in three components: the *overturning moment* M_x , *rolling resistance moment* M_y and the *self-aligning moment* M_z . A wheel torque T can be applied along the tire rotation axis [4].

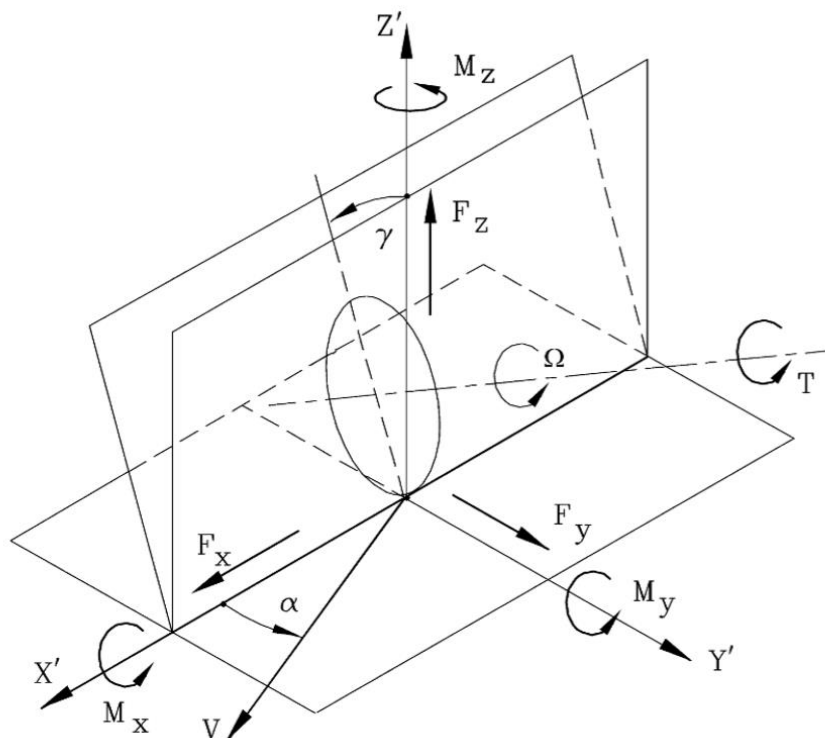


FIGURE 2.6 Reference system used to study the forces exchanged between tire and ground

As *sideslip angle* we define the angle between the direction of the wheel hub motion and the $X'Z'$ plane, while the angle between the very same plane and the wheel equatorial plane is the *camber angle* and is positive if the upper part of the wheel points toward the vehicle [4].

The forces on the plane of the ground are exerted thanks to adhesion phenomena between the tire and the ground that occur thanks to the attraction forces of the molecules of the two elements (*physical adhesion*) and to the dissipation in the *local deformation* of the material [4].

The ratio between longitudinal and vertical force is the *longitudinal friction coefficient*:

$$\mu_x = \frac{F_x}{F_z}$$

Similarly, the *lateral friction coefficient* is:

$$\mu_y = \frac{F_y}{F_z}$$

If a braking or driving moment is applied to the wheel, the tread band is circumferentially deformed near the contact zone, for this reason the peripheral speed of the wheel change during rolling. The effective rolling radius in the contact point is different from the one of the undeformed wheel: the instantaneous centre of rotation doesn't lie anymore on the ground (Fig 2.7) and the angular velocity Ω of the wheel is lower than Ω_0 characterizing free rolling in same conditions [4].

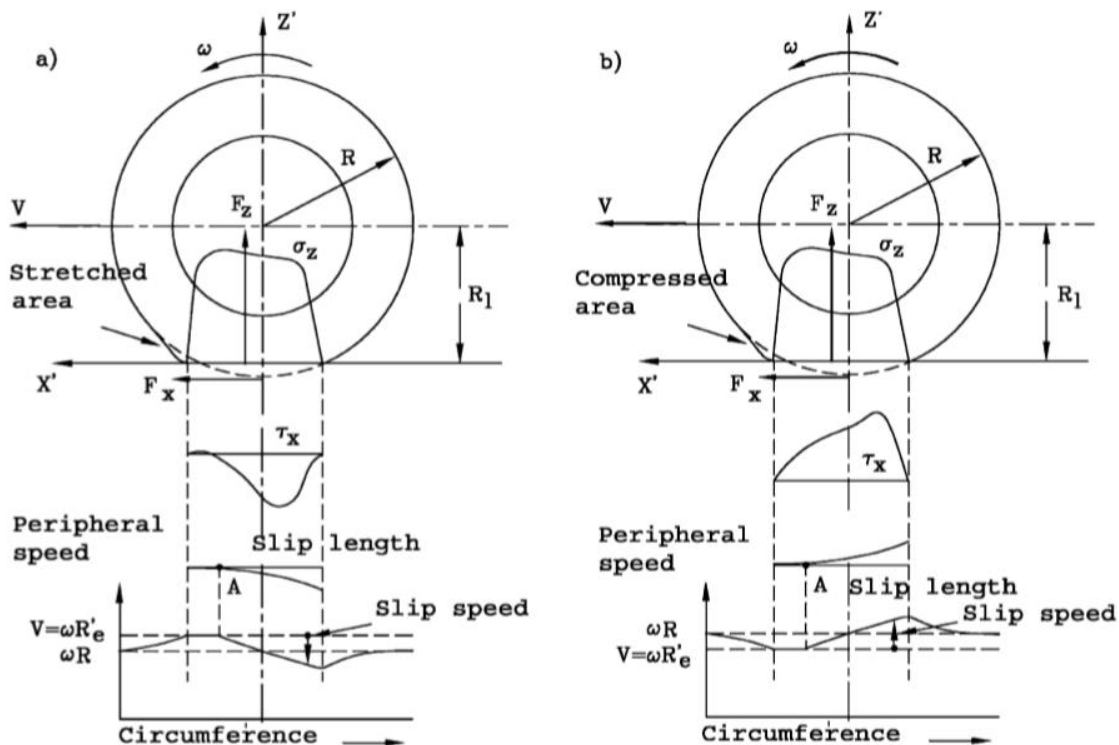


FIGURE 2.7. Contact pressure distribution for a braking (a) and driving (b) wheel.

In this condition it's possible to define a *longitudinal slip* as:

$$\kappa = \frac{\Omega}{\Omega_0} - 1 = \frac{v}{V}$$

Where v is the linear speed in the contact point (Fig 2.8).

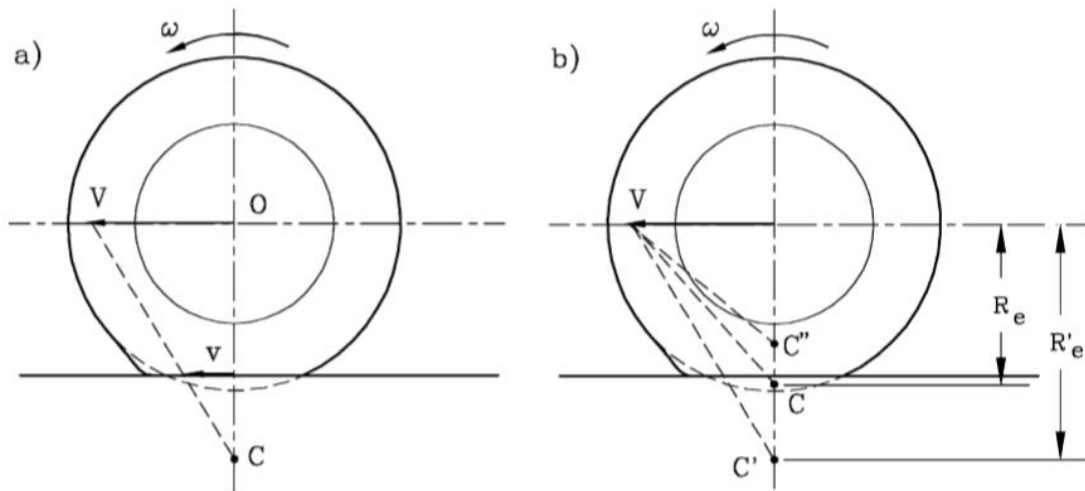


FIGURE 2.8. (a) Centre of instantaneous rotation and slip speed for a braking wheel. (b) Instantaneous centre of rotation by pure rotation C, by braking C' and by traction C''.

The longitudinal force that the wheel exchange with the road is function of the slip and vanishes with $\kappa = 0$. The function is antisymmetric, and the forces grows linearly for small values of slip, then reaches a peak and decrease (Fig 2.9). The lower limit for $\kappa = -1$ occurs in braking with the wheel locked and free sliding. There's no upper limit for slip, but the wheels simply spin while the vehicle is not moving [4].

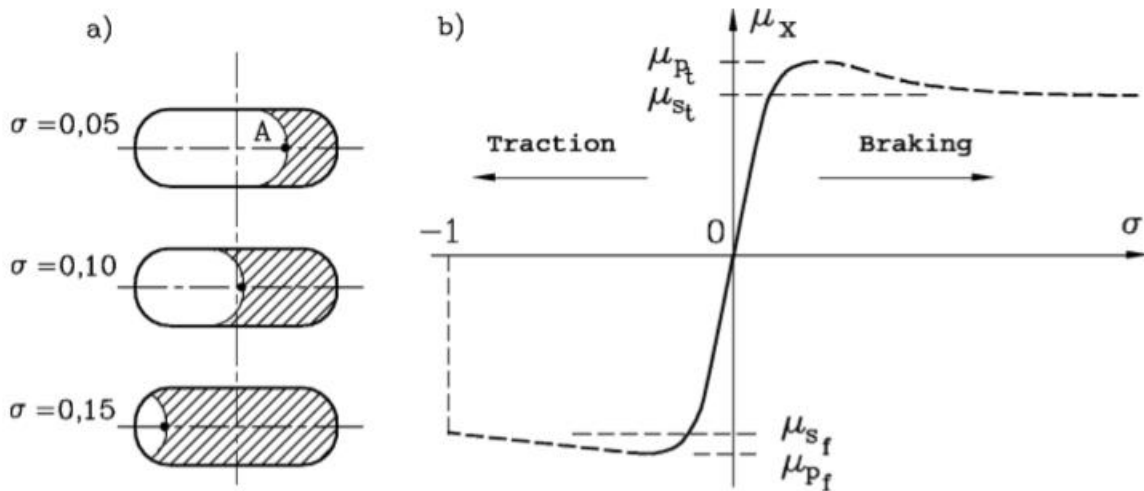


FIGURE 2.9. (a) Slipping area for different values of slip σ . (b) Qualitative diagram of μ_x in function of the longitudinal slip σ .

As it can be seen in Fig 2.9, the maximum friction occurs for limited values of slip, for this reason devices as ABS (Antilock Braking System) avoid the locking of the wheel and maintain in a restricted range the slip, optimizing braking.

The lateral force F_y has a similar relation with sideslip angle and it's again linked with the compliance of the tire. The presence of a sideslip angle means that the velocity of the centre of the wheel does not lie in its mean plane [4]. The contact area divides in a leading zone (in which no

sliding occurs) and a trailing zone that grows with the sideslip and in which the tread slips toward the mean plane (Fig 2.10) [4].

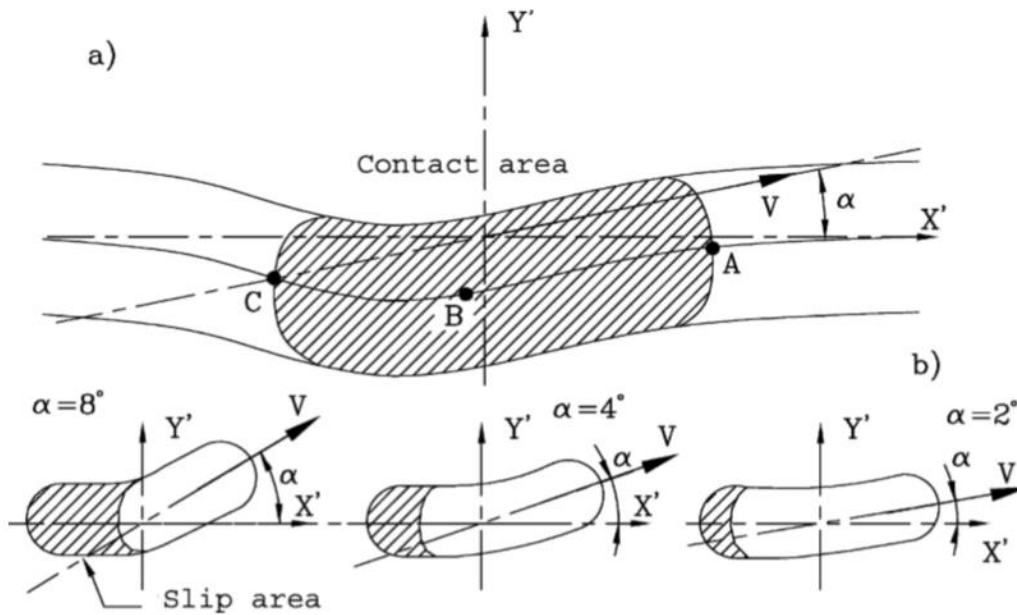


FIGURE 2.10. Wheel-road contact in presence of sideslip. (a) path of a point on the tread on the equator plane; (b) contact zone and slip zone for different values of α (not in scale).

The resultant of the distribution of side forces is not applied at the centre of the contact zone but at a distance t called *pneumatic trail* (Fig 2.11). The product of the force and the trail is the *self-aligning moment* $M_z = F_y t$. At high sideslip the distribution of the τ_y is more even and the pneumatic trail decrease, also the lateral force starts decreasing after the peak and consequently the moment drops (Fig 2.12 b) and can even change direction [4].

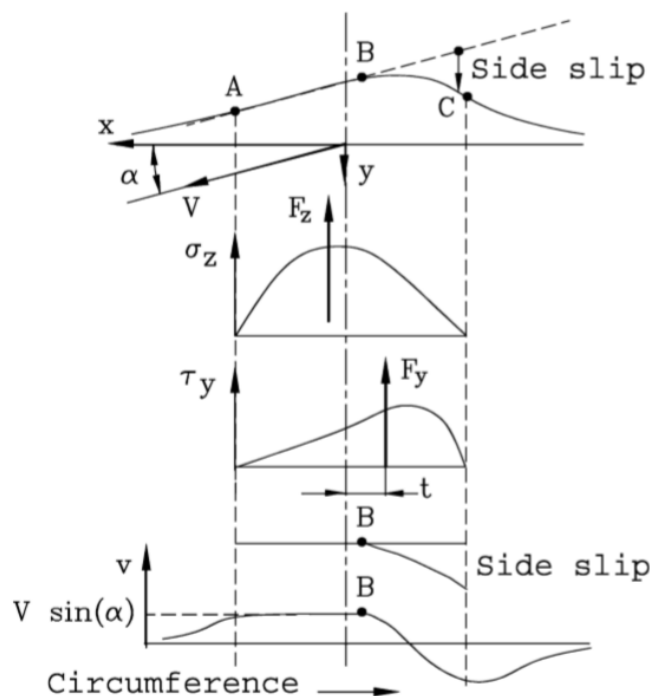


FIGURE 2.11. Lateral deformation, distribution of the pressures σ_z e τ_y , slip and lateral speed for a cornering tire.

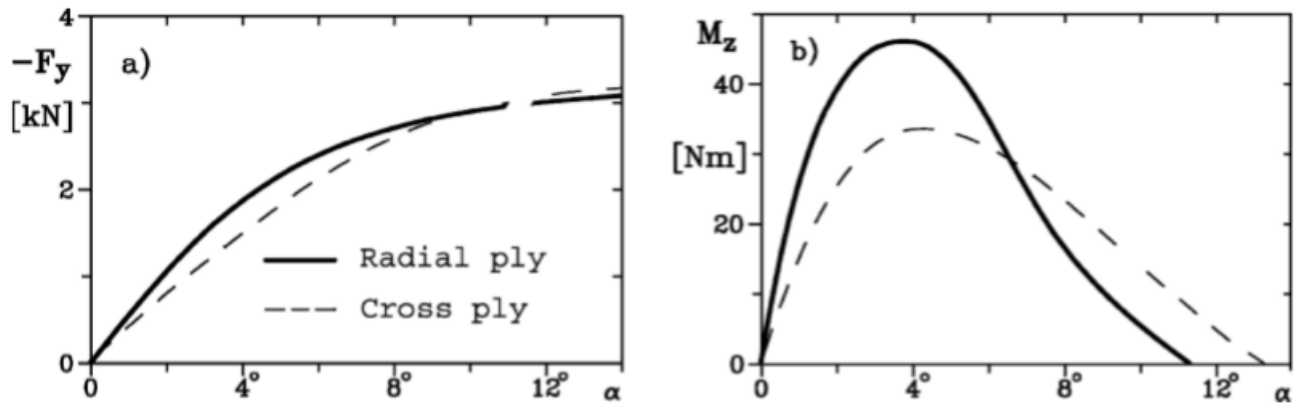


FIGURE 2.12. Lateral force F_y and self-aligning moment M_z for different tires subjected to the same load, with same size and inflation pressure.

2.1.3 Pacejka's Magic Formula MF 5.2

A widely used semi-empirical model to calculate steady state force and moments characteristics is the so-called Magic Formula by Hans B. Pacejka.

The general form of the formula holds for given values of vertical load and vertical load and it's the following [10]:

$$y = D \sin[C \operatorname{atan}\{Bx - E(Bx - \operatorname{atan} Bx)\}]$$

With:

$$Y(X) = y(x) + S_V$$

$$x = X + S_H$$

Where Y is the output variable (F_x, F_y, M_z), X the input variable (κ or α) and:

- B the stiffness factor
- C the shape factor
- D the peak value
- E the curvature factor
- S_V the vertical shift
- S_H the horizontal shift

The magic formula produces an anti-symmetrical curve passing through the origin, reaching a maximum and then tending to an asymptote (Fig 2.13). The horizontal and vertical shift allow the curve to have an offset respect to the origin (usually caused by camber, rolling resistance and conicity of the tire). Deviations from the symmetric behaviour can be accommodated by the shape factor E that is made dependent from the sign of the abscissa [10].

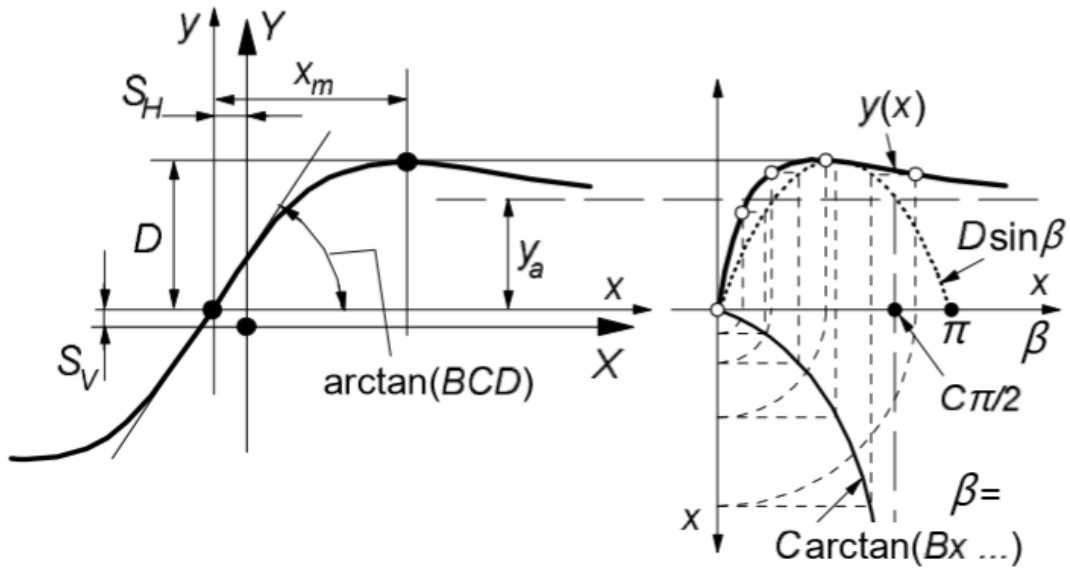


FIGURE 2.13 Curve produced by the magic formula. With meaning of curve parameters.

The product BCD corresponds to the slope of the curve at the origin, for small values of slip the relation with forces and moments is linear [10].

All the factors are function of vertical load and camber angle, the dependence is described by a series of parameters that are specific for the tire at a given inflation pressure. The following formulas refer to [10]

Regarding the longitudinal behaviour, the *slip stiffness* (the slope at the origin) is:

$$BCD_x = K_x = F_z(p_{Kx1} + p_{Kx2}df_z)e^{p_{Kx3}df_z}$$

The peak adherence coefficient:

$$\mu_{xpeak} = p_{Dx1} + p_{Dx2}df_z$$

Concerning lateral behaviour, the cornering stiffness (BCD_y) is equal to:

$$BCD_y = K_y = p_{Ky1}F_{z0} \sin \left[2 \operatorname{atan} \left(\frac{F_z}{p_{Ky2}F_{z0}} \right) \right]$$

And the peak lateral adherence:

$$\mu_{ypeak} = (p_{Dy1} + p_{Dy2}df_z)(1 - p_{Dy3}\gamma^2)$$

Where:

$$df_z = \frac{F_z - F_{z0}}{F_{z0}}$$

Is the dimensionless load increment respect to the nominal F_{z0} , γ the camber angle and p the parameters of the tire.

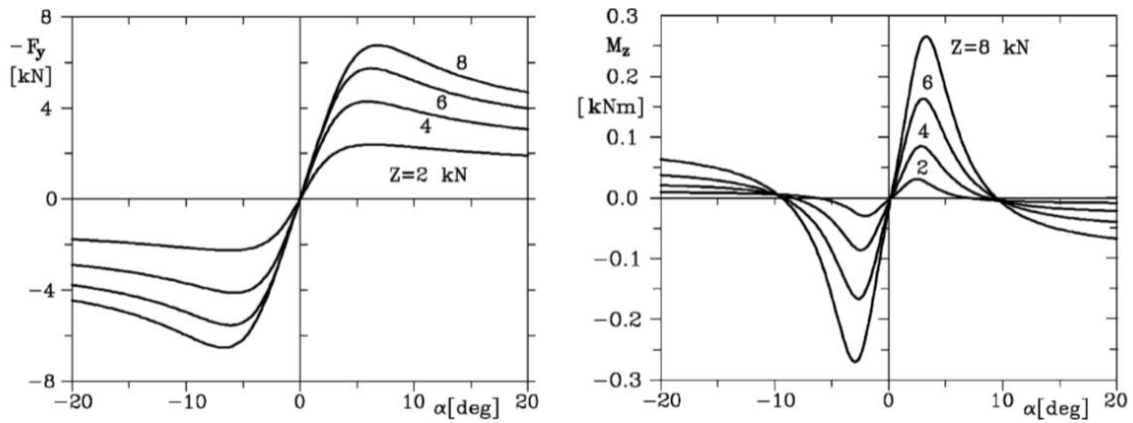


FIGURE 2.14. Curves $F_y(\alpha)$ and $M_z(\alpha)$ obtained with the magic formula.

2.1.4 Improved Magic Formula to take in account inflation pressure changes MF 6.2

Over the years the Magic Formula saw several improvements on the accuracy and capability of the model. From the 6 version of the formula, introduced by I. J. M. Besselink, A. J. C. Schmeitz and H.B. Pacejka in [11] and to which we will refer trough the paragraph:

- The effect of inflation pressure changes was introduced, eliminating the need to have a different set of parameters for each pressure condition.
- The description of camber was improved, allowing bigger angles and making superfluous the use of a special formula for motorcycles.
- A better description of tire dynamics was introduced, making it consistent between MF-Swift and MF-Tire models.

Being the Magic Formula a semi-empirical tire model, each individual tire characteristic has to be analysed for the impact of changes of pressure. The main effects identified were:

- Changes in longitudinal stiffness, cornering stiffness and camber stiffness.
- Changes of the peak friction coefficients, both longitudinal and lateral.
- Reduction of pneumatic trail increasing inflation pressure.

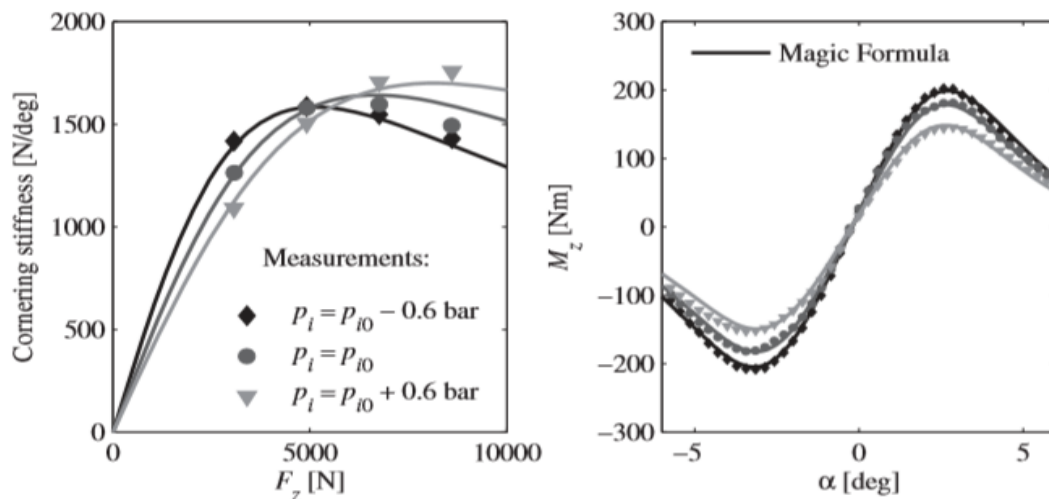


FIGURE 2.15. Tire pressure effects for a passenger car tyre; left: cornering stiffness and right: self-aligning moment.

To take in account pressure, an increment from the nominal one is introduced:

$$dp_i = \frac{p_i - p_{i0}}{p_{i0}}$$

The formula for longitudinal slip stiffness becomes:

$$K_x = F_z(p_{Kx1} + p_{Kx2}df_z)e^{p_{Kx3}df_z}(1 + p_{px1}dp_i + p_{px2}dp_i^2)$$

For the peak adherence coefficient:

$$\mu_{xpeak} = (p_{Dx1} + p_{Dx2}df_z)(1 - p_{Dy3}\gamma^2)(1 + p_{px3}dp_i + p_{px4}dp_i^2)$$

The cornering stiffness is equal to:

$$K_y = p_{Ky1}(1 + p_{py2}dp_i)F_{z0} \sin \left[p_{Ky4} \operatorname{atan} \left(\frac{F_z}{(p_{Ky2} + p_{ky5}\gamma^2)(1 + p_{py2}dp_i)F_{z0}} \right) \right] (1 - p_{Ky3}|\gamma|)$$

And the peak lateral adherence:

$$\mu_{ypeak} = (p_{Dy1} + p_{Dy2}df_z)(1 - p_{Dy3}\gamma^2)(1 + p_{py3}dp_i + p_{py4}dp_i^2)$$

2.2 Longitudinal dynamics

In this paragraph we will refer to [12]. Considering the vehicle as a rigid body, neglecting suspensions and compliance of the tires and assuming that the x axis is parallel to the ground, the longitudinal equilibrium is:

$$m\ddot{x} = \sum_{\forall i} F_{xi}$$

Where F_{xi} are all the forces acting in longitudinal direction, like braking or driving forces, drag, rolling resistance etc.

2.2.1 Load distribution

Longitudinal dynamics is influenced by the distribution of normal forces: being a vehicle with more than three wheels statically indeterminate, the load distribution is determined by the suspensions. However, assuming the system symmetric about xz plane, the two wheels of each axle are equally loaded. A two-axle vehicle can be considered as a beam on two supports (statically determined) and can be modelled as a rigid body.

With the vehicle at a standstill on a level road the normal forces are:

$$\begin{cases} F_{z1} = mg \frac{b}{l} \\ F_{z2} = mg \frac{a}{l} \end{cases}$$

In the more general case of a vehicle moving with a longitudinal grad angle α (Fig 2.16) the dynamic equilibrium in x and z direction and the rotations about O can be computed:

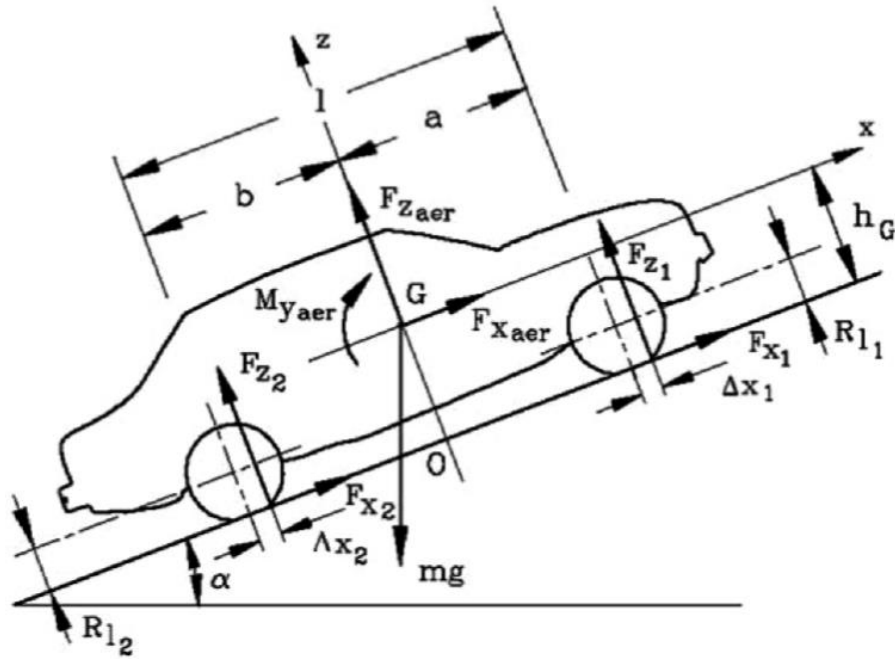


FIGURE 2.16. Forces acting on a vehicle moving on an inclined road

$$\begin{cases} F_{x1} + F_{x2} + F_{xaer} - mg\sin(\alpha) = m\dot{V} \\ F_{z1} + F_{z2} + F_{zaer} - mg\cos(\alpha) = 0 \\ F_{z1}(a + \Delta x_1) - F_{z2}(b - \Delta x_2) + mgh_g\sin(\alpha) - M_{aer} + |F_{xaer}|h_g = mh_g\dot{V} \end{cases}$$

The Δx_i are the offsets from the point of contact of the normal force and they take in account rolling resistance.

Solving the second and third equation in the normal forces:

$$\begin{cases} F_{z1} = mg \frac{(b - \Delta x_2)\cos(\alpha) - h_g\sin(\alpha) - K_1V^2 - \frac{h_g}{g}\dot{V}}{l + \Delta x_1 - \Delta x_2} \\ F_{z2} = mg \frac{(a + \Delta x_1)\cos(\alpha) + h_g\sin(\alpha) - K_2V^2 + \frac{h_g}{g}\dot{V}}{l + \Delta x_1 - \Delta x_2} \end{cases}$$

Where:

$$\begin{cases} K_1 = \frac{\rho S}{2mg} [C_x h_g - lC_{My} + (b - \Delta x_2)C_z] \\ K_2 = \frac{\rho S}{2mg} [-C_x h_g + lC_{My} + (a + \Delta x_1)C_z] \end{cases}$$

2.2.2 Braking in ideal conditions

In the condition of ideal braking, all the wheels brake with the same longitudinal friction coefficient μ_x .

The total braking force is so:

$$F_x = \sum_{\forall i} \mu_{xi} F_{zi}$$

The deceleration, considering also the effect of drag, rolling resistance and slope is consequently equal to:

$$\frac{dV}{dt} = \frac{\sum_{\forall i} \mu_{xi} F_{zi} - \frac{1}{2} \rho S C_x V^2 - f \sum_{\forall i} F_{zi} - mg \sin(\alpha)}{m}$$

In ideal braking, neglecting drag and rolling resistance that are usually far smaller than braking forces, the deceleration becomes:

$$\frac{dV}{dt} = \mu_x \left[g \cos \alpha - \frac{1}{2m} \rho V^2 S C_z \right] - g \sin \alpha$$

That on level road with no lift (like on most passenger vehicles) becomes:

$$\frac{dV}{dt} = \mu_x g$$

The braking manoeuvre will cause a load transfer and the normal forces can be calculated neglecting aerodynamic effects as:

$$\begin{cases} F_{z1} = \frac{m}{l} \left[g b \cos(\alpha) - g h_g \sin(\alpha) - \frac{h_g dV}{dt} \right] \\ F_{z2} = \frac{m}{l} \left[g b \cos(\alpha) + g h_g \sin(\alpha) + \frac{h_g dV}{dt} \right] \end{cases}$$

The contribution to the braking force of each single axle can be obtained multiplying the normal load for the adherence:

$$\begin{cases} F_{x1} = \mu_{x1} F_{z1} \\ F_{x2} = \mu_{x2} F_{z2} \end{cases}$$

2.3 Lateral dynamics

According to how their path is controlled, vehicles can be classified in:

- Kinematic guided vehicles, in which the trajectory is determined by kinematic constraints
- Piloted vehicles, where the trajectory is changed exerting forces on the vehicle.

The first condition is an abstraction, all the forces needed are provided by the constraint, that should be infinitely stiff [4].

In road vehicles instead, the driver operates the steering wheel imposing the wheels to work with a sideslip angle and generate forces to change trajectory. The linearity of the tire behaviour and the high value of cornering stiffness however give to the driver the impression of a kinematic driving [4]. Throughout all paragraph we will refer to [12].

2.3.1 Low speed or kinematic steering

In kinematic steering the velocities of the centres of the wheels lie on their midplanes: that means that the sideslip angles are vanishing small. In this condition the wheels cannot exert cornering forces to balance the centrifugal force due to the curvature of the trajectory, so the model holds for cornering at vanishing small speed.

Considering a front steering vehicle, the condition for kinematic steering is that the perpendiculars to the mid planes of all wheels meet in a single point O (Fig 2.17).

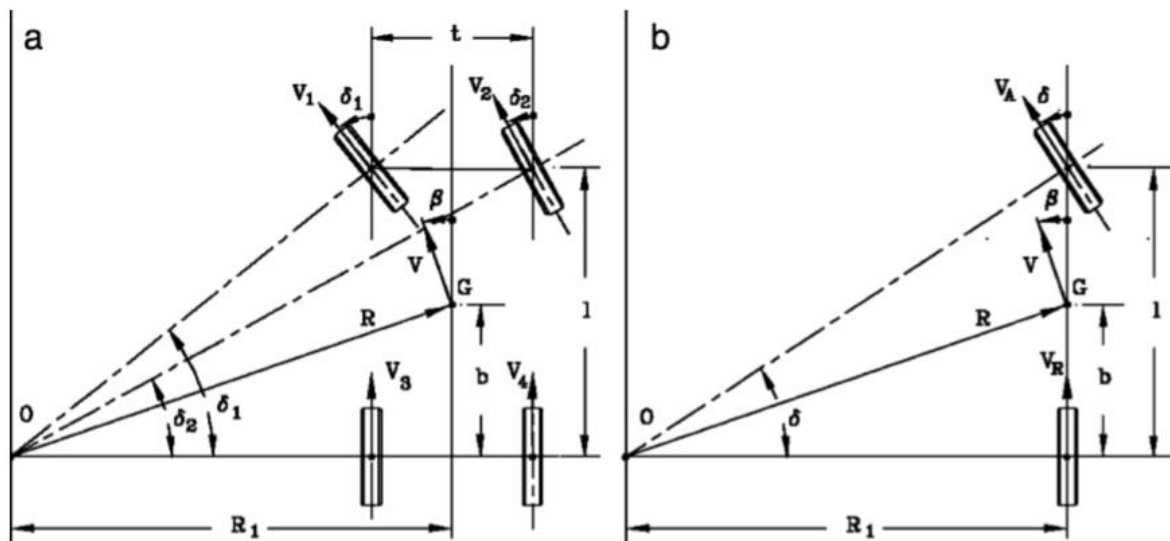


FIGURE 2.17. Kinematic steering for a four-wheeled and for a two-wheeled vehicle

From simple geometrical considerations, the steering angles to have kinematic steering can be found:

$$\tan(\delta_1) = \frac{l}{R_1 - \frac{t}{2}}$$

$$\tan(\delta_2) = \frac{l}{R_1 + \frac{t}{2}}$$

Eliminating R_1 between the two equations, the direct relationship between the angles is:

$$\cot(\delta_1) - \cot(\delta_2) = \frac{t}{l}$$

A device that allow wheels to be steer according to this relation is referred to *Ackerman Steering*, but no actual system follow exactly the equation.

Many efforts have been made in the past to get as close as possible to Ackerman geometry, however the importance of kinematic steering is often overestimated considering that:

- A wheel sideslip angle is always present, steering
- Most suspensions cause an additional steering angle with roll
- In most cases steering wheels have a toe in angle
- Suspension stroke and deformation cause additional steering

If the radius of curvature is much bigger respect to the track t the system can be considered as *mono-track* (Fig 18-b) so equivalent to a two-wheel vehicle. In this condition the radius is equal to:

$$R = \sqrt{b^2 + R_1^2} = \sqrt{b^2 + l^2 \cot^2 \delta}$$

Where δ is the steering angle of the equivalent mono-track model.

If the radius is big enough, $R \approx R_1 \approx l \cot \delta \approx \frac{l}{\delta}$

The equation can be rewritten as:

$$\frac{1}{R\delta} \approx \frac{1}{l}$$

This ratio is called *curvature gain* and defines the response of the vehicle in terms of curvature $\frac{1}{R}$ to a steering angle δ . The curvature gain is therefore a sort of transfer function for the directional control and in kinematic conditions is equal to the reciprocal of the wheelbase.

Another important transfer function of the vehicle are the *sideslip angle gain* defined as the response in sideslip of the vehicle to a steering input:

$$\frac{\beta}{\delta} = \frac{b}{l}$$

And the *acceleration gain* (the response in terms of lateral acceleration)

$$\frac{V^2}{R\delta} = \frac{V^2}{l}$$

2.3.2 Ideal steering

If the speed is not vanishingly small, the wheels work with a sideslip angle to generate cornering forces.

Consider a rigid vehicle moving on a level road with transversal slope α_t (Fig 2.18): neglecting aerodynamic forces, the equilibrium along η axis (parallel to the road surface, passing through the centre of mass of the vehicle and intersecting the vertical for the centre of the path) can be written equating the wheel forces to the centrifugal force.

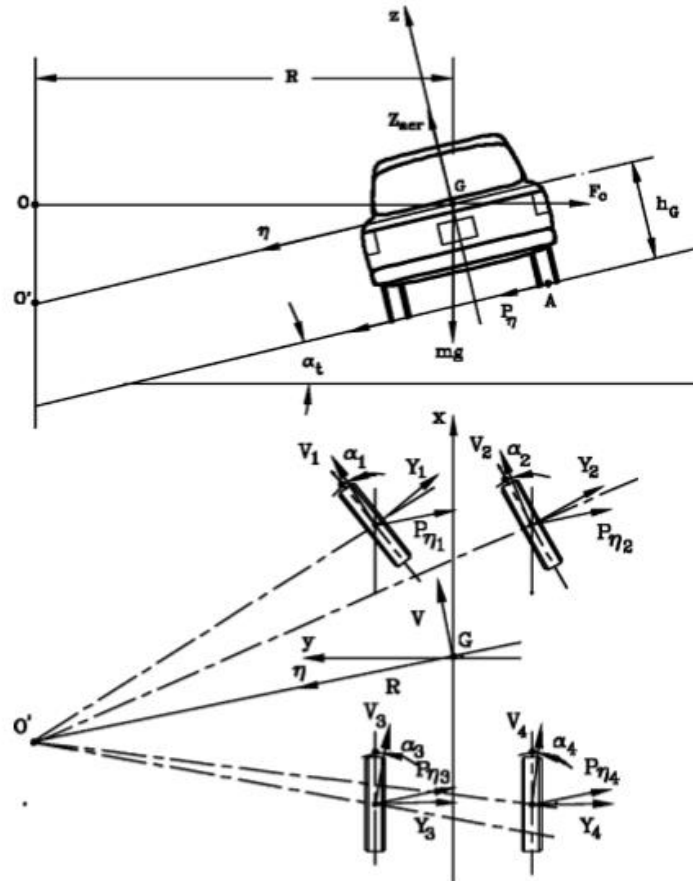


FIGURE 2.18 Simplified model for dynamic steering

With $\alpha_t = 0$:

$$\frac{mV^2}{R} = \sum_{\forall i} P_{\eta i}$$

Similarly to the definition of ideal braking, the assumption in ideal steering is that μ_y is the same for all the wheels. Moreover in a first approximation the $P_{\eta i}$ can be considered equal to the cornering forces F_{y_i} . The total vertical force exerted by the vehicle on the road is $F_z = mg$.

So, the previous equation becomes:

$$\frac{mV^2}{R} = \sum_{\forall i} F_{y_i} = \sum_{\forall i} F_{z_i} \mu_{y_i} = \mu_y mg$$

And the lateral acceleration can be calculated as:

$$\frac{V^2}{R} = \mu_y g$$

Therefore, the maximum acceleration allowed by the adherence of the tires depends on the maximum friction coefficient:

$$\left(\frac{V^2}{R}\right)_{max} = \mu_{yp}g$$

Another limitation to the maximum lateral acceleration of the vehicle comes from the danger of rollover, that occurs if the resultant of forces in the yz plane crosses the road surface outside point A (Fig 2.18).

Computing the equilibrium of the moments about point A :

$$M_A = -\frac{t}{2}mg + h_g \frac{mV^2}{R}$$

The rollover occurs with $M_A = 0$. So the maximum acceleration is:

$$\left(\frac{V^2}{R}\right)_{max} = \frac{t}{2h_g}g$$

According to the magnitude of $\frac{t}{2h_g}$ and μ_{yp} , the acceleration is limited by the first condition reached.

$$\left(\frac{V^2}{R}\right)_{max} = g \min\left\{\mu_{yp}, \frac{t}{2h_g}\right\}$$

Introducing the effect of the slope and aerodynamics the equilibrium in η direction becomes:

$$\frac{mV^2}{R} \cos(\alpha_t) - mg \sin(\alpha_t) = \sum_{\forall i} P_{\eta i} = \sum_{\forall i} F_{zi} \mu_{yi}$$

The normal force exerted on the road is instead:

$$F_z = mg \cos(\alpha_t) + \frac{mV^2}{R} \sin(\alpha_t) - \frac{1}{2} \rho C_z S V^2$$

The maximum acceleration allowed by adherence is computed:

$$\left(\frac{V^2}{R}\right)_{max} = g \frac{\tan(\alpha_t) + \mu_{yp}(1 - MV^2)}{1 - \mu_{yp} \tan(\alpha_t)}$$

Where the ratio M is:

$$M = \frac{\rho S C_z}{2mg \cos(\alpha_t)}$$

The moment about point A is:

$$M_A = -\frac{t}{2} \left[mg \cos(\alpha_t) + \frac{mV^2}{R} \sin(\alpha_t) - \frac{1}{2} \rho C_z S V^2 \right] + h_g \left[\frac{mV^2}{R} \cos(\alpha_t) - mg \sin(\alpha_t) \right]$$

Consequently, the rollover limit condition is:

$$\left(\frac{V^2}{R} \right)_{max} = g \frac{\tan(\alpha_t) + \frac{t}{2h_g} (1 - MV^2)}{1 - \frac{t}{2h_g} \tan(\alpha_t)}$$

The maximum lateral acceleration is limited by the condition that is reached first:

$$\left(\frac{V^2}{R} \right)_{max} = g \min \left\{ \frac{\tan(\alpha_t) + \mu_{yp} (1 - MV^2)}{1 - \mu_{yp} \tan(\alpha_t)}, \frac{\tan(\alpha_t) + \frac{t}{2h_g} (1 - MV^2)}{1 - \frac{t}{2h_g} \tan(\alpha_t)} \right\}$$

Most vehicles are designed to reach the sliding limit before rollover ($\mu_{yp} < \frac{t}{2h_g}$), the rollover condition can be reached tough in commercial vehicles and SUVs with an high centre of gravity.

The model is a rough approximation of the actual situation as it based on the assumptions that all wheels have the same side force coefficients μ_y , that all the forces are directed along η axis and neglecting load transfer and the influence of suspensions.

2.3.3 Simplified approach for high speed cornering

Considering the distribution of cornering forces between the axles, the sideslip angle of the vehicle and the wheels, a more accurate model can be developed.

Assume that the vehicle is moving at constant velocity on a level road, the path is circular with a radius of curvature much bigger than the wheelbase. Consequently, all the angles are small and the system can be modelled as mono-track.

Referring to Fig 2.19, neglecting aerodynamic forces and self-aligning moments, the equilibrium about y axis is:

$$\frac{mV^2}{R} \cos(\beta) = \sum_{\forall i} F_{xi} \sin(\delta_i) + \sum_{\forall i} F_{yi} \cos(\delta_i)$$

While the equilibrium of moments around G point is:

$$\sum_{\forall i} F_{xi} \sin(\delta_i) x_i + \sum_{\forall i} F_{yi} \cos(\delta_i) x_i = 0$$

If the angles are small the equations reduce to

$$\begin{cases} \frac{mV^2}{R} = \sum_{\forall i} F_{yi} \\ \sum_{\forall i} F_{yi} x_i = 0 \end{cases}$$

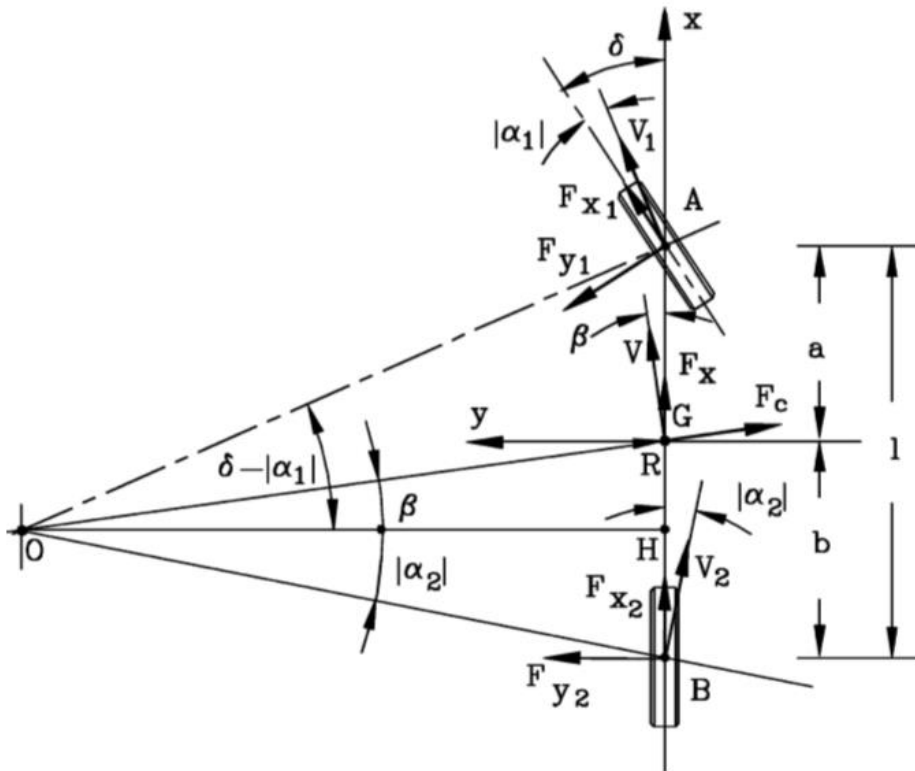


FIGURE 2.19 Mono-track model to study the handling of a two-axle vehicle.

Solving the equations:

$$F_{y1} = \frac{mV^2 b}{R l}$$

$$F_{y2} = \frac{mV^2 a}{R l}$$

For small sideslip angles, the relation with the side force is linear through the cornering stiffness:

$$F_{y1} = C_1 \alpha_1$$

$$F_{y2} = C_2 \alpha_2$$

C_1 and C_2 are the cornering stiffnesses of the whole axle, that is equal to the sum of the cornering stiffnesses of the single wheels.

Consequently, the sideslip angles for front and rear axle are equal to:

$$\alpha_1 = \frac{mV^2}{R} \frac{b}{C_1 l}$$

$$\alpha_2 = \frac{mV^2}{R} \frac{a}{C_2 l}$$

From simple geometrical considerations:

$$\delta - \alpha_1 + \alpha_2 = \frac{l}{R}$$

Substituting:

$$\delta = \frac{l}{R} + \frac{mV^2}{Rl} \left(\frac{b}{C_1} - \frac{a}{C_2} \right)$$

The curvature gain is therefore:

$$\frac{1}{R\delta} = \frac{1}{l} \frac{1}{1 + K_{us} \frac{V^2}{gl}}$$

Where

$$K_{us} = \frac{mg}{l^2} \left(\frac{b}{C_1} - \frac{a}{C_2} \right)$$

Is the *understeer coefficient* of the vehicle, a non-dimensional quantity sometimes expressed in radians. It grows with b and C_2 and decrease with a and C_1 . Through its effect on cornering stiffness, the inflation pressure affects the curvature gain of the vehicle.

As it was said before, in kinematic conditions:

$$\frac{1}{R\delta} = \frac{1}{l}$$

The lateral acceleration gain is:

$$\frac{V^2}{R\delta} = \frac{V^2}{l} \frac{1}{1 + K_{us} \frac{V^2}{gl}}$$

From geometrical considerations the vehicle sideslip angle is:

$$\beta = \frac{b}{R} - \alpha_2$$

So, the sideslip angle gain is:

$$\frac{\beta}{\delta} = \frac{b}{l} \left(1 - \frac{maV^2}{blC_2} \right) \frac{1}{1 + K_{us} \frac{V^2}{gl}}$$

2.3.4 High speed cornering

The previous model considered only cornering forces and steady state operation. A three degrees of freedom model that overcomes these limitations can be developed and to keep it simple the following assumptions are made:

- The sideslip angles of the vehicle and of the wheels are small. Also the yaw velocity $\dot{\psi}$ can be considered a small quantity.
- The vehicle is modelled as a rigid body on a flat surface: roll, pitch and vertical displacements due to suspensions are neglected.

Considering the inertial reference frame XY in Fig 2.20, the coordinates of the center of mass G and the yaw angle between x and X can be used as generalized coordinates:

$$\begin{cases} m\ddot{X} = F_X \\ m\ddot{Y} = F_Y \\ J_z\ddot{\psi} = M_z \end{cases}$$

Where F_X, F_Y and M_z are the total forces acting in X and Y directions and the total yaw moment in $z \equiv Z$.

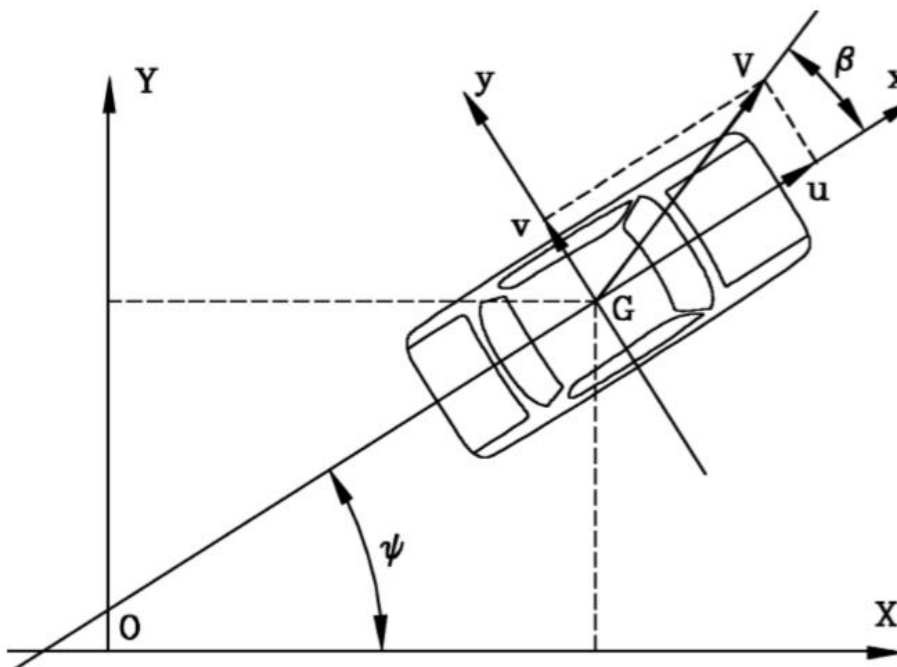


FIGURE 2.20 Reference frame to study of the motion of a rigid vehicle.

In order to obtain a linearized model is better to refer to the non-inertial frame of the vehicle xy avoiding dealing with the trigonometric functions of yaw angle that cannot be considered small and would prevent linearization.

Transposing to the non-inertial frame, the equations become:

$$\begin{cases} m(\dot{u} - rv) = F_X \\ m(\dot{v} + ru) = F_Y \\ J_z \dot{r} = M_z \end{cases}$$

Where r is the yaw speed $\dot{\psi}$ and u and v are the components of speed in x and y direction.

With a small vehicle sideslip, the velocities become:

$$\begin{cases} u = V \cos(\beta) \approx V \\ v = V \sin(\beta) \approx V\beta \end{cases}$$

Moreover rv is the product of two small quantities and can be neglected. V can be considered a known function of time, with the unknown of the longitudinal forces to follow a certain speed behaviour.

So the equations reduce in linear form in F_x , β and r :

$$\begin{cases} m\dot{V} = F_X \\ mV(\dot{\beta} + r) + m\dot{V}\beta = F_Y \\ J_z \dot{r} = M_z \end{cases}$$

Neglecting the interaction between longitudinal and lateral forces, the first equation can be uncoupled and the lateral behaviour can be studied on his own as a function of β and r .

The sideslip angles of the wheels can be expressed in terms of generalized velocities: referring to Fig 2.21, the velocity of the centre P_i of the contact area of the i th wheel is equal to:

$$\vec{V}_{P_i} = \vec{V}_G + r \wedge (\overline{P_i - G}) = \begin{cases} u - ry_i \\ v + rx_i \end{cases}$$

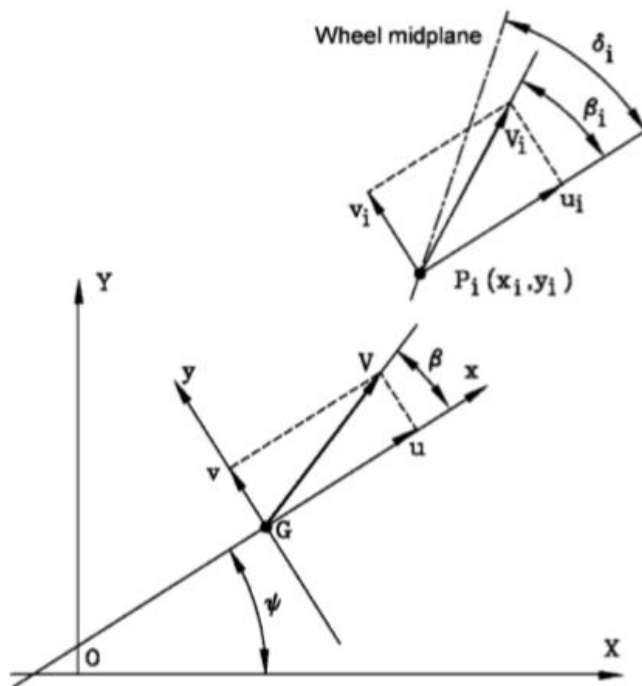


FIGURE 2.21 Position and velocity of the centre P_i of the contact area of the i -th wheel.

The angle β_i between x axis and the velocity of P_i can be calculated as:

$$\beta_i = \text{atan} \left(\frac{v_i}{u_i} \right) = \text{atan} \left(\frac{v + rx_i}{u - ry_i} \right) \approx \text{atan} \left(\frac{V\beta + rx_i}{V - ry_i} \right) \approx \left(\frac{V\beta + rx_i}{V - ry_i} \right)$$

Where the approximations hold for small angles. The sideslip of the wheel is equal to:

$$\alpha_i = \beta_i - \delta_i = \left(\frac{V\beta + rx_i}{V - ry_i} \right) - \delta_i \approx \left(\frac{V\beta + rx_i}{V} \right) - \delta_i \approx \beta + \frac{rx_i}{V} - \delta_i$$

Noting that the term ry_i is far smaller than V .

Thanks to these approximations y_i doesn't appear in the equation and the sideslip for the wheels of the same axle are equal. That allows to work in term of axles and consider a mono-track model.

The sideslip angles for front and rear axle in a front steering vehicle are:

$$\begin{cases} \alpha_1 = \beta + \frac{a}{V}r - \delta \\ \alpha_2 = \beta - \frac{b}{V}r \end{cases}$$

The total force in y direction is equal to:

$$F_y = \sum_{\forall i} F_{xi} \sin(\delta_i) + \sum_{\forall i} F_{yi} \cos(\delta_i) + \frac{1}{2} \rho V_r^2 SC_y + F_{ye}$$

Where F_{ye} takes in account external forces. The yaw moment is instead:

$$M_z = \sum_{\forall i} F_{xi} \sin(\delta_i) x_i + \sum_{\forall i} F_{yi} \cos(\delta_i) x_i + \sum_{\forall i} M_{zi} + \frac{1}{2} \rho V_r^2 SC_{Mz} + M_{ze}$$

Where with M_{zi} are defined the self-aligning moments of the wheels while M_{ze} takes in account external moments.

Linearizing, the equation of lateral force become:

$$F_y = \sum_{\forall i} F_{yi} + \frac{1}{2} \rho V_r^2 SC_y + F_{ye}$$

Cornering forces can be written as a linear function of the sideslip angle, considering the cornering stiffness of the axle:

$$F_{yi} = -C_i \alpha_i = -C_i \left(\beta + \frac{rx_i}{V} - \delta_i \right)$$

With small sideslip also aerodynamic force has a linear behaviour and depends on β , so the aerodynamic coefficient can be written as:

$$C_y = (C_y)_\beta \beta$$

Finally, the expression of lateral force can be reduced to the linear equation:

$$F_y = Y_\beta \beta + Y_r r + Y_\delta \delta + F_{ye}$$

Where:

$$Y_\beta = - \sum_{\forall i} C_i + \frac{1}{2} \rho V_r^2 S (C_y)_\beta$$

$$Y_r = - \frac{1}{V} \sum_{\forall i} x_i C_i$$

$$Y_\delta = \sum_{\forall i} C_i$$

In the same way also the yaw moment can be linearized:

$$M_z = N_\beta \beta + N_r r + N_\delta \delta + M_{ye}$$

Introducing the self-aligning moment stiffness $(M_{zi})_\alpha$ and the aerodynamic moment coefficient as $C_{Mz} = (C_{Mz})_\beta \beta$.

The terms appearing in the equation are equal to:

$$N_\beta = - \sum_{\forall i} [-x_i C_i + (M_{zi})_\alpha] + \frac{1}{2} \rho V_r^2 S (C_y)_\beta$$

$$N_r = - \frac{1}{V} \sum_{\forall i} [-x_i^2 C_i + (M_{zi})_\alpha x_i]$$

$$N_\delta = \sum_{\forall i} [x_i C_i + (M_{zi})_\alpha]$$

$Y_\beta, Y_r, Y_\delta, N_\beta, N_r$ and N_δ are called derivatives of stability.

The final expression of the equations of motion is then:

$$\begin{cases} mV(\dot{\beta} + r) + m\dot{V}\beta = Y_\beta \beta + Y_r r + Y_\delta \delta + F_{ye} \\ J_z \dot{r} = N_\beta \beta + N_r r + N_\delta \delta + M_{ye} \end{cases}$$

The two equations are first order differential equations for the two unknown β and r , while δ can be considered as an input and the external forces and moments disturbances.

The curvature gain for this model in steady state is equal to:

$$\frac{1}{R\delta} = \frac{Y_\delta N_\beta - N_\delta Y_\beta}{V[N_\beta(mV - Y_r) + N_r Y_\beta]}$$

The acceleration gain:

$$\frac{V^2}{R\delta} = \frac{V[Y_\delta N_\beta - N_\delta Y_\beta]}{N_\beta(mV - Y_r) + N_r Y_\beta}$$

The sideslip gain:

$$\frac{\beta}{\delta} = \frac{-N_{\delta}(mV - Y_r) - N_r Y_{\delta}}{N_{\beta}(mV - Y_r) + N_r Y_{\beta}}$$

Also a yaw velocity gain can be introduced:

$$\frac{r}{\delta} = \frac{Y_{\delta} N_{\beta} - N_{\delta} Y_{\beta}}{N_{\beta}(mV - Y_r) + N_r Y_{\beta}}$$

2.3.5 Definition of understeer and oversteer

A *neutral steer* vehicle has at any speed a response to a steering input that is constant and equal to that in kinematic conditions (Fig 2.22a). This condition occurs for $K_{us} = 0$ and doesn't mean however that the vehicle actually steers kinematically, being the sideslip of the wheels different from 0 and β different to the kinematic value.

If $K_{us} > 0$ the curvature gain decreases increasing the speed of the vehicle, the response is smaller than in kinematic conditions and to maintain constant the radius of the path the driver has to increase the steering angle at higher speeds. A vehicle behaving this way is said *understeer*.

If $K_{us} < 0$ the curvature gain increases with the speed until it diverges at a *critical speed* and the system becomes unstable.

$$V_{cr} = \sqrt{\frac{gl}{K_{us}}}$$

A vehicle behaving this way is said to be *oversteer*.

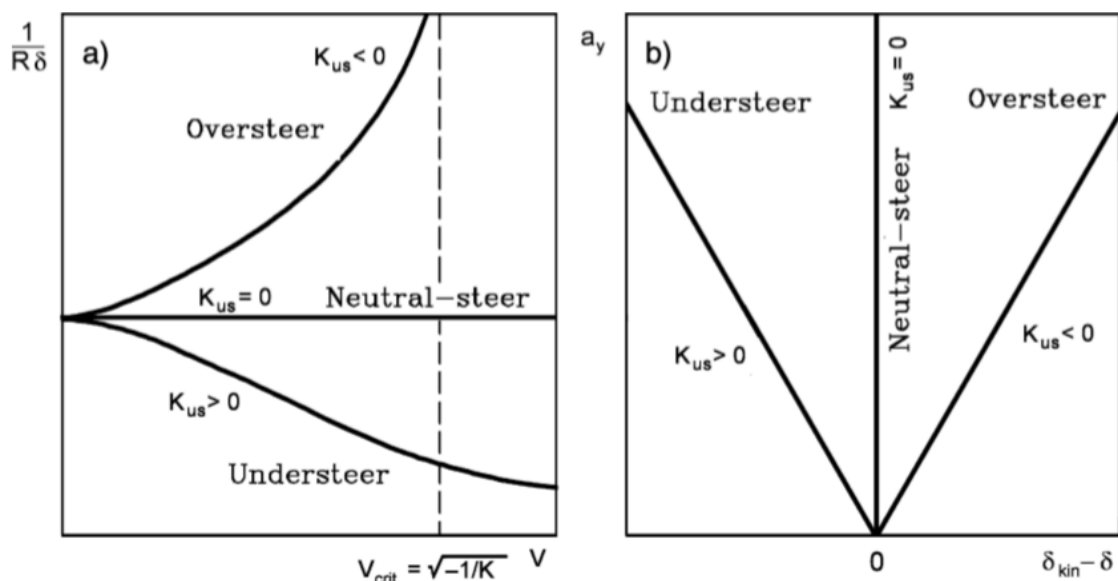


FIGURE 2.22 Steady state response to a steering input. Path curvature gain as a function of speed (a) and handling diagram (b) for an oversteer, an understeer and a neutral steer vehicle.

The plot in Fig.2.22 b is the *handling diagram* where the lateral acceleration is plotted in function of $\delta_{kin} - \delta$

Another definition can come from sideslip angles: referring to Fig 2.23, when the speed tends to 0, the vehicle steers kinematically and the centre of curvature is O ; the sideslip angles in this condition vanish. At higher speed the wheels work with sideslip angles: in neutral steer $\alpha_1 = \alpha_2$, the angle $BO'A$ is equal to $\delta - \alpha_1 + \alpha_2 = \delta$ as in kinematic conditions and the radius is equal to the kinematic one; the centre of curvature however moves to O' . Understeer vehicles corner with $|\alpha_1| > |\alpha_2|$, the radius R'' is bigger than the kinematic one and the path centre is O'' . Oversteer vehicles finally work with $|\alpha_1| < |\alpha_2|$, the center is O''' and the radius R''' is smaller.

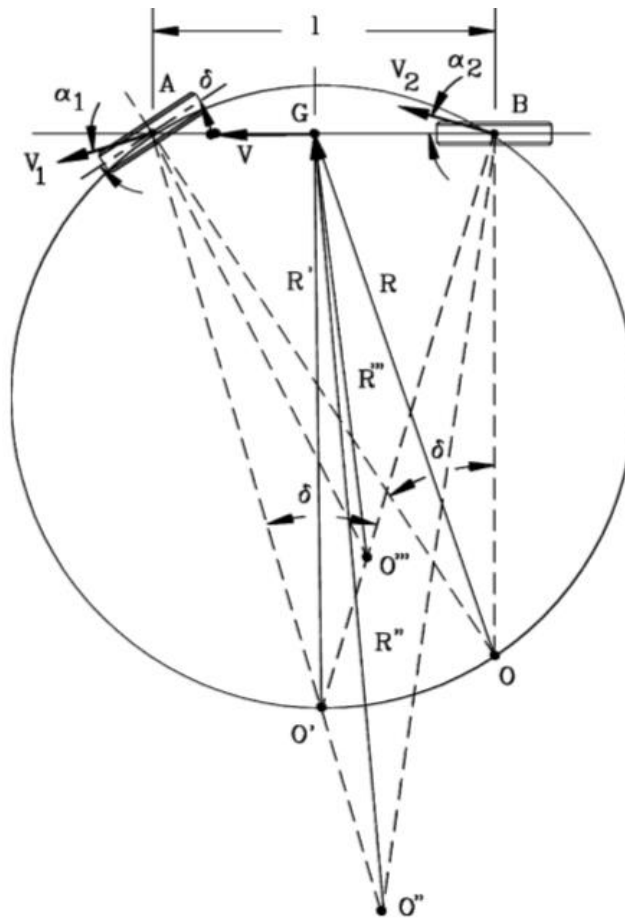


FIGURE 2.23 Geometrical definition of steering behaviour of a single axle steering vehicle.

Considering the derivatives of stability, the dependence on V of the curvature gain is no more monotonic, and the behaviour can change from oversteer to understeer or vice-versa throughout the speed range (Fig 2.24).

Instead to refer to the condition:

$$\frac{1}{R\delta} = \frac{1}{l}$$

Neutral steer can be defined by an incremental definition:

$$\frac{d}{dV} \left(\frac{1}{R\delta} \right) = 0$$

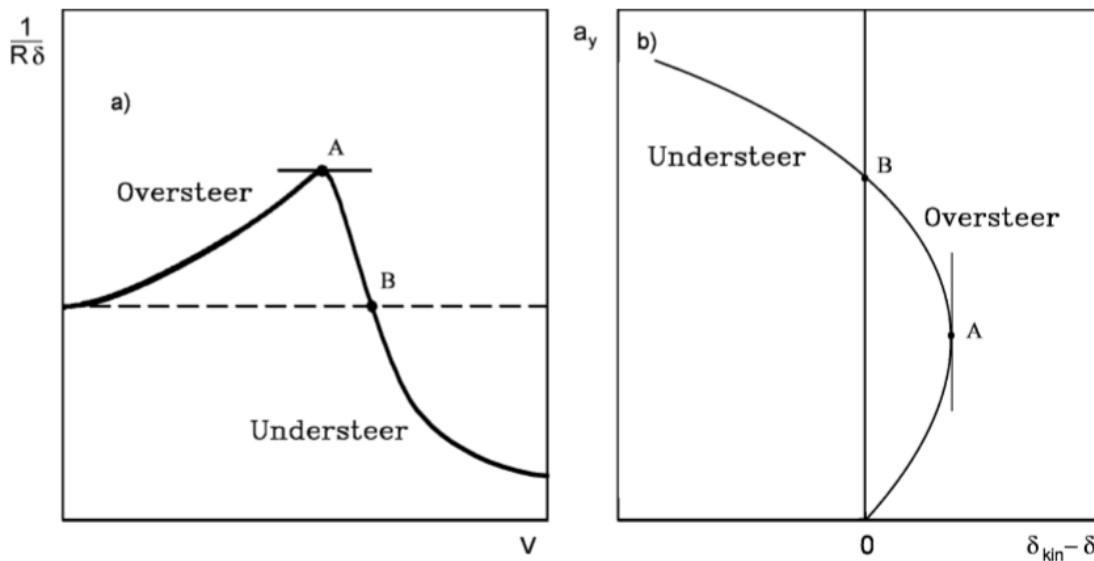


FIGURE 2.24 Steady state response to a steering input. Plot of the path curvature gain as a function of speed (a) and handling diagram (b) for a vehicle that at low speed is oversteer and then becomes understeer at high speed

Referring to Fig 2.24, according to the absolute definition, the condition of neutral steer is on point *B*, while according to the incremental is on point *A*.

So the incremental definition of understeer is for:

$$\frac{d}{dV} \left(\frac{1}{R\delta} \right) < 0$$

While oversteer occurs for:

$$\frac{d}{dV} \left(\frac{1}{R\delta} \right) > 0$$

The incremental definition suits better the sensation of the driver, that obviously doesn't know the value of the kinematic radius but can sense the variation of the curvature path increasing the speed.

A typical condition of understeer is when front wheels lose grip and front tires cannot exploit lateral forces, the grip can be however restored braking or releasing the accelerator pedal as the deceleration implies a load transfer on the front axle. For this reason, most passenger cars are designed to have an understeer behaviour. Oversteer instead, cause instability and can lead to spin out. A corrective manoeuvre would imply correct regulation of the accelerator and a counter-steer action.

3 The effect of inflation pressure on tire performance

Pacejka MF-5.2 parameters for three different tires at different levels of pressure were provided by Michelin:

| Destination of use | Designation | Pressure levels | | | |
|--------------------------|-------------|-----------------|---------|----------|-------|
| | | 1,8 bar | 2,2 bar | 2,6 bar | |
| Passenger Car | 185/65 R 15 | 1,8 bar | 2,2 bar | 2,6 bar | |
| Light Commercial Vehicle | 225/65 R 16 | 3,5 bar | 4 bar | 4,75 bar | |
| Light Commercial Vehicle | 195/75 R 16 | 3,5 bar | 4 bar | 4,5 bar | 5 bar |

TABLE 3.1 Tire models provided by Michelin (The nominal pressure for each tire is highlighted in red).

The first tire was used in the simulations on a Fiat Grande Punto 1.3 MultiJet 75 cv, the other two on an Iveco Daily MY2014. Thanks to the magic formula the characteristics of force and moments for the different inflation pressures and in different load conditions were plotted.

3.1 Tire 185/65 R 15

Two load conditions are considered for the Punto, one with only the driver (1352 kg) and one in full load (1762 kg). On the experimental tests held in Balocco the static loads on each wheel were the following:

| Total Load | Front Left Tire | Front Right Tire | Rear Left Tire | Rear Right Tire |
|------------|-----------------|------------------|----------------|-----------------|
| 1351.6 kg | 431 kg | 422 kg | 253.6 kg | 245 kg |
| 1762 kg | 433 kg | 420.5 kg | 457 kg | 451.5 kg |

TABLE 3.2 Distribution on the wheels for the two load conditions examined (Grande Punto)

The loads chosen in the plots are the lowest (253.6 kg = 2488 N) and the highest (457 kg = 4483 N).

3.1.1 Longitudinal analysis

In Fig. 3.1 the longitudinal adherence is plotted against the slip rate for the three levels of pressure: the low load condition is plotted in full lines, the high load in dashed lines.

The maximum adherence occurs at 1,8 bar, then decreases non-linearly for higher inflation pressures; increasing the load instead the adherence decrease, especially for higher levels of slip. The effect on the peak adherence is examined in Fig 3.2.

The longitudinal slip stiffness is unaffected by pressure as can be seen in detail in Fig 3.3; it's instead greater for the high load condition: that means that the adherence has a greater slope and reach higher values for low values of slip compared to the minimum load condition.

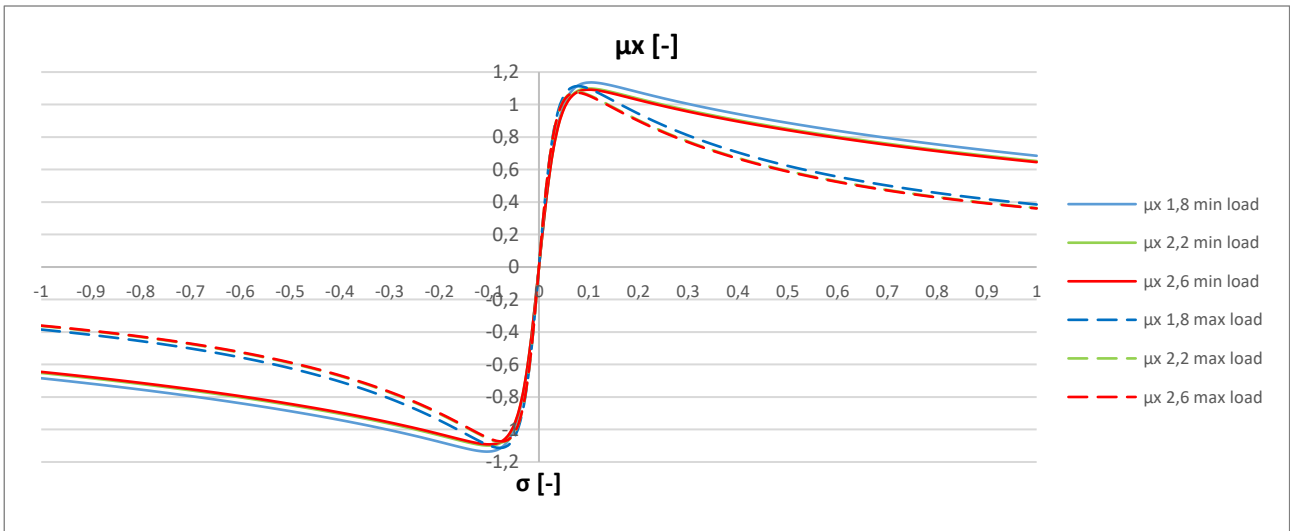


FIGURE 3.1 Longitudinal adherence in function of slip for different levels of pressure and load (Tire 185/65 R 15)

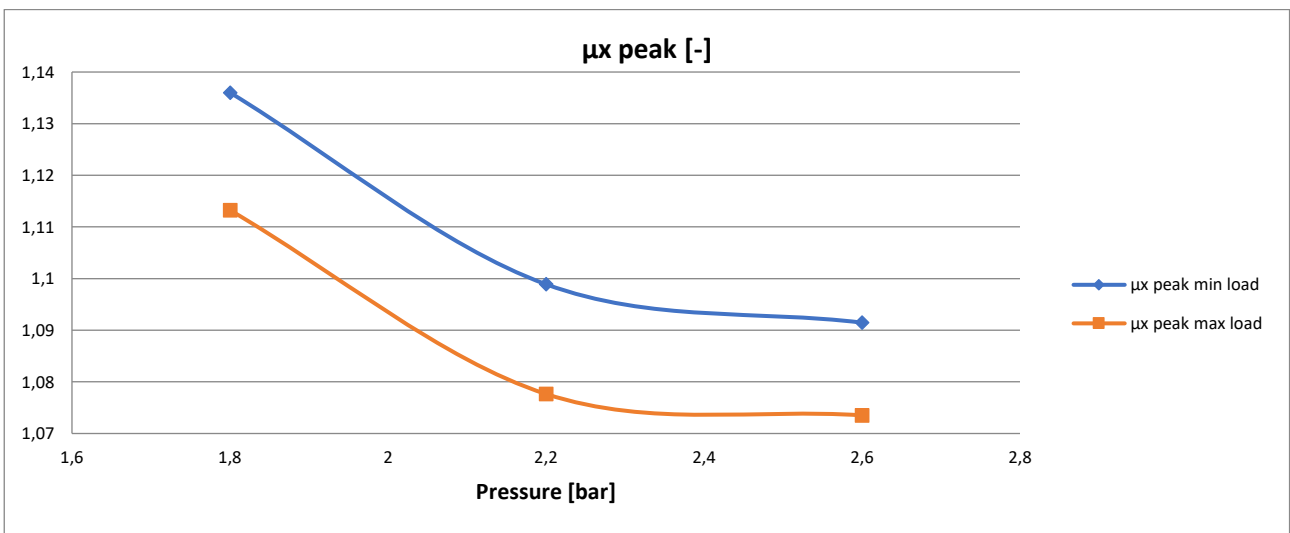


FIGURE 3.2 Effect of pressure and load on the peak value of adherence (Tire 185/65 R 15).

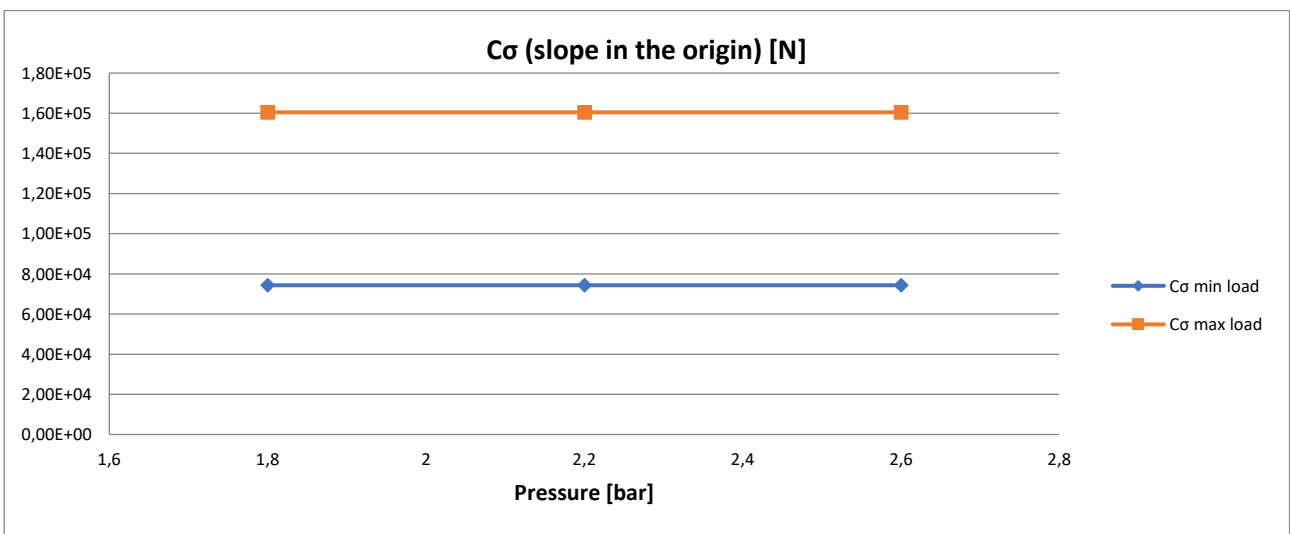


FIGURE 3.3 Effect of pressure and load on longitudinal slip stiffness (Tire 185/65 R 15).

3.1.2 Lateral analysis

Also lateral adherence is bigger for lower levels of pressure and lower load (Fig 3.4), the effect of inflation pressure on the peak lateral adherence is more linear compared to the longitudinal (Fig 3.5).

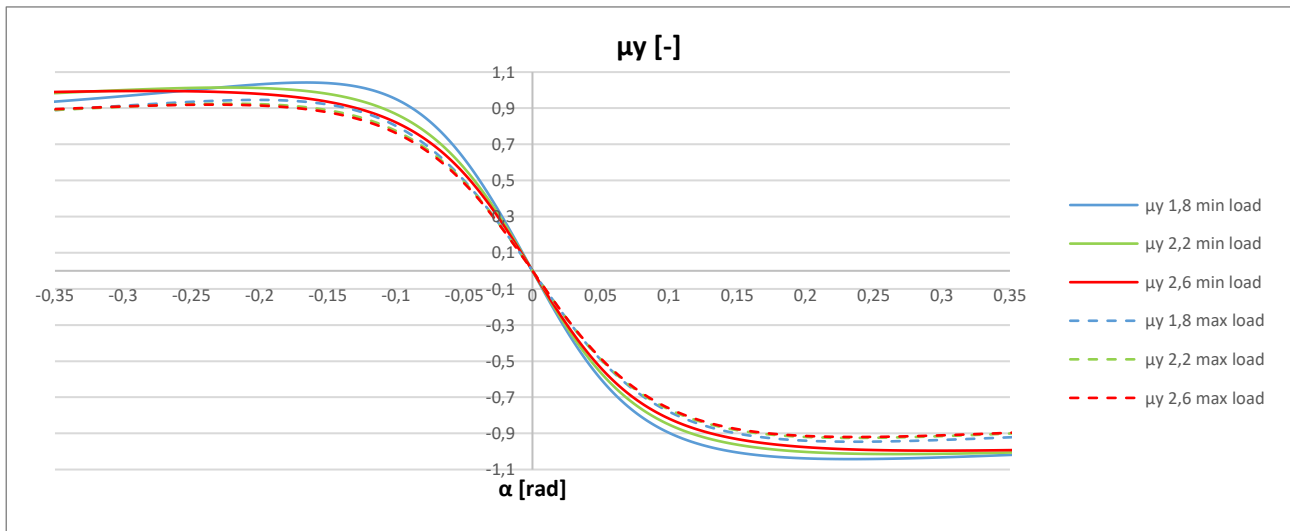


FIGURE 3.4 Lateral adherence in function of sideslip for different levels of pressure and load (Tire 185/65 R 15).

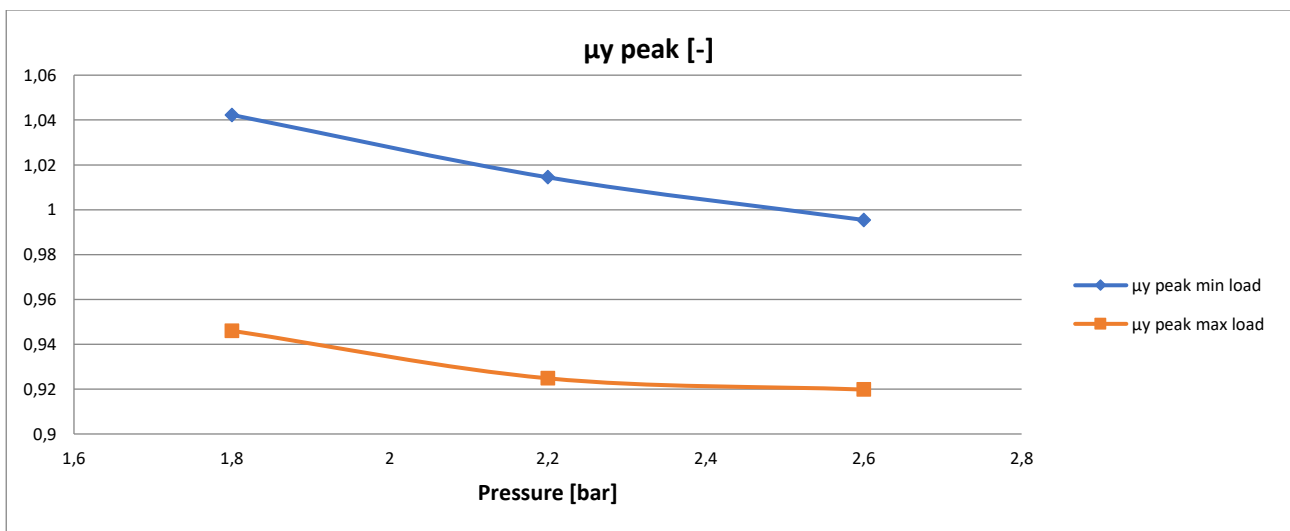


FIGURE 3.5 Effect of pressure and load on peak lateral adherence (Tire 185/65 R 15)

The absolute value of cornering stiffness decreases increasing inflation pressure for the low load condition, while is almost constant in the maximum load condition (Fig 3.6). This behaviour is justified by the effect of load on cornering stiffness: as it can be seen from figure 3.7 for low loads the cornering stiffness grows linearly and it's bigger for low inflation pressure until point A (near the maximum load condition), then the cornering stiffness for higher pressures continues to grow, becoming bigger than the ones for lower pressure, that reach a saturation.

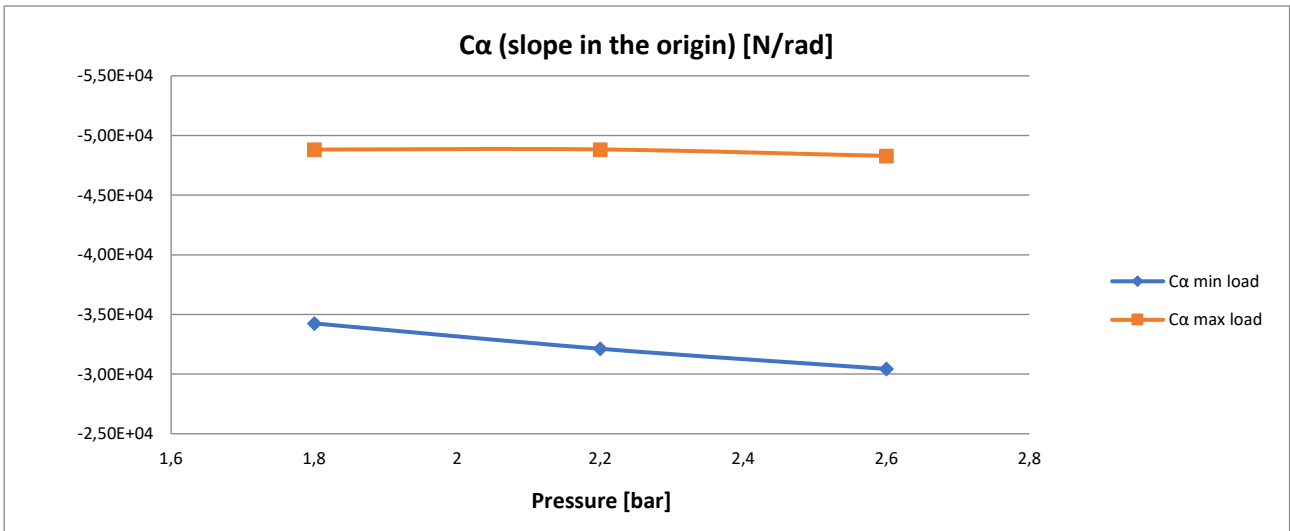


FIGURE 3.6 Cornering stiffness in function of pressure for the two load conditions (Tire 185/65 R 15)

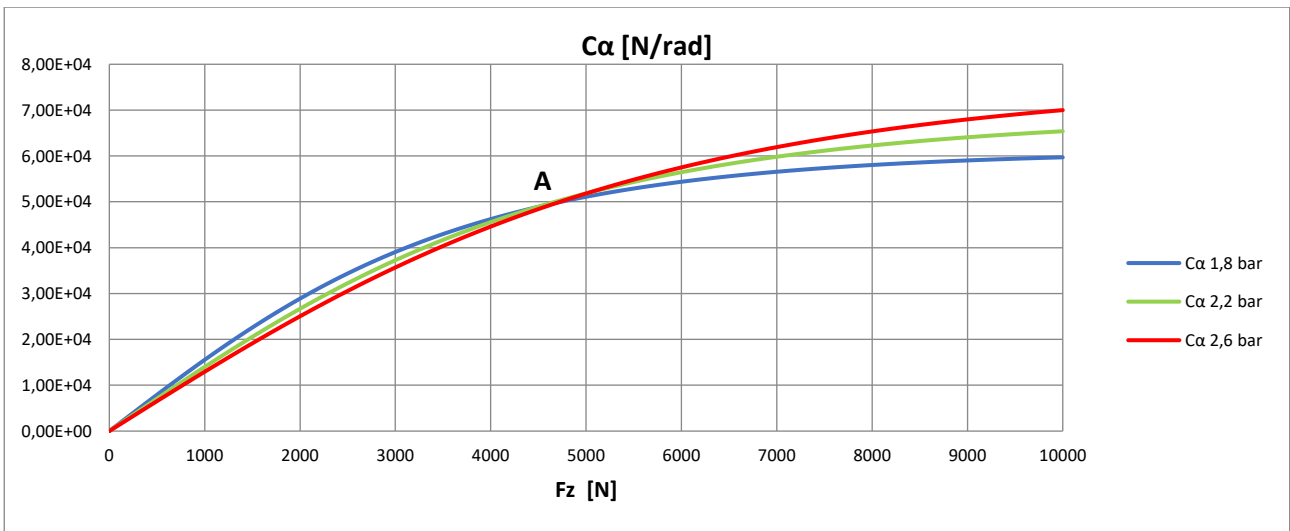


FIGURE 3.7 Effect of pressure and load on cornering stiffness (Tire 185/65 R 15)

So, for low loads, recalling the influence of cornering stiffness on the understeer coefficient, a pressure increase on front tires would make the vehicle more understeer and a pressure increase on rear tires would make it more understeer. The effect instead become opposite for loads bigger than the ones corresponding to point A (that are actually reached in dynamic conditions). The effect is obviously bigger in vehicles subjected to great load changes like trucks and buses as it was experimentally observed by Fancher P.S. in [13] and M K Al-Solihat, S Rakheja, and A K W Ahmed in [14] . This behaviour is again confirmed in the study of the tires used on the light commercial vehicle Iveco Daily and on its very simulations with ADAMS car.

3.1.3 Self aligning moment

The self-aligning moment decrease increasing the inflation pressure and increase increasing the load (Fig 3.8). The aligning moment stiffness decrease too with pressure almost linearly and it's bigger for the maximum load condition (Fig 3.9).

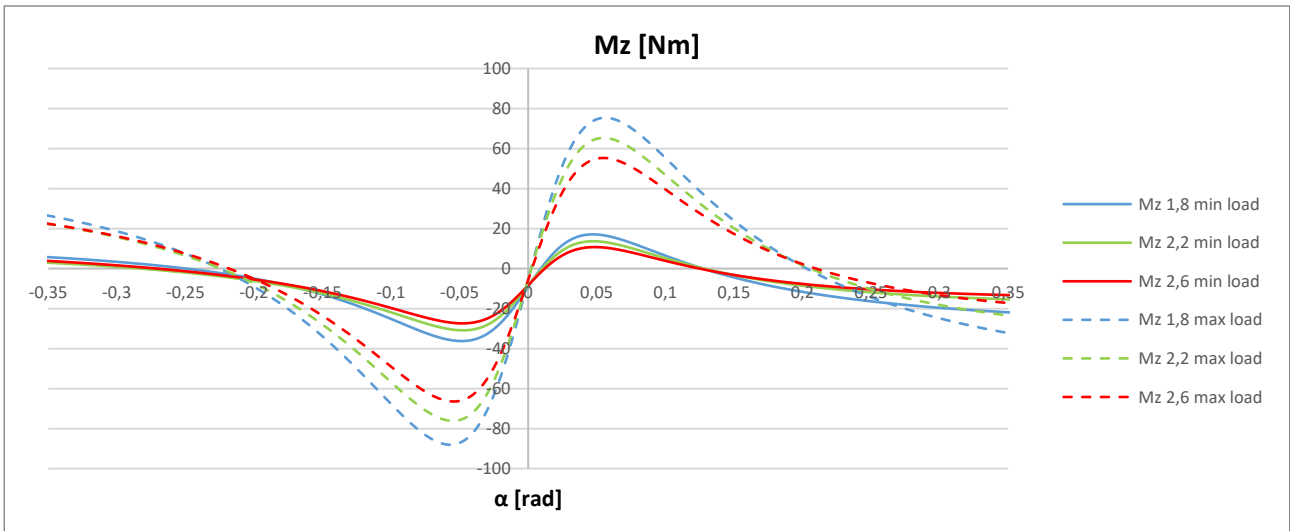


FIGURE 3.8 Self-aligning-moment in function of sideslip for different values of inflation pressure and load (Tire 185/65 R 15)

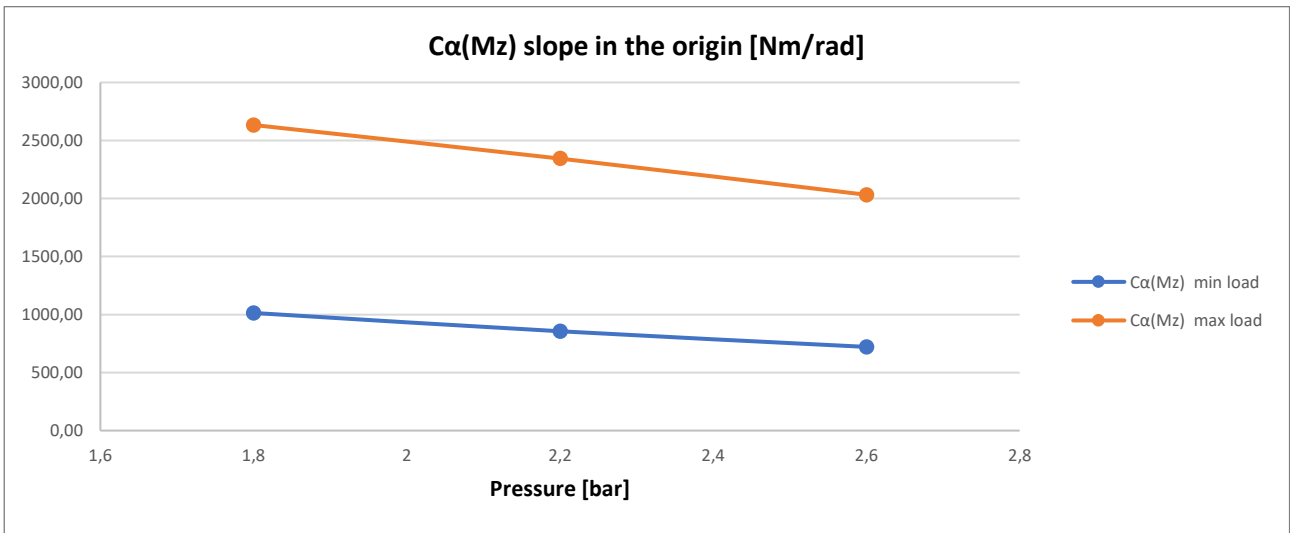


FIGURE 3.9 Effect of pressure and load on self-aligning moment stiffness (Tire 185/65 R 15)

3.1.4 Summary table of the results

In Table 3.3 the percentage variation of the main tire parameters from the nominal pressure condition is summarized.

| Load | $F_z = 2488 \text{ N}$ | | | $F_z = 4483 \text{ N}$ | | |
|----------------|------------------------|-------------------|----------|------------------------|-------------------|----------|
| | -0,4 bar | 2,2 bar (Nominal) | +0,4 bar | -0,4 bar | 2,2 bar (Nominal) | +0,4 bar |
| μ_{xp} | +3,38% | 1,10 | -0,69% | +3,30% | 1,08 | -0,39% |
| C_σ | +0% | 7,43E+04 N | +0% | +0% | 1,6E+05 N | +0% |
| μ_{yp} | +2,74% | 1,01 | -1,87% | +2,29% | 0,92 | -0,54% |
| C_α | +6,61% | 3,21E+04 N/rad | -5,26% | -0,02% | 4,88E+04 N/rad | -1,11% |
| M_{zMax} | +25,23% | 13,65 Nm | -21,37% | +15,44% | 65,29 Nm | -15,33% |
| $C_{Mz\alpha}$ | +18,41% | 856 Nm/rad | -15,74% | +12,34% | 2344 Nm/rad | -13,32% |

TABLE 3.3 Effect of inflation pressure on main tire parameters for two load conditions (Tire 185/65 R 15)

3.2 Tire 225/65 R 16

The vehicle was tested as unladen (2363 kg) and in full load (3500 kg). In the former condition the load is distributed at 56% on the front, in the latter at the 43%. The vertical forces on the wheels for the two conditions are computed in table 3.4.

| Total Load | Load on front axle (per wheel) | Load on rear axle (per wheel) |
|------------|--------------------------------|-------------------------------|
| 2363 kg | 6500 N | 5000 N |
| 3500 kg | 7360 N | 9770 N |

TABLE 3.4 Distribution on the wheels for the two load conditions examined (Iveco Daily)

The MF parameters of the tire are available for three levels of pressure (3,5, 4 , 4,75 bar) and again the lowest (5000 N) and the highest (9770 N) load are considered in the plots.

3.2.1 Longitudinal analysis

In Fig. 3.10 the longitudinal adherence is plotted in function of the slip. The effect of pressure is different for unladen and full loaded vehicle: in the former case the adherence grows almost linearly increasing pressure, in the latter the opposite occurs. In Fig. 3.11 the effect on peak adherence is plotted.

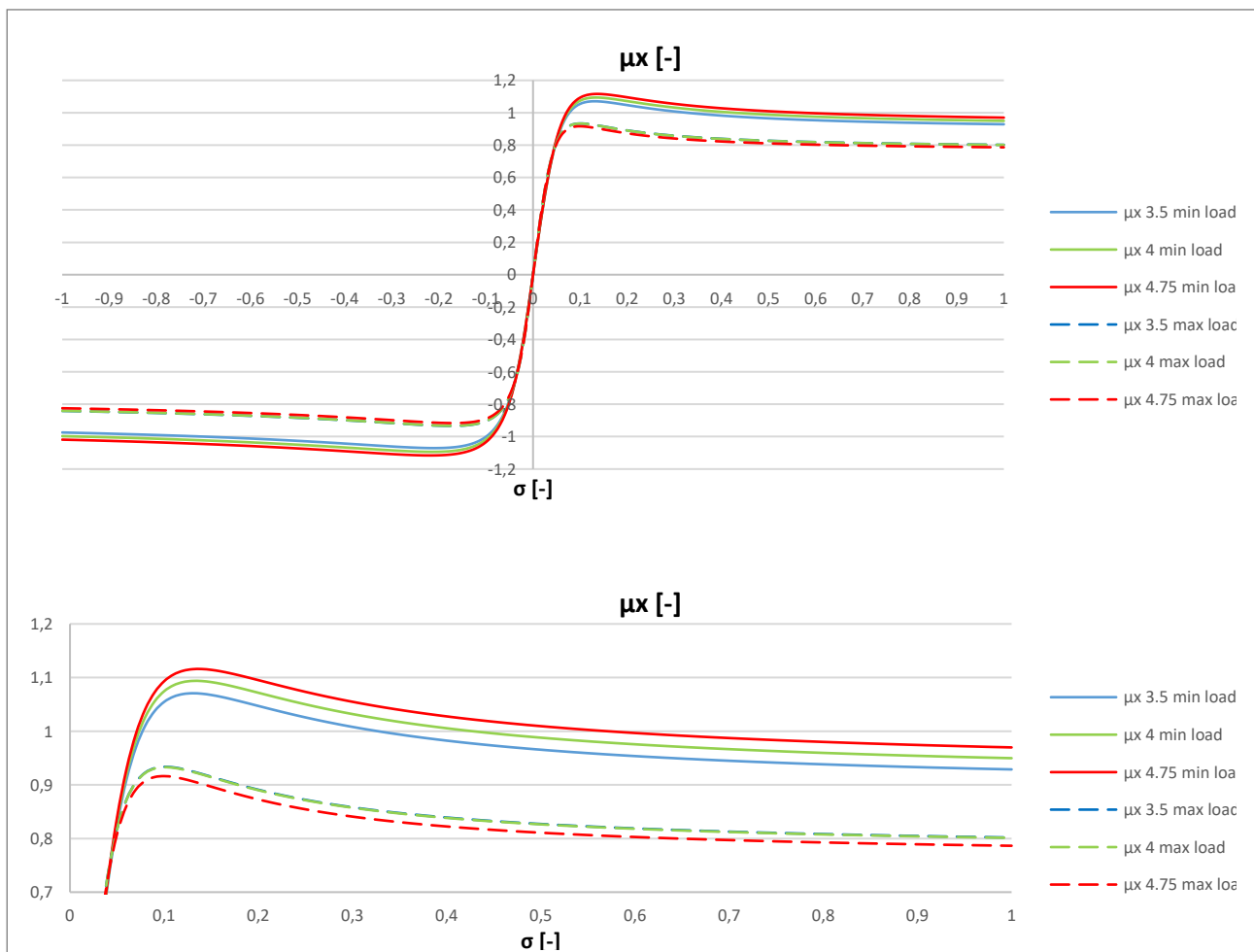


FIGURE 3.10 Longitudinal adherence in function of slip for different levels of pressure and load (Tire 225/65 R 16)

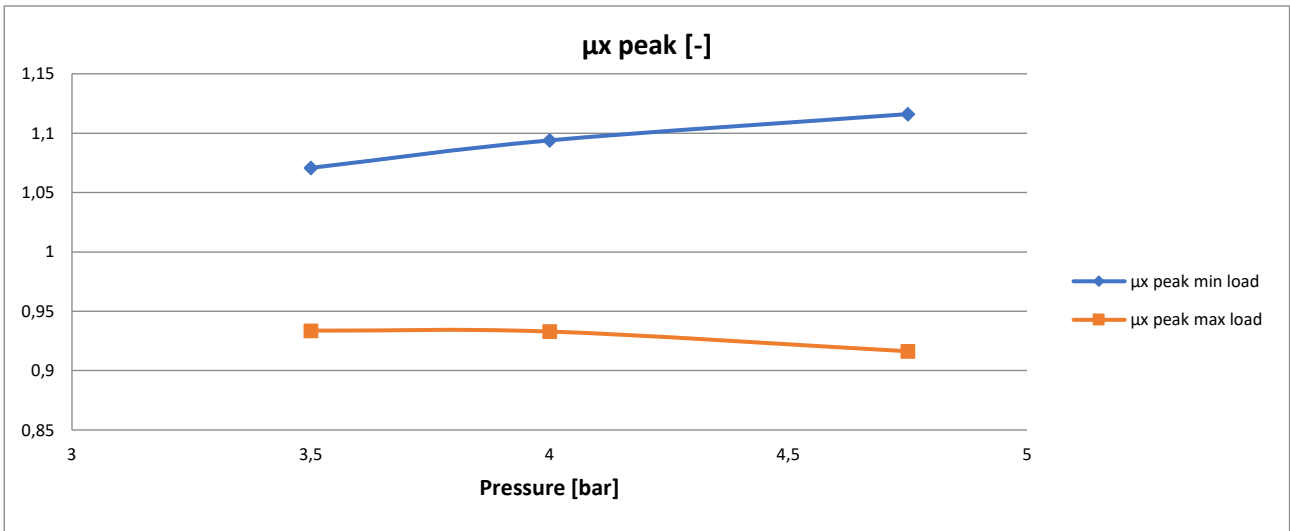


FIGURE 3.11 Effect of pressure and load on peak longitudinal adherence (Tire 225/65 R 16)

The longitudinal slip stiffness remains instead constant changing the pressure and it's higher for the fully loaded vehicle (Fig 3.12).

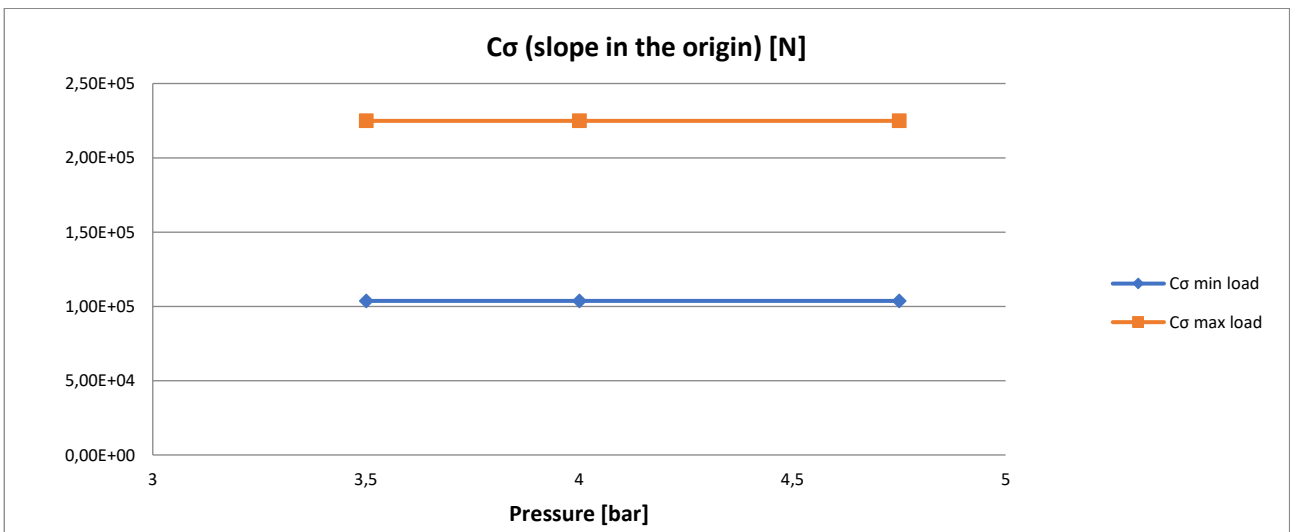


FIGURE 3.12 Effect of pressure and load on longitudinal slip stiffness (Tire 225/65 R 16)

3.2.2 Lateral analysis

The lateral adherence is at first bigger at lower pressure, having a greater slope, however the curve for 4,75 bar reaches a higher peak, while the one for 3,5 bar start decreasing for higher levels of slip (Fig 3.13). On Fig 3.14 is plotted the peak lateral adherence, the effect of pressure is important, especially at unladen vehicle where the gain in adherence is more than 11% bigger increasing the pressure at 4,75 bar from the nominal one. On Figure 3.15 Instead is plotted the effect on cornering stiffness.

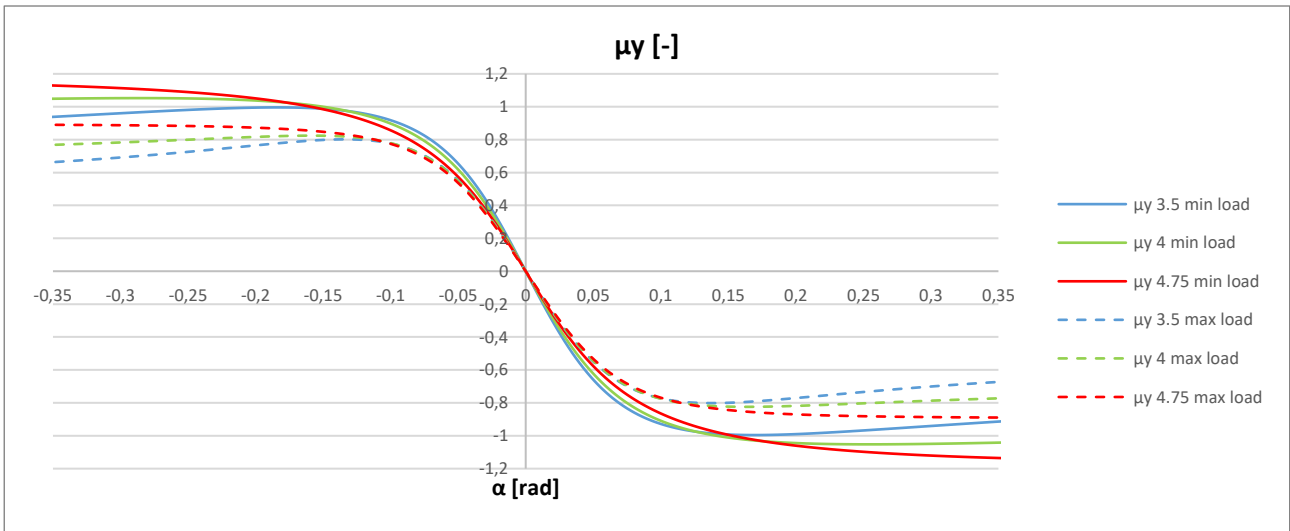


FIGURE 3.13 Lateral adherence in function of sideslip angle for different levels of pressure and load (Tire 225/65 R 16)

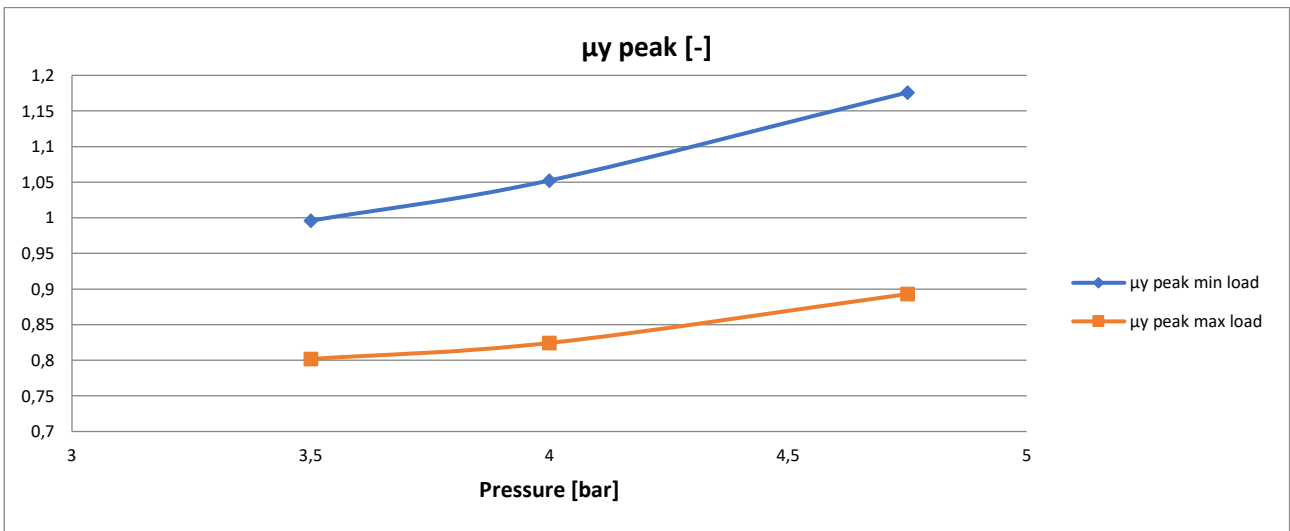


FIGURE 3.14 Effect of pressure and load on peak lateral adherence (Tire 225/65 R 16)

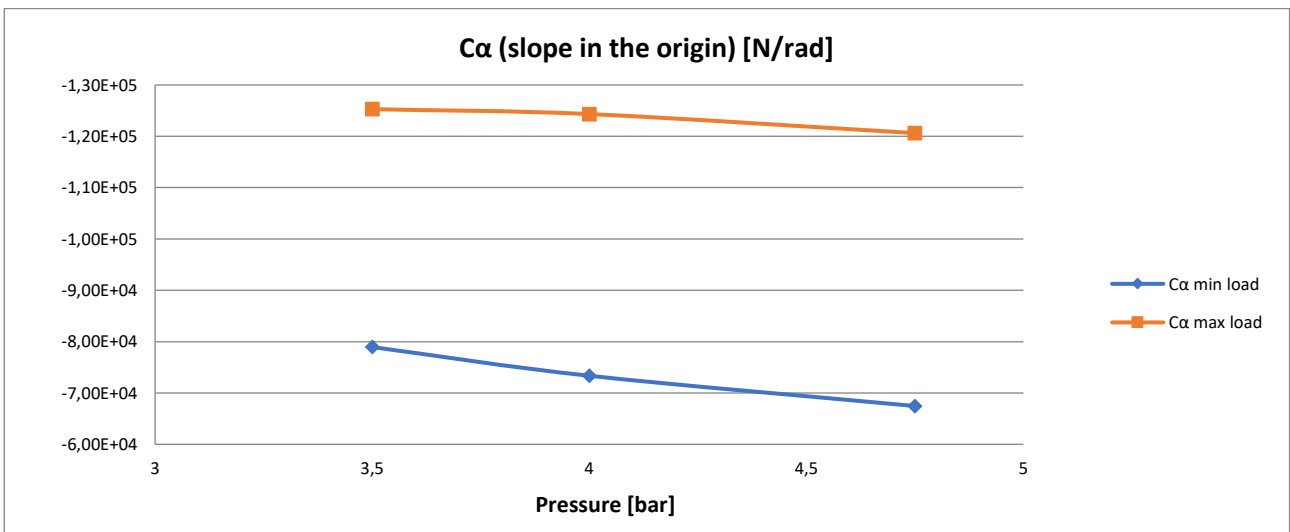


FIGURE 3.15 Effect of pressure and load on cornering stiffness (Tire 225/65 R 16)

For the static loads here considered the cornering stiffness decrease increasing inflation pressure in both load conditions (Fig 3.15), the variation is bigger at unladen vehicle. The “cross point” after which the trend becomes opposite occurs in fact after 11000 N of vertical load (Fig 3.16). This loads are however reached in dynamic condition for the fully loaded vehicle due to the inertia load transfer.

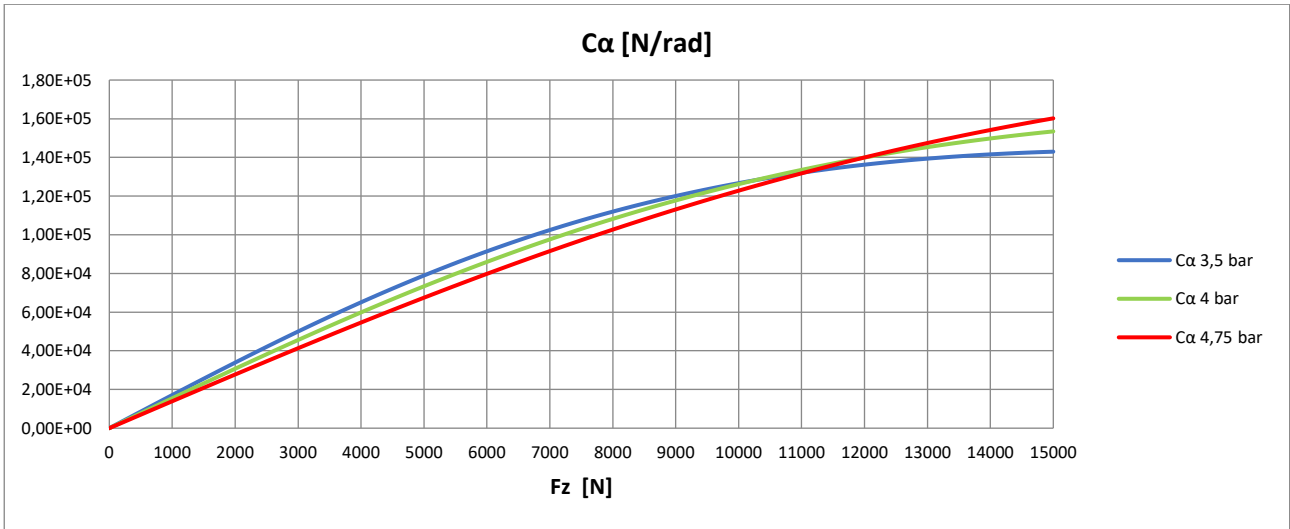


FIGURE 3.16 Effect of pressure and load on cornering stiffness (Tire 225/65 R 16)

3.2.3 Self aligning moment

A lower pressure results in a higher self-aligning moment in both load conditions (Fig 3.17). Also the stiffness increase decreasing pressure, the trend is almost linear (Fig 3.18). The moment changes its sign at approximately the same value of sideslip for all inflation pressures, however at 3,5 bar the moment remains low for high levels of sideslip.

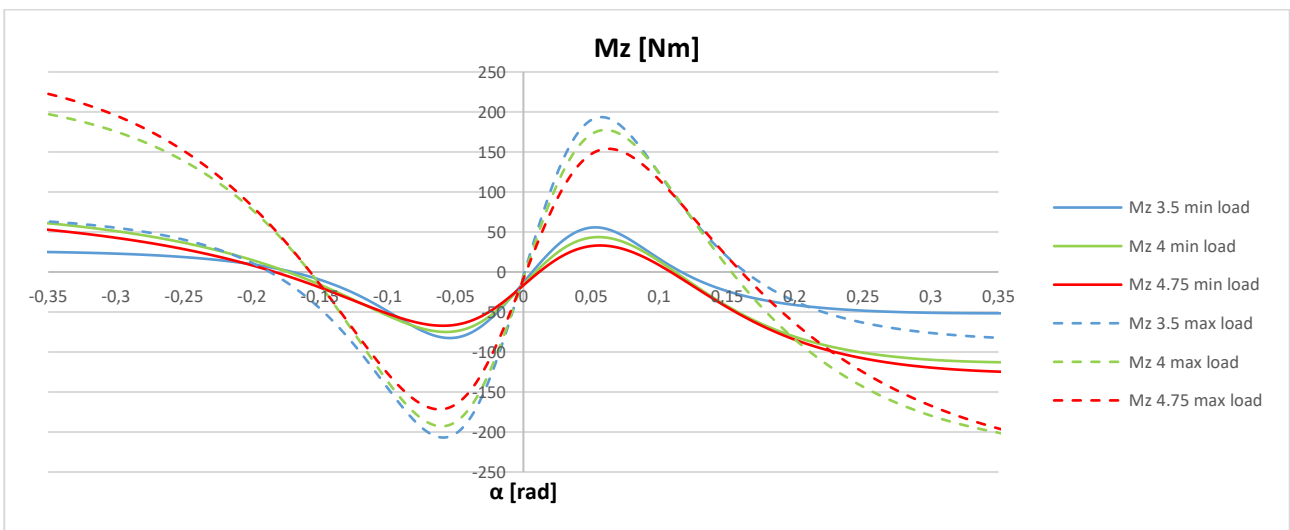


FIGURE 3.17 Self aligning-moment in function of sideslip for different values of inflation pressure and load (Tire 225/65 R 16)

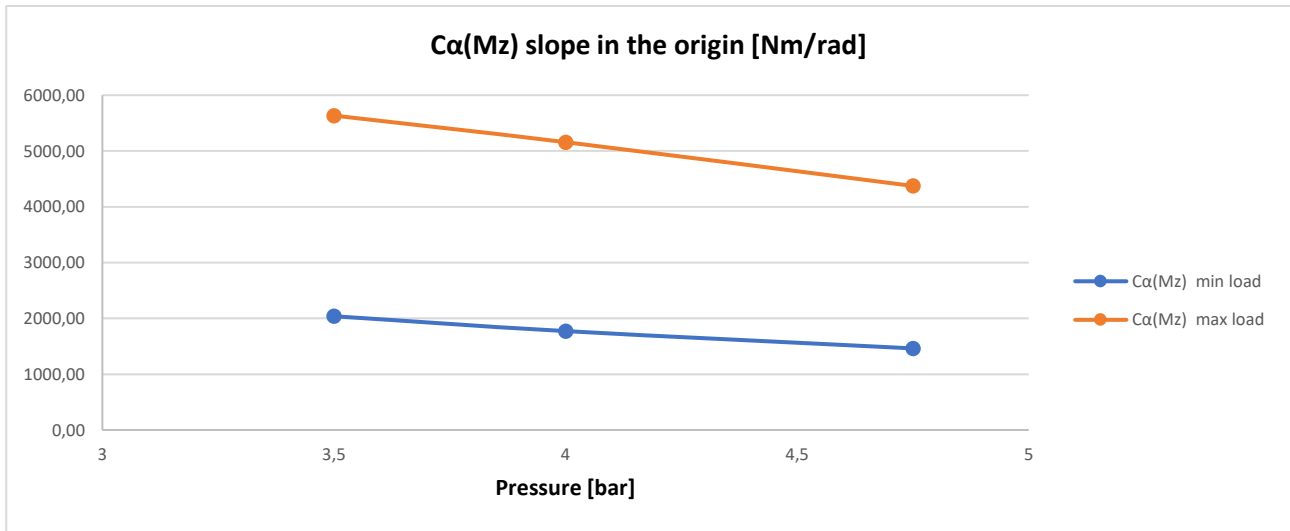


FIGURE 3.18 Effect of pressure and load on self-aligning moment stiffness (Tire 185/65 R 15)

3.2.4 Summary table of the results

In Table 3.5 the percentage variation of the main tire parameters from the nominal pressure condition is summarized.

| Load | $F_z = 5000\text{ N}$ | | | $F_z = 9770\text{ N}$ | | |
|----------------|-----------------------|-----------------|-----------|-----------------------|-----------------|-----------|
| | -0,5 bar | 4 bar (Nominal) | +0,75 bar | -0,5 bar | 4 bar (Nominal) | +0,75 bar |
| μ_{xp} | -2,12% | 1,09 | +2,03% | +0,08% | 0,93 | -1,78% |
| C_σ | +0% | 1,04E+05 N | +0% | +0% | 2,25E+05 N | +0% |
| μ_{yp} | -5,36% | 1,05 | +11,74% | -2,74% | 0,82 | +8,33% |
| C_α | +7,62% | 7,34E+04 N/rad | -8,04% | +7,68% | 1,24E+05 N/rad | -2,97% |
| M_{zMax} | +27,81% | 43,60 Nm | -24,07% | +9,05% | 177,51 Nm | -13,27% |
| $C_{Mz\alpha}$ | +15,02% | 1772 Nm/rad | -17,52% | +9,24% | 5158 Nm/rad | -15,21% |

TABLE 3.5 Effect of inflation pressure on main tire parameters for two load conditions (Tire 225/65 R 16)

3.3 Tire 195/75 R 16

This second tire was also used in the Iveco Daily simulations, the vertical loads considered are the same as before (5000 N and 9770 N) but data for four levels of pressure are available: 3.5, 4, 4.5 and 5 bar.

3.3.1 Longitudinal analysis

When the vehicle is unladen the adherence grows with pressure until 4,5 bar, then at 5 bar it decreases. In the full loaded condition instead the effect of pressure is minimum, a small decrease in adherence increasing inflation pressure is registered (Fig 3.19). In Fig 3.20 is plotted the effect on the peak adherence value.

The slope shows not change with pressure and it's higher at higher load (Fig 3.21) the values are almost the same of the tire 225/65 R16.

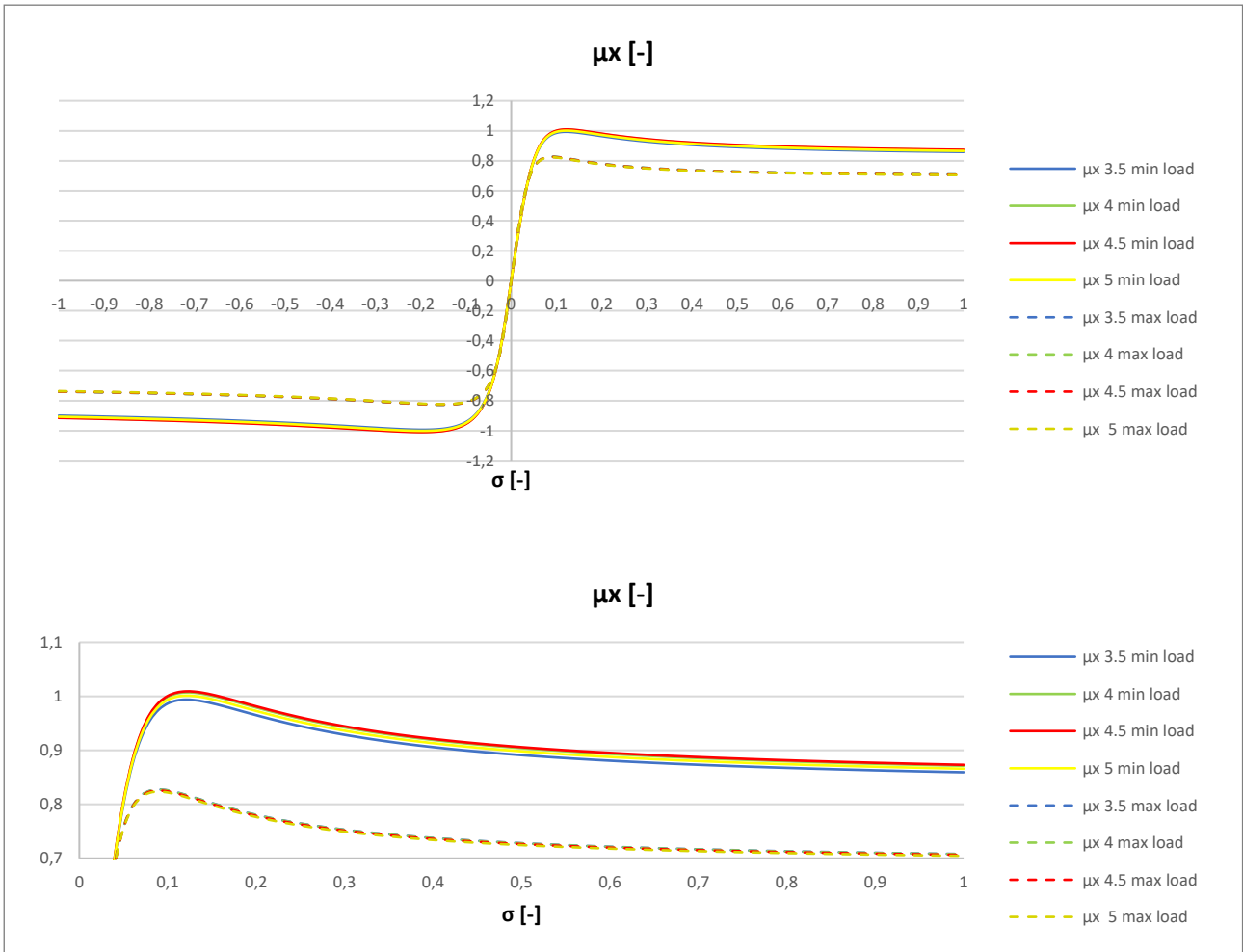


FIGURE 3.19 Longitudinal adherence in function of slip for different levels of pressure and load (Tire 195/75 R 16)

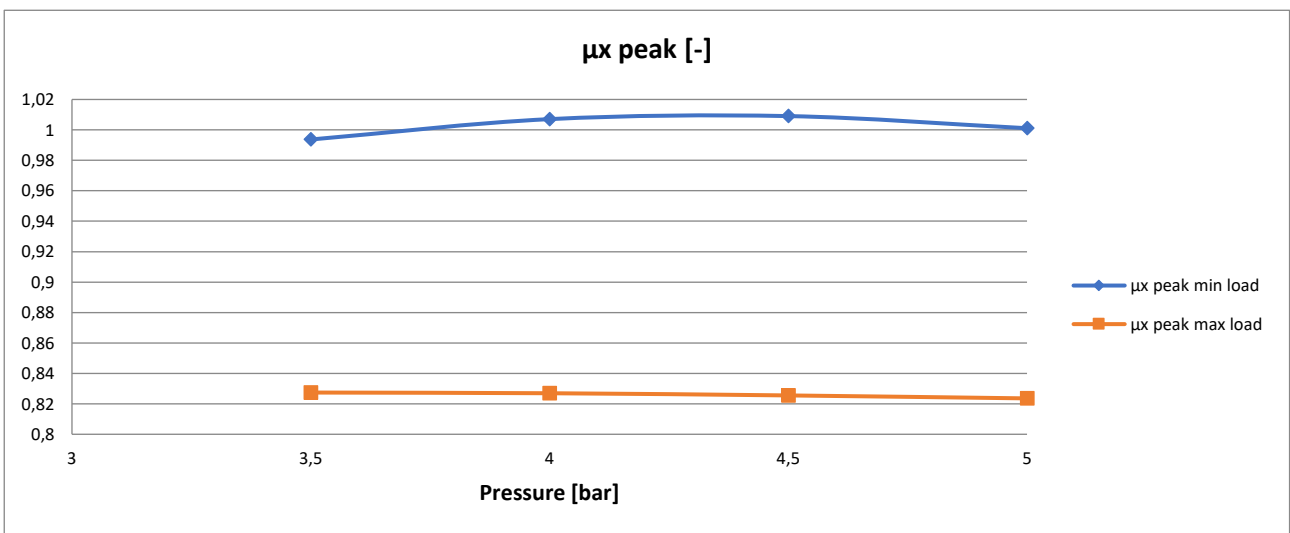


FIGURE 3.20 Effect of pressure and load on peak longitudinal adherence (Tire 195/75 R 16)

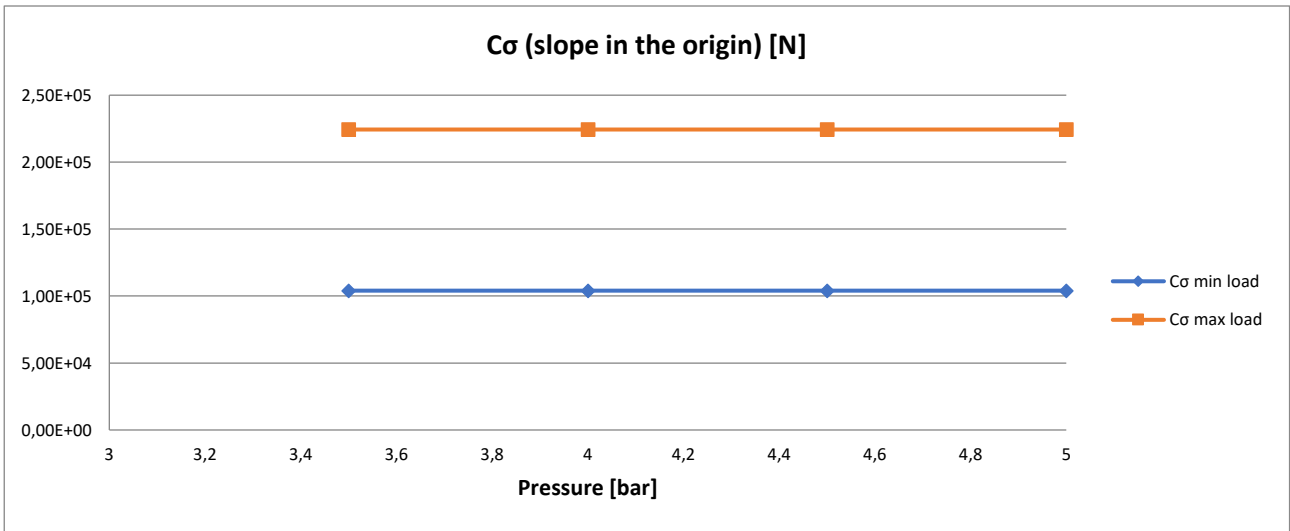


FIGURE 3.21 Effect of pressure and load on longitudinal slip stiffness (Tire 195/75 R 16)

3.3.2 Lateral analysis

For high levels of sideslip angle the adherence grows with pressure, with small angles instead lower pressures allow higher lateral adherence (Fig 3.22). In Figure 3.23 is plotted the effect on the peak lateral adherence.

For this tire the change of the trend of cornering stiffness in function of pressure is more present: the stiffness decrease with pressure at low load while it increases at full load (Fig 3.24).

Plotting the cornering stiffness in function of the vertical load (Fig 3.25) it can be observed that the cross-point of the curves is at approximately 8500 N so is reached also in static conditions by the fully loaded vehicle.

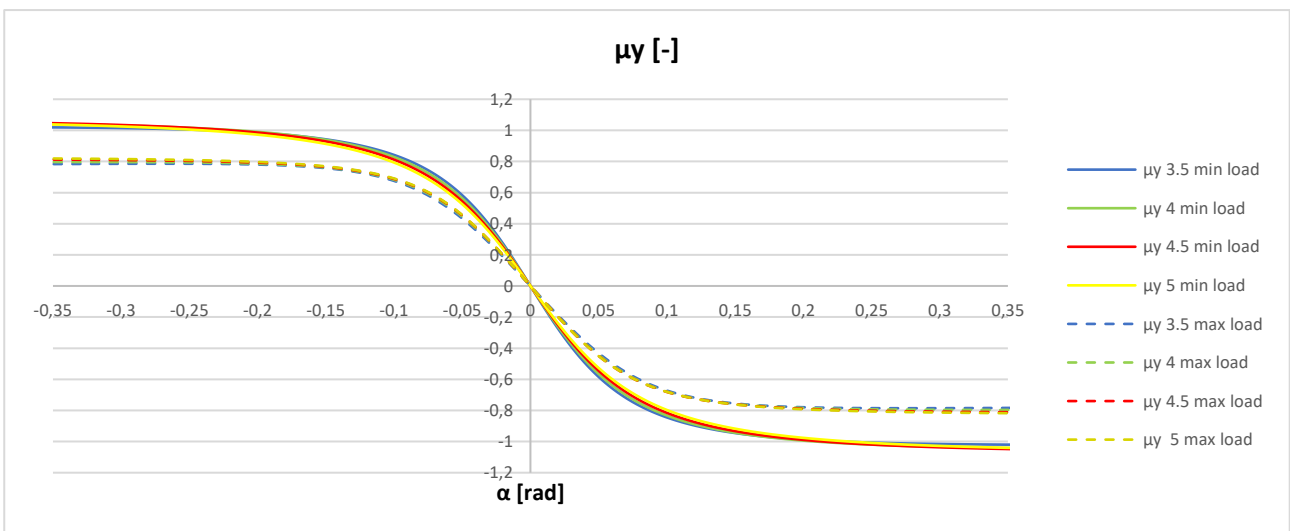


FIGURE 3.22 Lateral adherence in function of sideslip angle for different levels of pressure and load (Tire 195/75 R 16)

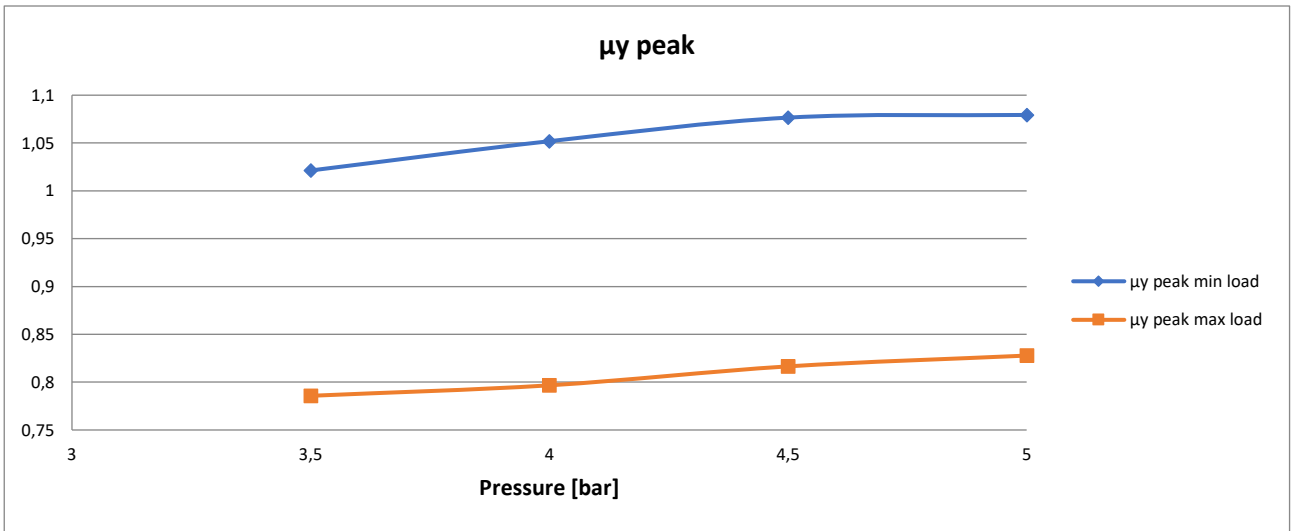


FIGURE 3.23 Effect of pressure and load on peak lateral adherence (Tire 195/75 R 16)

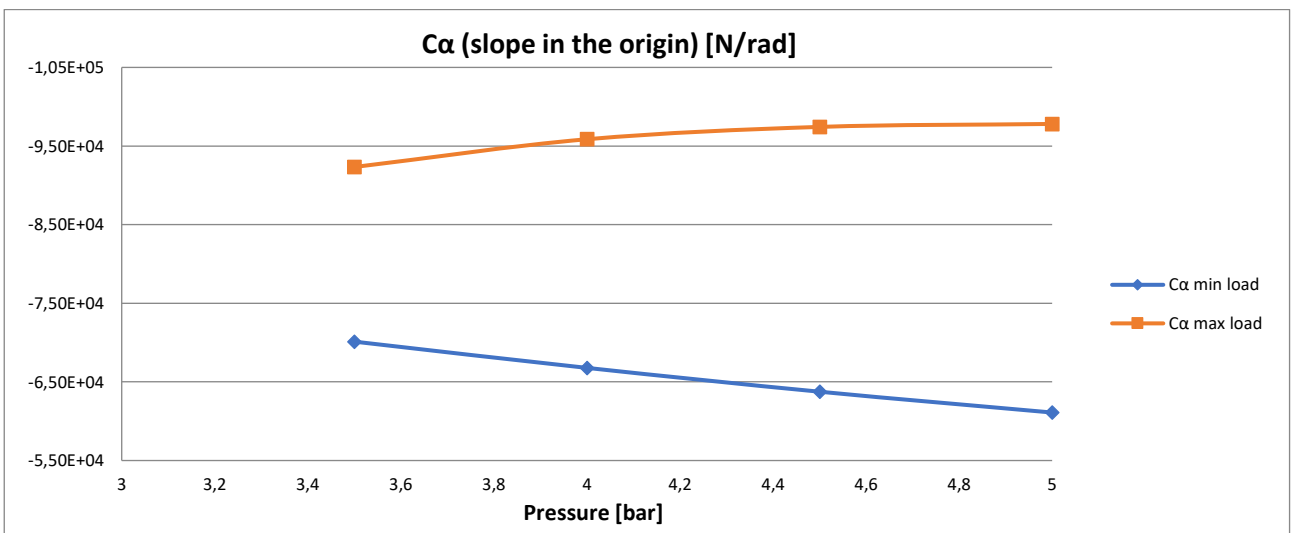


FIGURE 3.24 Effect of pressure and load on cornering stiffness (Tire 195/75 R 16)

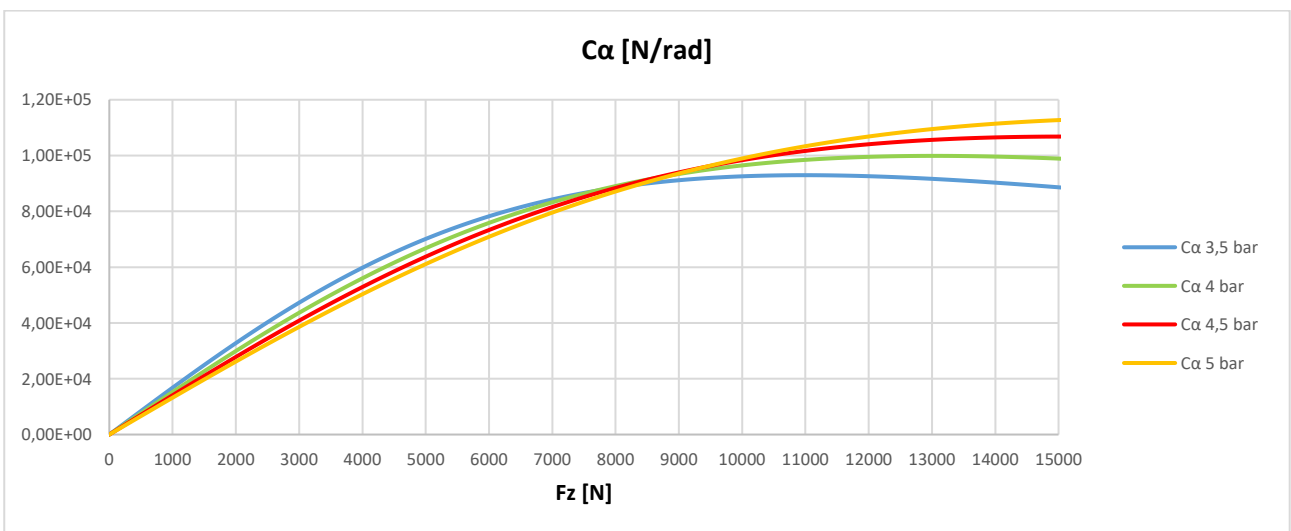


FIGURE 3.25 Effect of pressure and load on cornering stiffness (Tire 195/75 R 16)

3.3.3 Self aligning moment

The self-aligning moment increase decreasing inflation pressure in both load conditions (fig 3.26), decreasing pressure makes also increase the moment stiffness (Fig 3.27). At 5 bar the moment is much smaller and drops for low values of sideslip angle changing its sign.

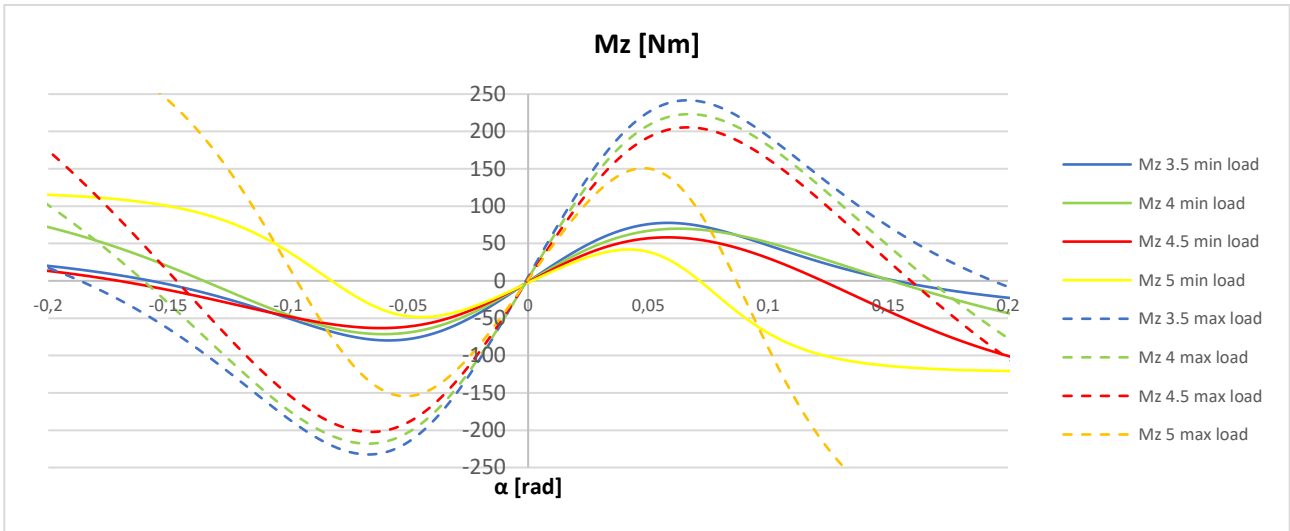


FIGURE 3.26 Self-aligning-moment in function of sideslip for different values of inflation pressure and load (Tire 195/75 R 16)

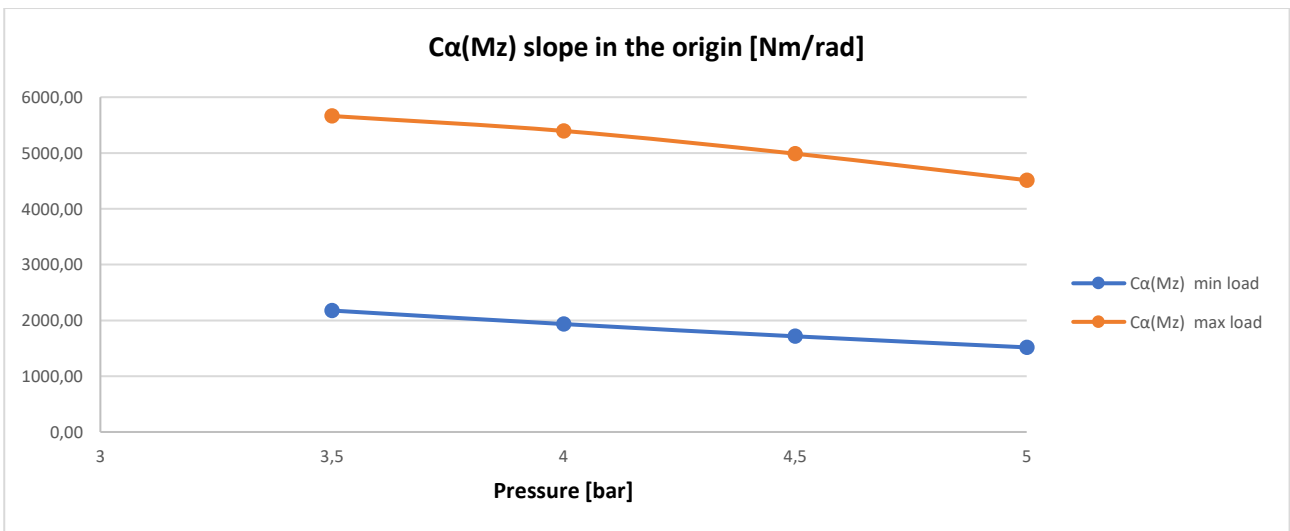


FIGURE 3.27 Effect of pressure and load on self-aligning moment stiffness (Tire 195/75 R 16)

3.3.4 Summary table of the results

In Table 3.6 the percentage variation of the main tire parameters from the nominal pressure condition is summarized.

| Load | $F_z = 5000\text{ N}$ | | | | $F_z = 9770\text{ N}$ | | | |
|----------------|-----------------------|--------------------|----------|---------|-----------------------|--------------------|----------|---------|
| | -0,5 bar | 4 bar (Nominal) | +0,5 bar | +1 bar | -0,5 bar | 4 bar (Nominal) | +0,5 bar | +1 bar |
| μ_{xp} | -1,33% | 1,01 | +0,20% | -0,59% | +0,05% | 0,83 | -0,17% | -0,41% |
| C_σ | +0% | 1,04E+05 N | +0% | +0% | +0% | 2,24E+05 N | +0% | +0% |
| μ_{yp} | -2,91% | 1,05 | +2,34% | +2,61% | -1,37% | 0,80 | +2,49% | +3,90% |
| C_α | +5,00% | 6,68E+04 N/rad | -4,54% | -8,51% | -3,68% | 9,59E+04 N/rad | +1,64% | +2,03% |
| M_{zMax} | +7,80% | 71,96 Nm | -19,15% | -41,74% | +8,31% | 223,16 Nm | -7,95% | -32,44% |
| $C_{Mz\alpha}$ | +12,53% | 1974 Nm/rad | -11,37% | -21,61% | +4,96% | 5395 Nm/rad | -7,55% | -16,35% |

TABLE 3.6 Effect of inflation pressure on main tire parameters for two load conditions (Tire 195/75 R 16)

4 Effect of inflation pressure on vehicle dynamics

In this section the effect of inflation pressure change on vehicle dynamics will be investigated through simulations on Adams Car of models of a Fiat Grande Punto and an Iveco Daily. Braking and Cornering manoeuvres were simulated and the results can be compared to the ones obtained by Pacejka's Magic Formula.

Additionally, in cooperation with Balocco Proving Ground the team ATPC performed experimental tests on the Punto that helped to validate previously made simulations and considerations and to improve the accuracy of the virtual models.

4.1 Fiat Grande Punto

As previously said the simulations were performed in two load conditions: one with driver only (1350 kg) and one at full load (1762 kg).

4.1.1 Braking

An emergency braking manoeuvre on a flat and dry road was simulated: the initial speed is 70 km/h and a 100% brake request is reached in 0.1 s (Fig 4.1)

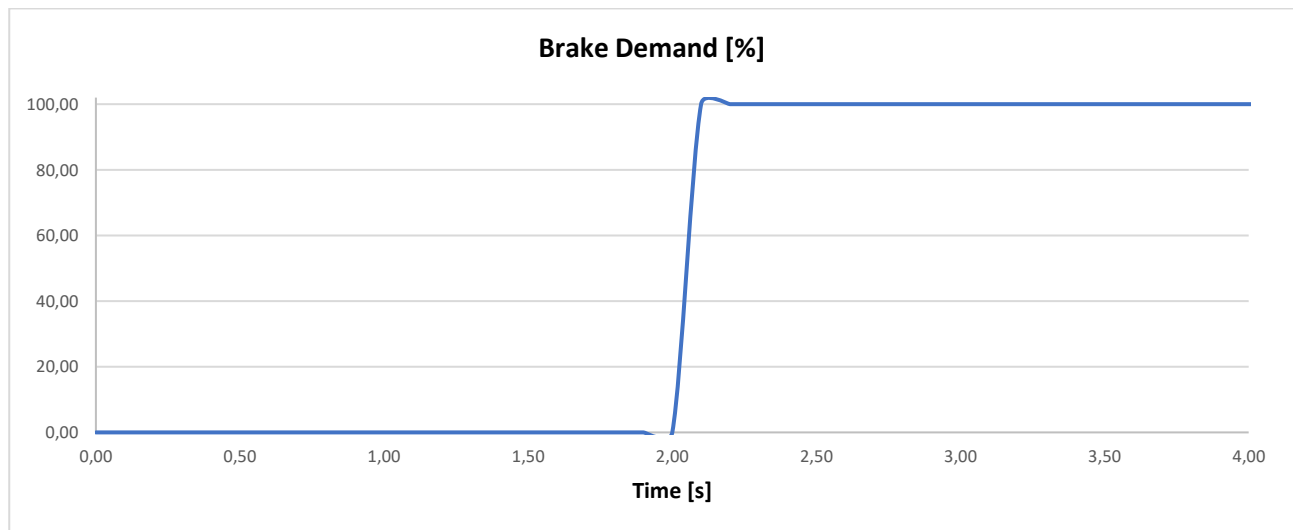


FIGURE 4.1 Brake demand (Grande Punto)

Examining the braking distance of the vehicle at 1350 kg and considering as reference the condition in which the inflation pressure is the recommended one (2,2 bar) it can be observed a reduction at lower pressures (Fig 4.2).

The minimum braking distance is reached with 1,8 bar inflation in front and rear tires, allowing a reduction of the 3,70% respect to the condition at nominal pressure.

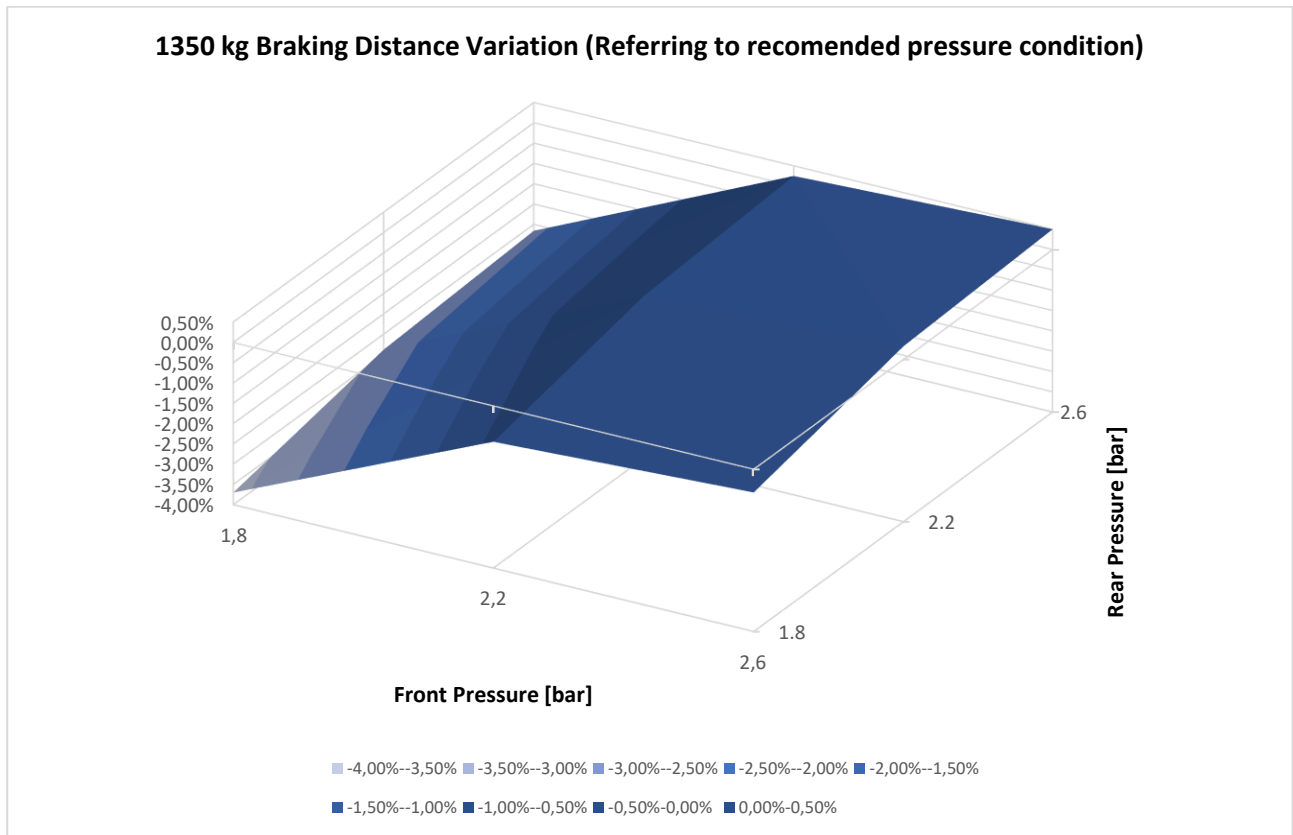


FIGURE 4.2 Braking distance variation compared to the condition at recommended inflation pressure (1350 kg Grande Punto)

Increasing the pressure at 2,6 bar in both front and rear axle wheels instead the braking distance increase of the 0,52%. It can also be observed that the influence of the pressure change is bigger in the front wheels: the deceleration in fact causes a load transfer on the front axle, the rear wheels then will contribute less to the braking manoeuvre. The load transfer and the pitch of the vehicle are encouraged by a lower pressure on the front axle and higher on the rear (Fig 4.3).

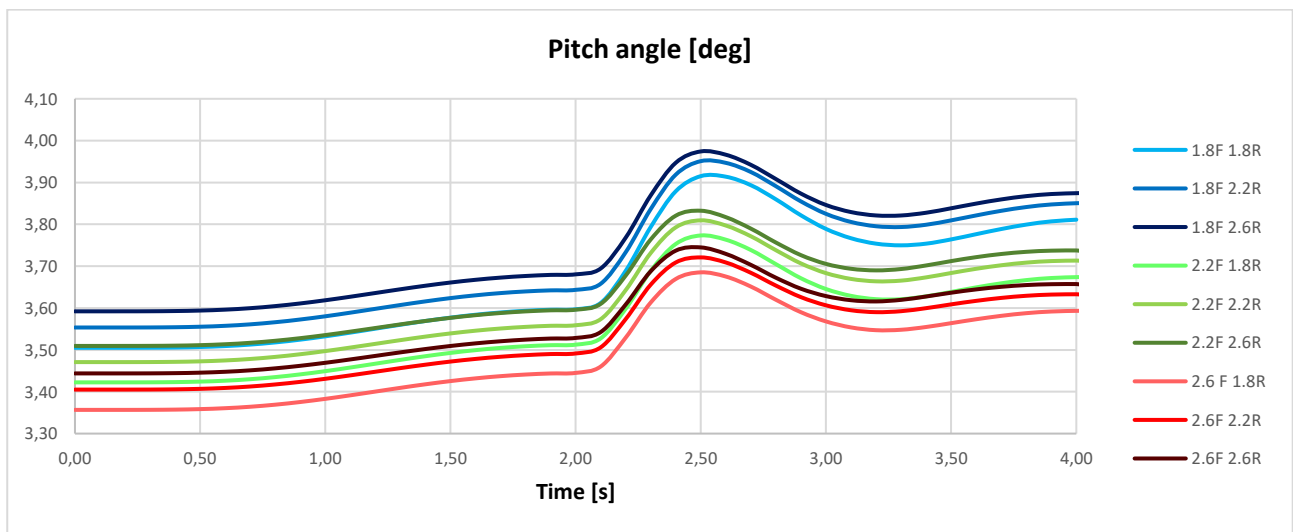


FIGURE 4.3 Pitch angle of the vehicle for different pressure conditions (1350 kg Grande Punto)

Repeating the simulation for the fully loaded vehicle (1762 kg) the braking distance increase, the effect of pressure however is really similar, causing a 3,73% distance decrease at 1,8 in both axles and a 0,46 increase at 2,6 bar (Fig 4.4). Also in this condition the effect of pressure is more important for the front axle.

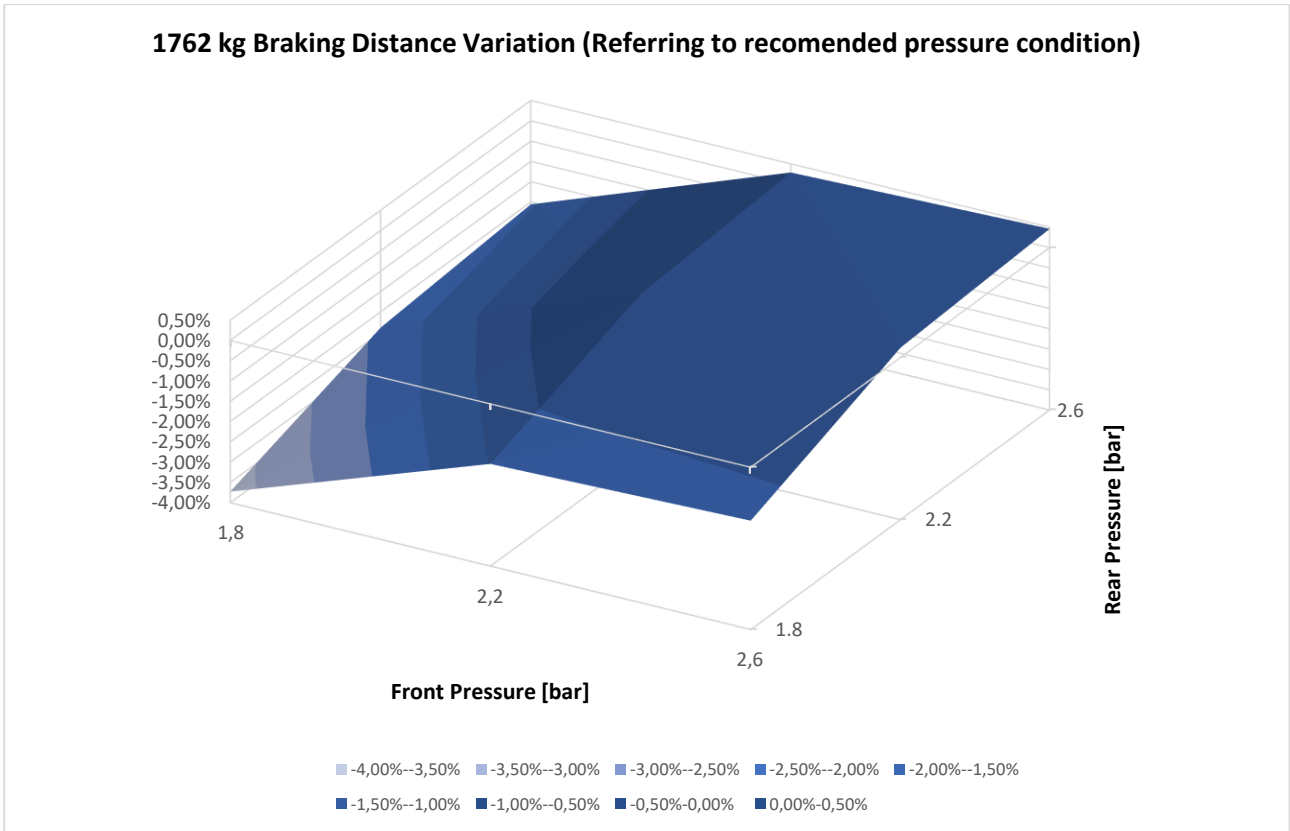


FIGURE 4.4 Braking distance variation compared to the condition at recommended inflation pressure (1762 kg Grande Punto)

The effect on the pitch is also similar but the angles are smaller for the full loaded vehicle (Fig 4.5).

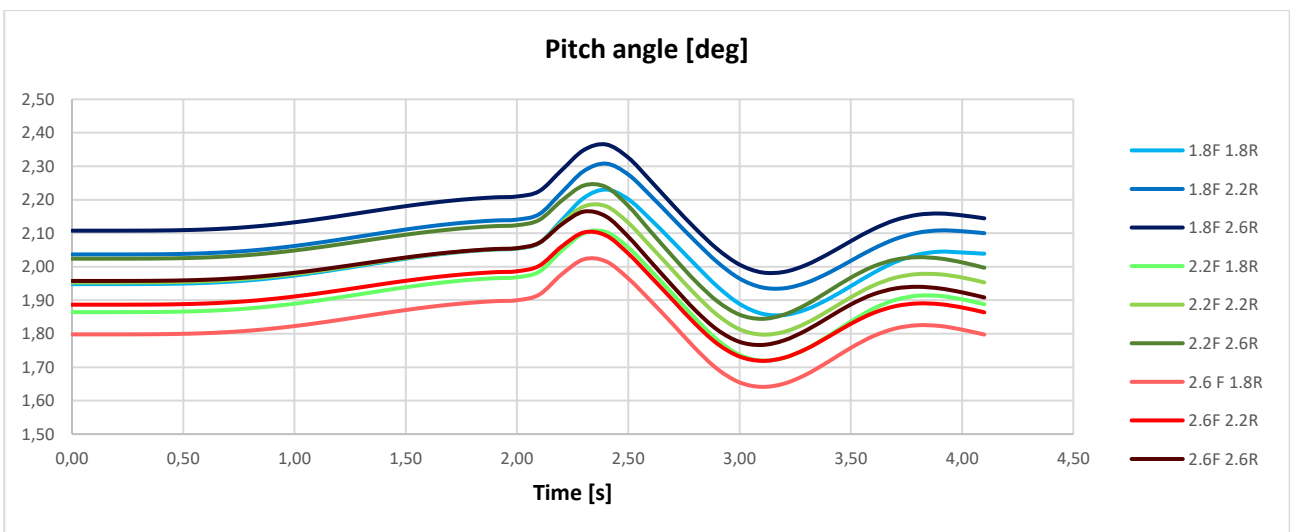


FIGURE 4.5 Pitch angle of the vehicle for different pressure conditions (1762 kg Grande Punto)

In Fig 4.6 instead, the braking distance for the fully loaded vehicle is compared to the one for the unladen vehicle at nominal pressure.

It can be observed that at 1,8 bar in both axles, the braking distance of the fully loaded vehicle is almost the same of the one reached by the unladen vehicle being even smaller of the 0,45%.

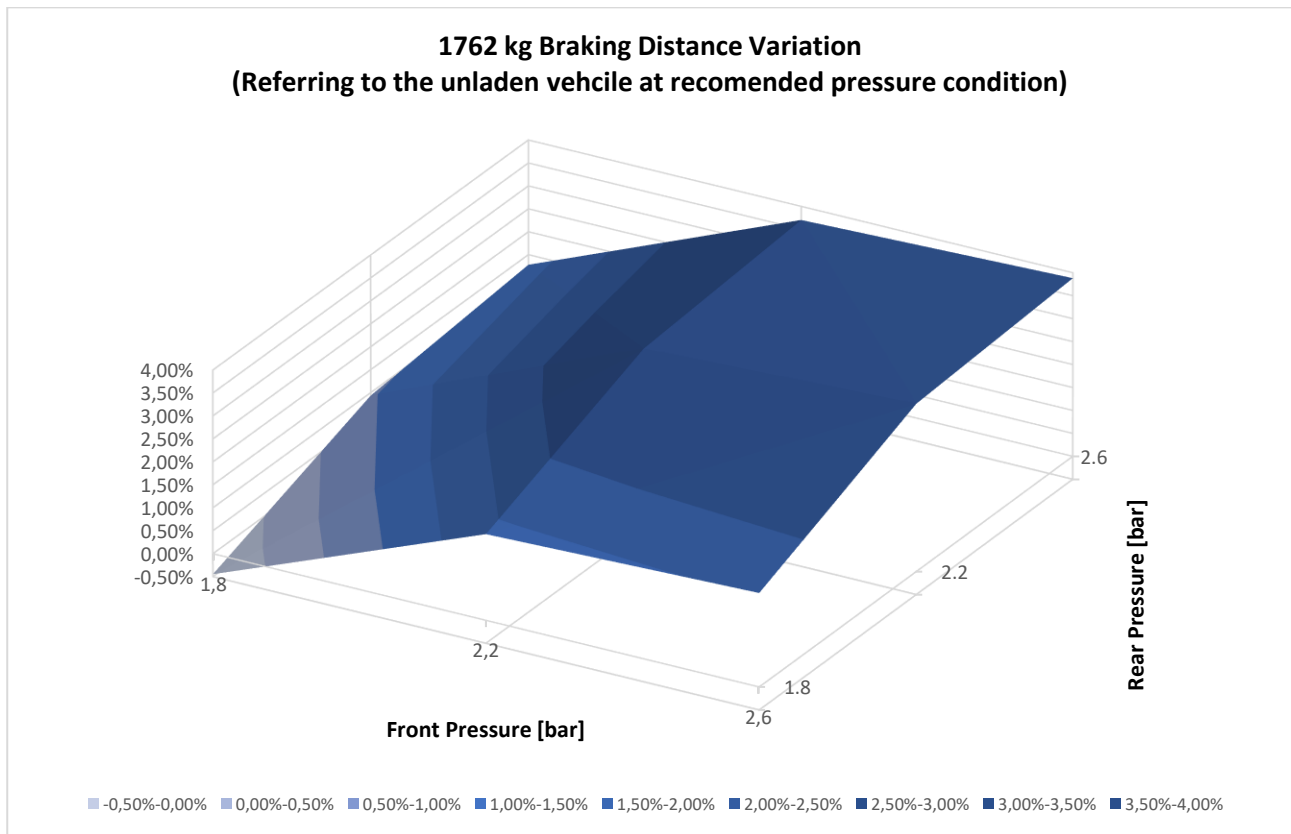


FIGURE 4.6 Braking distance variation compared to the unladen condition at recommended inflation pressure (1763 kg Grande Punto)

4.1.2 Analysis of braking results and literature overview

In both load conditions a lower pressure in both axles optimizes the braking distances of about 3,7%, however increasing inflation pressure in the optics of reduction of rolling resistance is not concerning for safety, causing an increase of braking distance of only the 0,5%.

So, two strategies can be developed, one to optimize braking distance and another to optimize fuel consumption. Using the first strategy the studied vehicle at full load is able to stop in the same space of the unladen one.

The results are consistent with the Magic Formula analysis according which the adherence grows decreasing tire pressure with similar variations in percentage.

Several tests campaigns were performed to investigate the effect of inflation pressure on braking distance for passenger vehicles: Vladimír Rievaj, Ján Vrábek and Anton Hudák in [15] carried out braking manoeuvres at different pressures, from 0,5 bar more to 0,5 bar less than the prescribed

inflation pressure. The tests showed an improvement of braking performance for the lower pressure (Fig 4.7).

| Name of results | Average values of braking | | |
|------------------------------------------------|---------------------------|------------|-----------|
| | decreased | prescribed | increased |
| Stopping distance[m] | 14.138 | 14.154 | 16.5 |
| Initial velocity[km.h ⁻¹] | 50.1 | 50.022 | 53.474 |
| Brake time[s] | 1.93 | 1.918 | 2.188 |
| Average brake deceleration[m.s ⁻²] | 7.938 | 7.814 | 7.236 |

FIGURE 4.7 Influence of pressure on braking performance

Other experimental tests by D. Hadryś, T. Węgrzyn and M. Miros [16] were performed on dry and wet road at 1, 2 and 3 bar on front tires. The experiments showed that the shortest stopping distance was reached at the recommended pressure on both dry and wet asphalt (Fig 4.8). It must be however considered that the pressure change is bigger and brings to a tire footprint reduction.

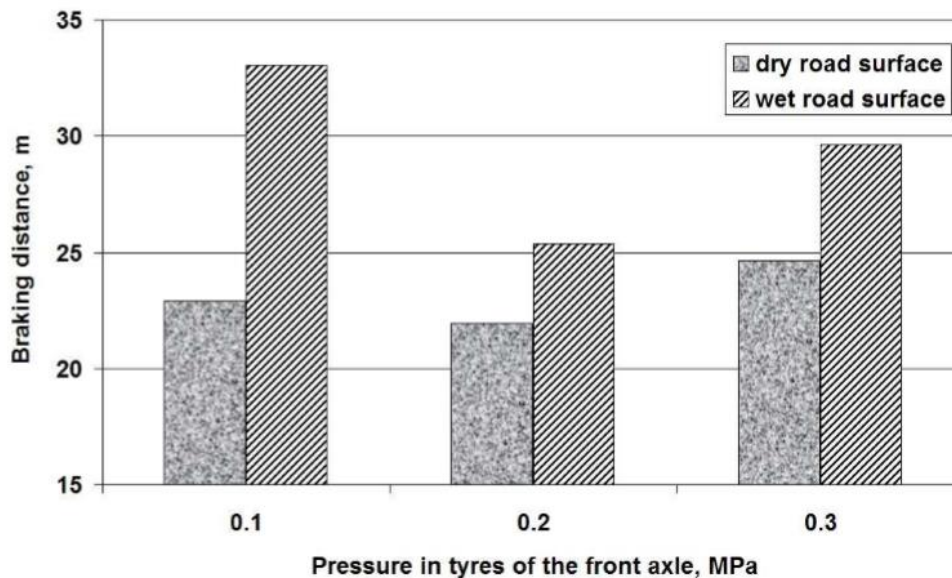


FIGURE 4.8 Influence of front tires pressure on braking distance.

4.1.3 Lateral Dynamics

For the two load conditions a step steer and a steering pad manoeuvre were performed. The ADAMS model was previously modelled with same dimensions, weights distribution and suspension typology of the actual car, then thanks to the experimental steering pad tests in cooperation with Balocco Proving Ground, the suspensions were tuned to better match the results obtained on the track.

4.1.3.1 Step Steer

A transient steer input is applied and then kept constant, the steering wheel angle chosen is 30° with an initial speed of 70 km/h. As previously said the effect of pressure on cornering stiffness change with the load. Considering the minimum load condition is useful to account the load transfer during the manoeuvre. In Figure 4.9 the load on each tire is indicated in the plot cornering stiffness vs vertical force.

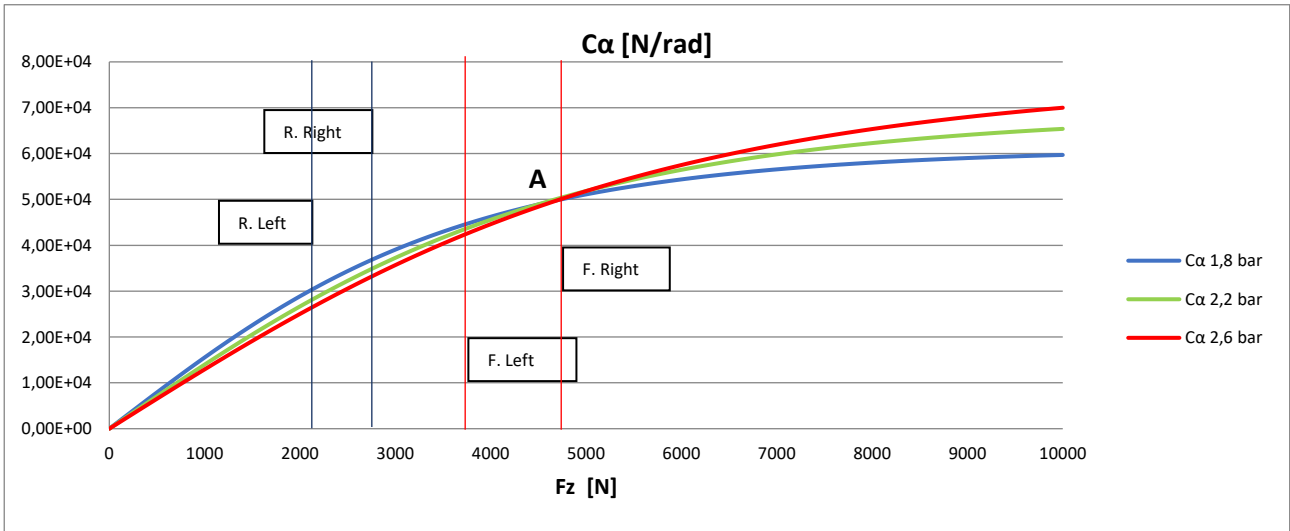


FIGURE 4.9 Cornering Stiffness in function of load for different pressures, the vertical load acting on the tires during a step steer manoeuvre is indicated (1350 kg Grande Punto)

The influence of pressure is clear for the rear axle, for which an increase of pressure causes a decrease of cornering stiffness. While this consideration is true also for the front left tire, it is not for the front right, that is more loaded and for which an increase of pressure leads to an increase of cornering stiffness.

On figure 4.10 are plotted the lateral accelerations in *g* registered for each pressure configuration.

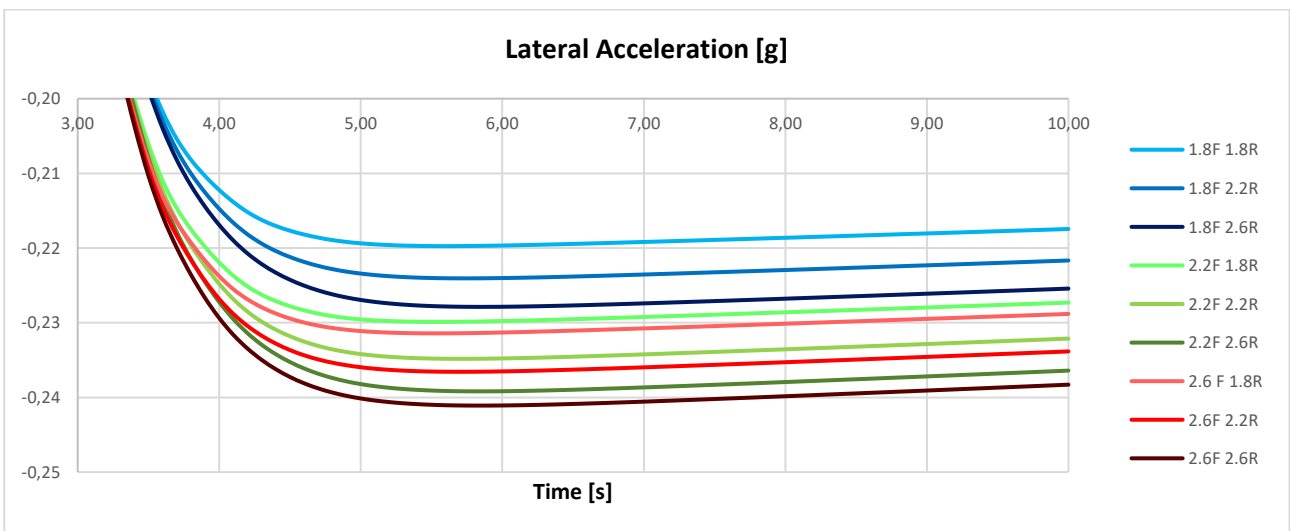


FIGURE 4.10 Lateral acceleration for different pressures (1350 kg Grande Punto)

A good measure of the cornering capability of the vehicle is the acceleration gain, that can be calculated as $\frac{a_y}{\delta}$. Considering the value of acceleration after the transient, the acceleration gain for the different pressure configurations is plotted in Fig 4.11.

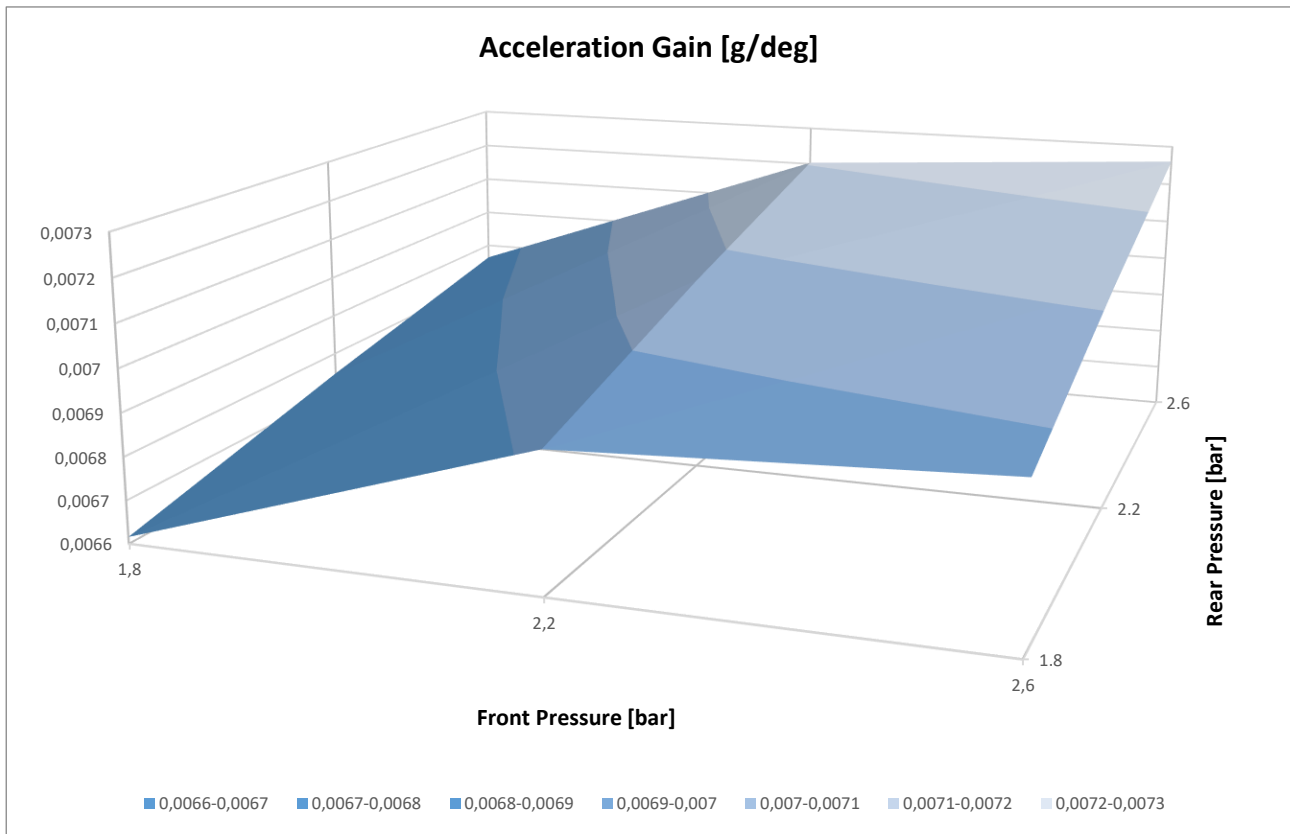


FIGURE 4.11 Acceleration Gain for different pressures (1350 kg Grande Punto)

It can be observed that both an increase of inflation pressure on the front and in the rear tires causes an increase of acceleration gain, so an increase of oversteer. That means that on the front axle prevailed the influence of the external tire, being more loaded and then capable to develop bigger cornering forces.

At 1762 kg, the centre of gravity moves back, and the load increase mostly on the rear axle. Examining the load transfer during the manoeuvre (Fig 4.12) it can be observed that this time both right wheels of front and rear axle are above point A, so higher pressures will cause a higher cornering stiffness. That means an increase of oversteer increasing front inflation pressure and an increase of understeer increasing rear pressure.

In Fig 4.13 are plotted the lateral accelerations. Unlike the lower load condition, the acceleration reached decrease with rear inflation pressure. Being the steering angle same for all simulations, bigger acceleration means bigger acceleration gain.

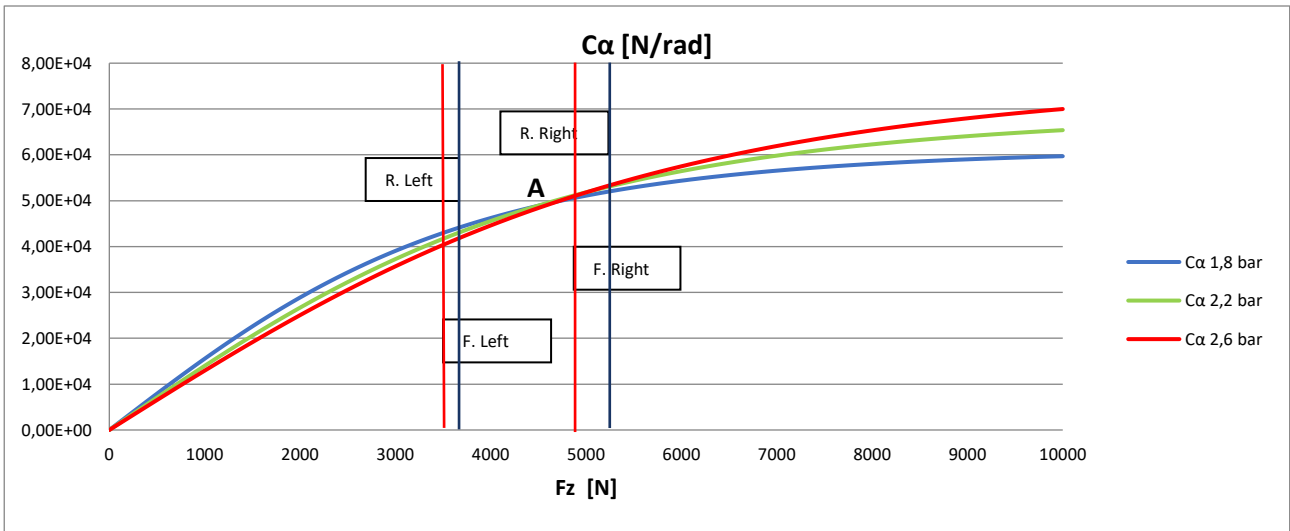


FIGURE 4.12 Cornering Stiffness in function of load for different pressures, the vertical load acting on the tires during a step steer manoeuvre is indicated (1762 kg Grande Punto)

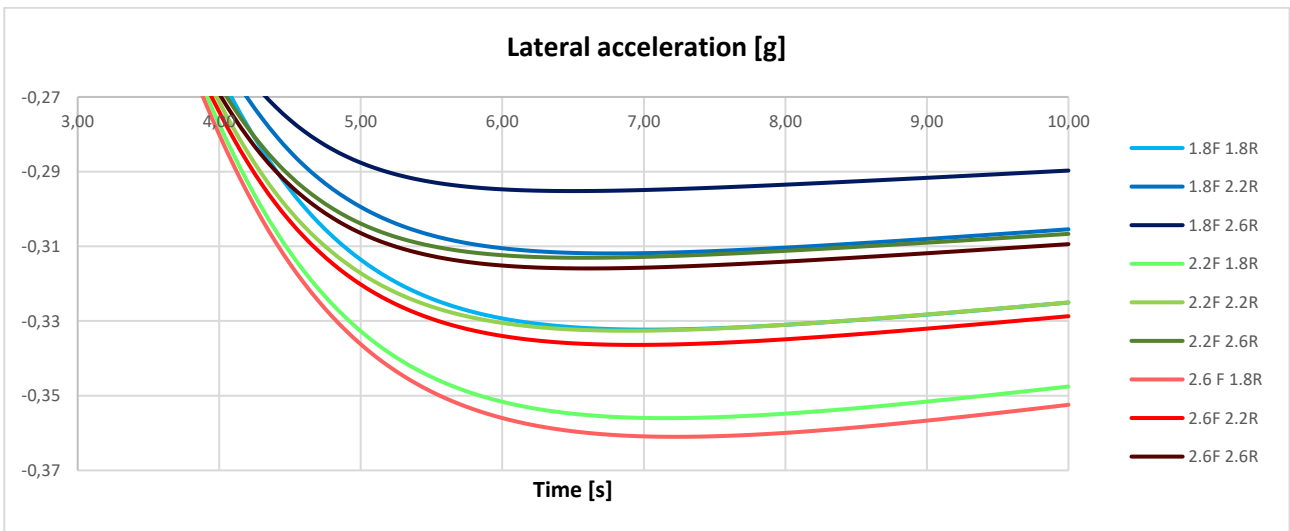


FIGURE 4.13 Lateral acceleration for different pressures (1762 kg Grande Punto)

The accelerations are bigger than in the 1350 kg condition: the increase of load on rear axle causes an increase of oversteer.

The effect on cornering behaviour is verified calculating the acceleration gain (Fig 4.14).

The minimum gain is obtained with 1,8 bar on front tires and 2,6 bar on rear tires. This configuration gives the vehicle a more understeer behaviour more similar to the one for the unladen vehicle.

A tool based on the three degrees of freedom model for vehicle dynamics (Par 2.3.4) was developed by the ATPC team to calculate the pressure configuration that brings the cornering behaviour of the vehicle at full load closer to the behaviour in standard B.

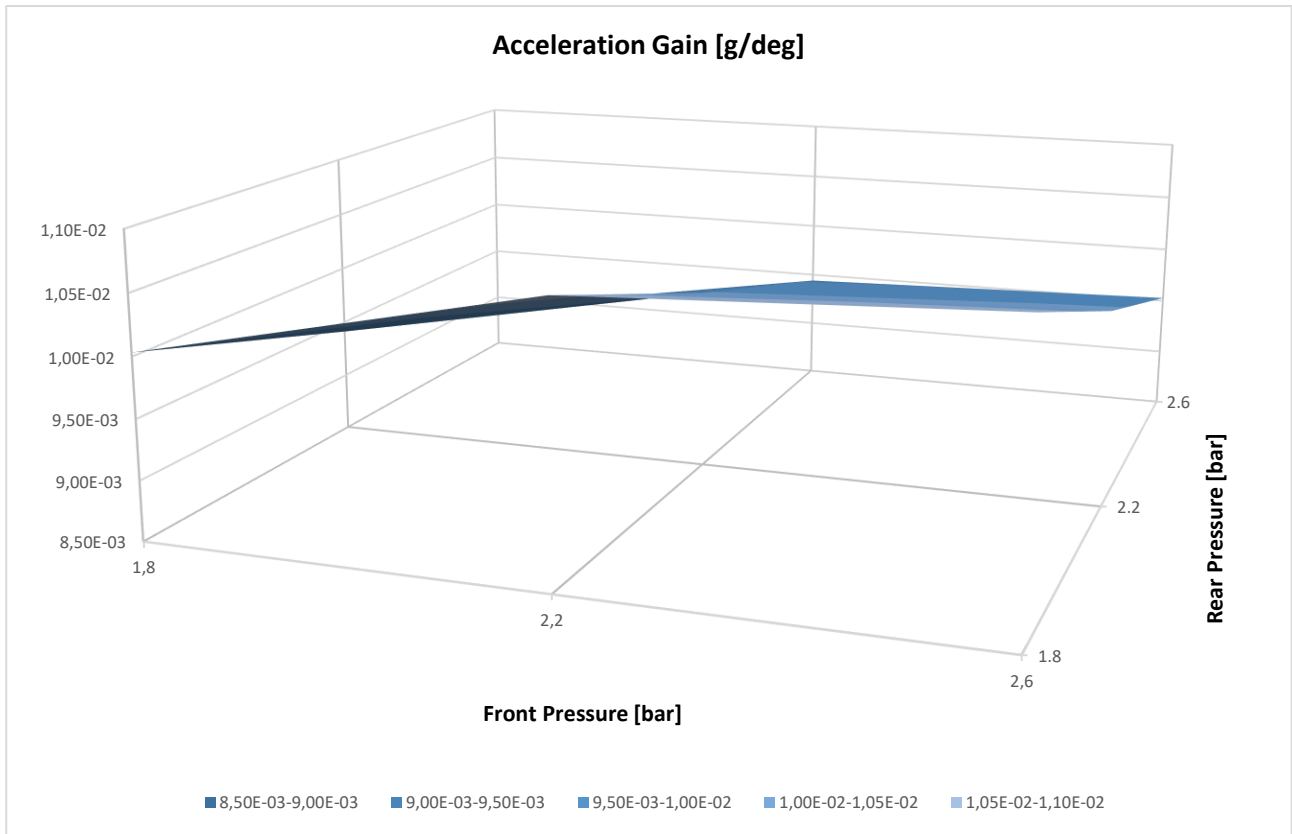


FIGURE 4.14 Acceleration Gain for different pressures (1762 kg Grande Punto)

4.1.3.2 Steering Pad

The steering pad manoeuvre consist in maintaining a constant curvature radius increasing gradually the acceleration. The simulations were performed for a 40m radius increasing lateral acceleration from 0.1g to 0.7g.

Being the trajectory fixed, an indication of the understeer or oversteer behaviour is the steering angle needed to maintain it. In Fig 4.15 is plotted the steering wheel angle for the vehicle at 1350kg.

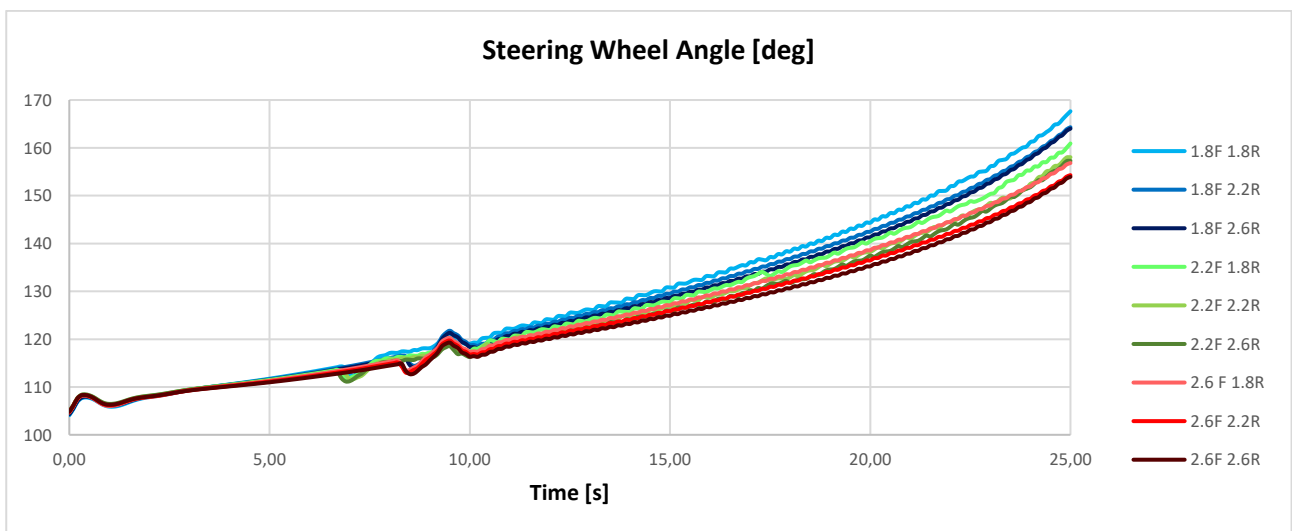


FIGURE 4.15 Steering wheel angle for different pressures (1350 kg Grande Punto)

A higher steering angle is needed at low inflation pressures, meaning that the vehicle becomes more understeer, confirming what was observed for the step steer manoeuvre.

From the steering angle, the curvature gain can be calculated as $\frac{1}{R\delta}$ where the curvature radius is constant and equal to 40 m. In Fig 4.16 is plotted the curvature gain in function of the vehicle speed.

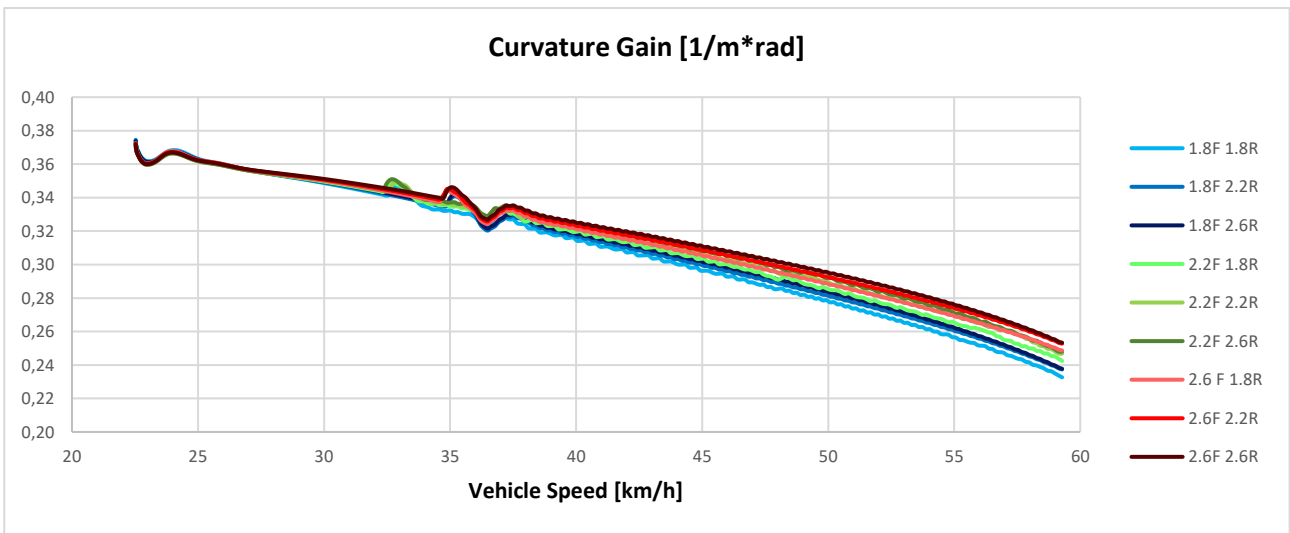


FIGURE 4.16 Curvature gain for different pressures (1350 kg Grande Punto)

The plot confirms a higher curvature gain (more oversteer) increasing front and rear pressure.

The same simulation was repeated for the vehicle at full load. In Fig 4.17 is plotted the steering wheel angle.

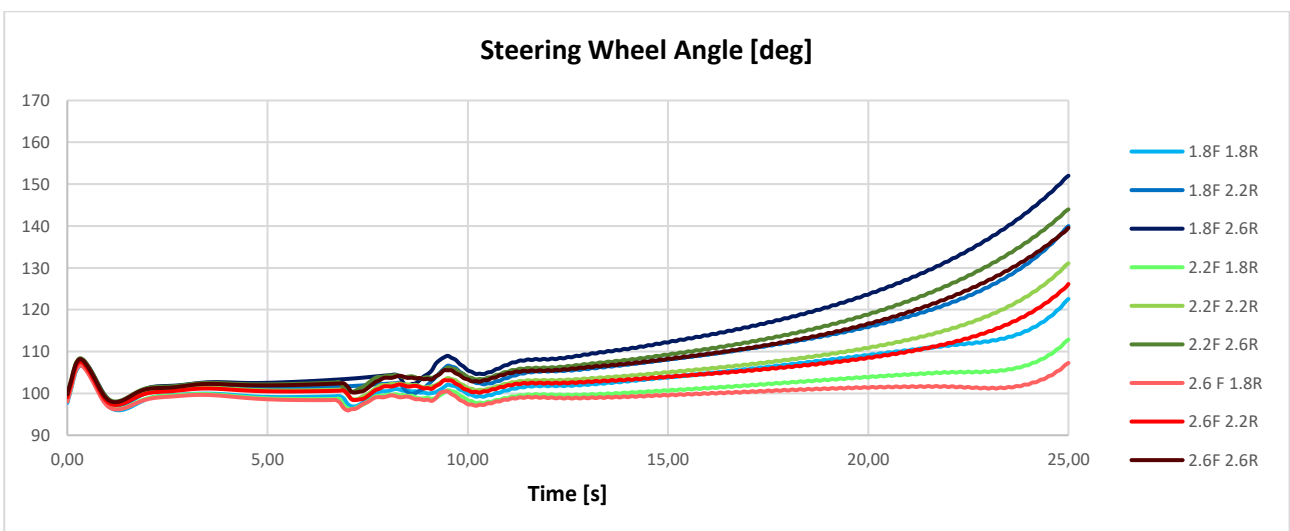


FIGURE 4.17 Steering wheel angle for different pressures (1762 kg Grande Punto)

The smaller angles needed indicate that the fully loaded vehicle is more oversteer.

Increasing front pressure, the oversteer behaviour is encouraged, the opposite occurs increasing rear pressure.

On Figure 4.18 is plotted the curvature gain, that again confirms the considerations made for the step steer.

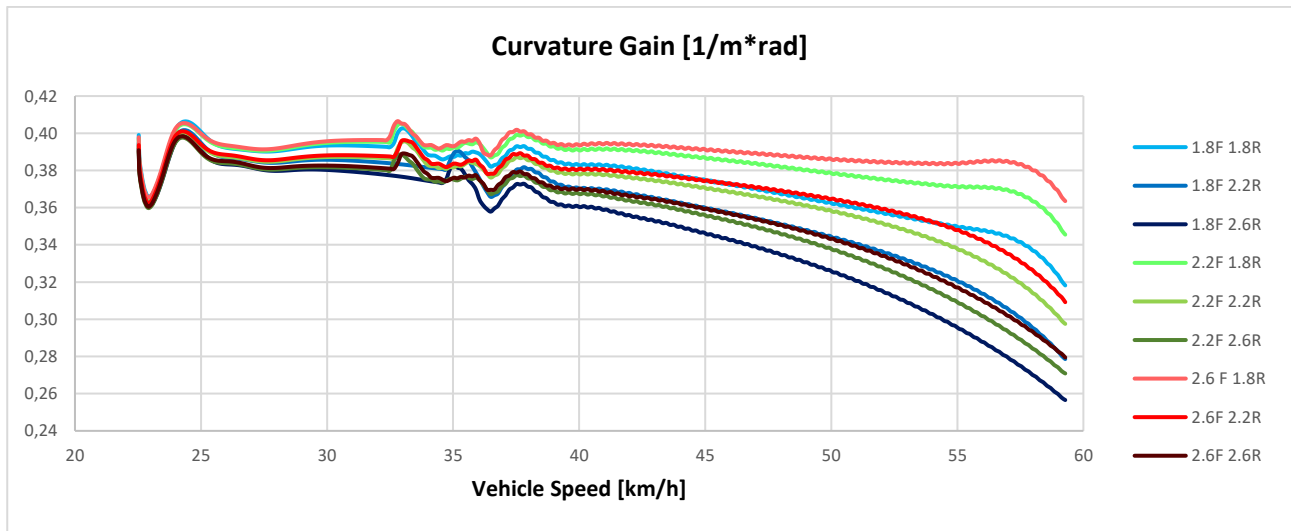


FIGURE 4.18 Curvature gain for different pressures (1762 kg Grande Punto)

4.1.4 Analysis of lateral dynamics results

The lateral dynamics of the vehicle is influenced by the load and the inflation pressure of the tire.

At low load an increase of pressure enhances the oversteer behaviour; at high load the same occurs for the front axle, while an increase on the rear axle has the opposite effect, making the vehicle more understeer. Knowing the change of load on the axles is possible to implement a strategy that permit to control the curvature gain of the vehicle restoring an understeer characteristic more similar to the one of the unladen vehicle.

4.2 Iveco Daily

The simulations were made in cooperation with Iveco and were performed for the unladen vehicle (2356 kg) and at full load (3500 kg). Two different tires were used, a 225/65 R16 and a 195/75 R16 more sensitive to pressure changes.

4.2.1 Braking (225/65 R16)

The initial speed is 70 km/h and a 100% brake request is reached in 0.1 s. It must be noted that the manoeuvres were performed without ABS. The effect on braking distance of the unladen vehicle is indicated in percentage variation respect to the prescribed inflation pressure in Fig 4.19.

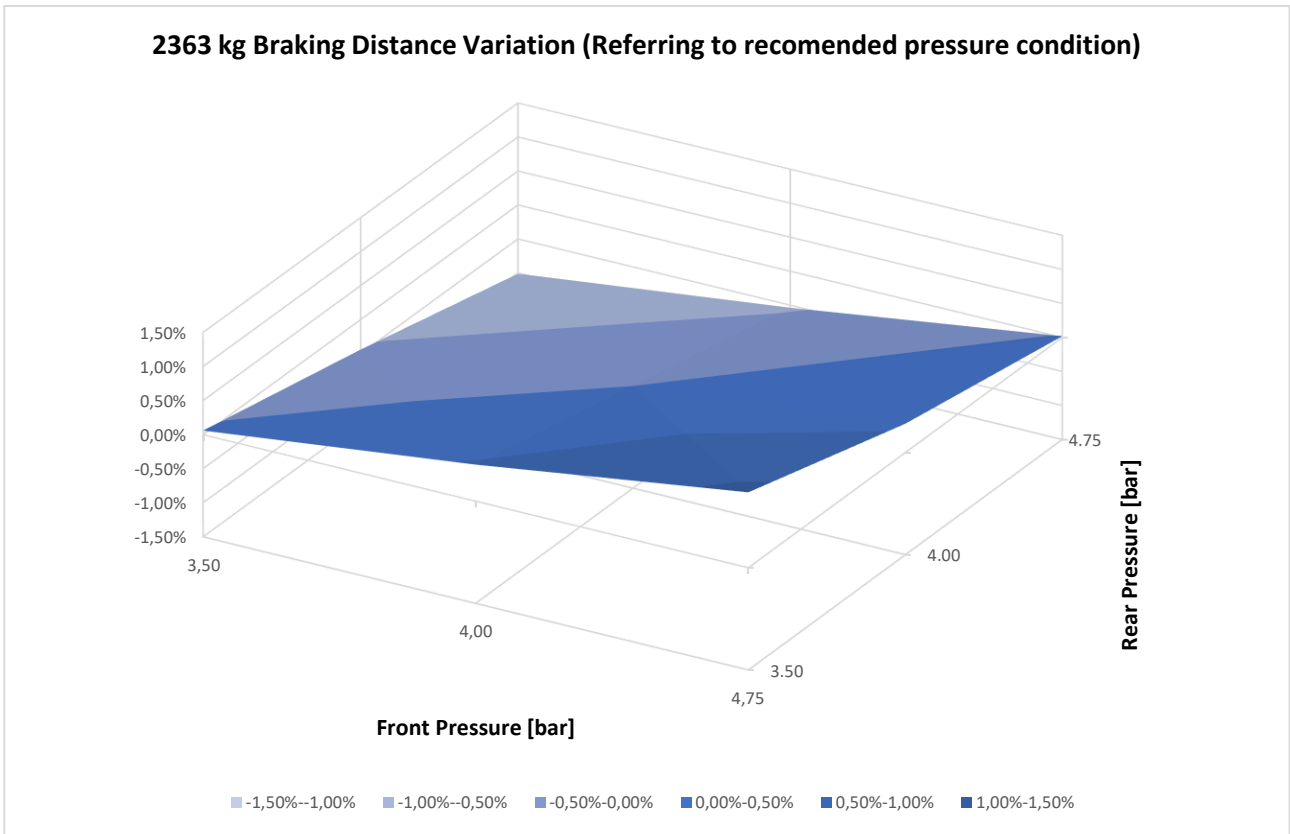


FIGURE 4.19 Braking distance variation compared to the condition at recommended inflation pressure (2363 kg IVECO Daily with 225/65 R16 Tires)

The stopping distance decreases almost linearly increasing rear pressure and decreasing front pressure. Consequently the minimum braking distance occurs at 3,5 bar on front tires and 4,75 bar on rear tires, allowing a reduction of 1.01% of braking distance. With 4,75 bar on front and 3,5 bar on rear instead the braking distance increase of the 1.11%.

The pitch is encouraged at lower front pressure and higher rear pressure (Fig 4.20).

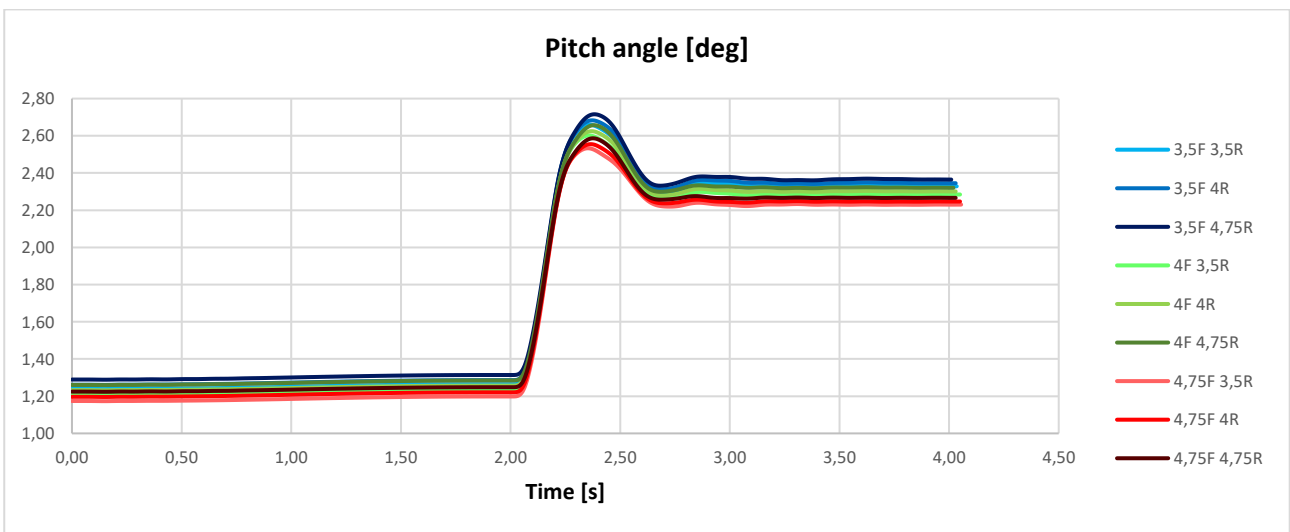


FIGURE 4.20 Pitch angle of the vehicle for different pressure conditions (2363 kg IVECO Daily with 225/65 R16 Tires)

For the fully loaded vehicle instead the smaller braking distance is achieved at 3,5 bar both on front and rear axle allowing though a reduction of only the 0,56%. The maximum pressure on both axles instead cause an increase of distance of the 0,93% (Fig 4.21).

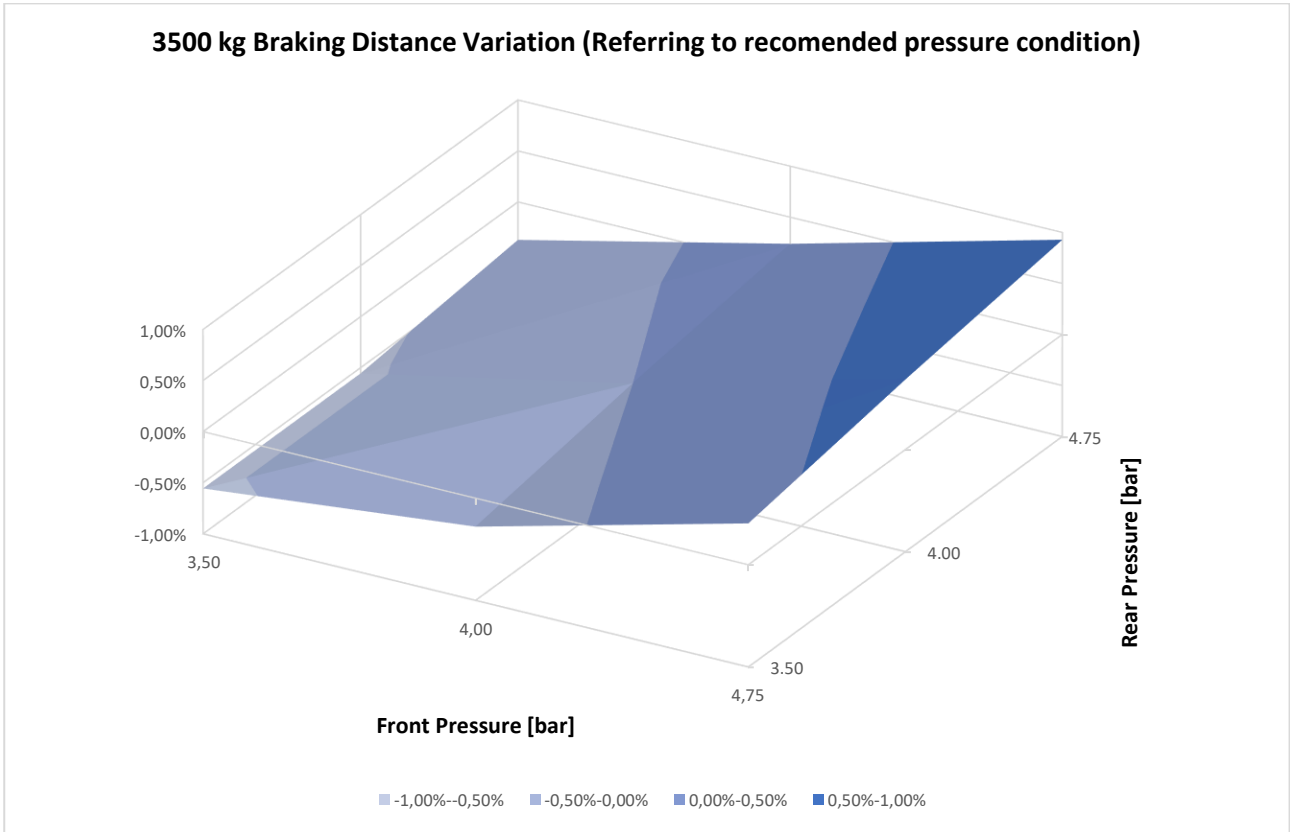


FIGURE 4.21 Braking distance variation compared to the condition at recommended inflation pressure (3500 kg IVECO Daily with 225/65 R16 Tires)

The effect on pitch angle is the same as for the unladen vehicle, the angles however are smaller, due to the bigger load on the rear axle (Fig 4.22).

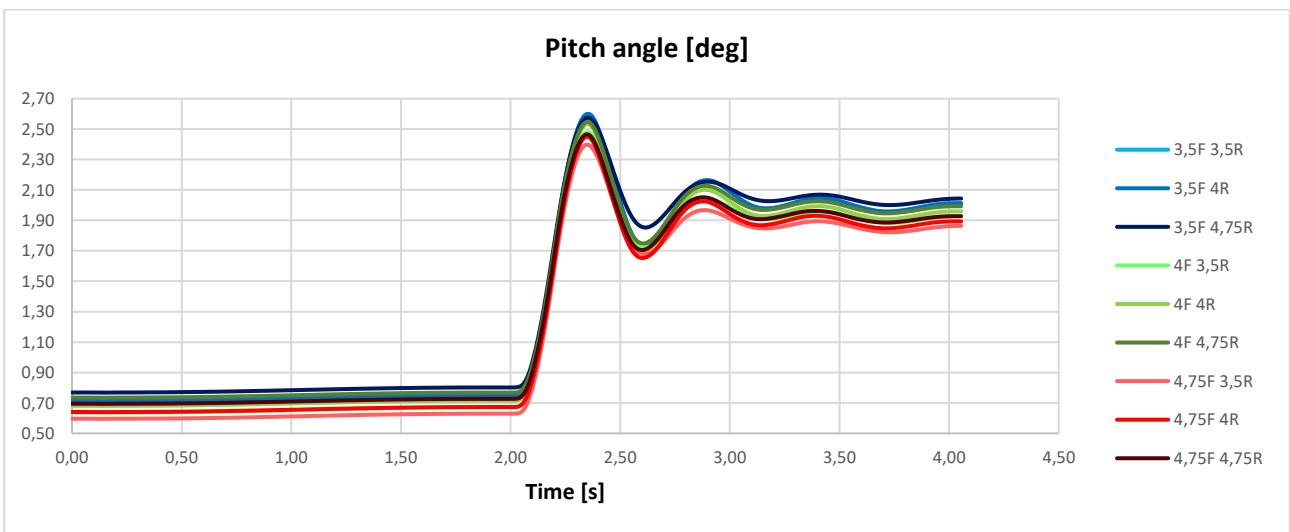


FIGURE 4.22 Pitch angle of the vehicle for different pressure conditions (3500 kg IVECO Daily with 225/65 R16 Tires)

4.2.2 Braking (195/75 R16)

The same braking manoeuvre is performed with a different tire with bigger aspect ratio. The effect on braking distance for the unladen vehicle is no more monotone (Fig 4.23).

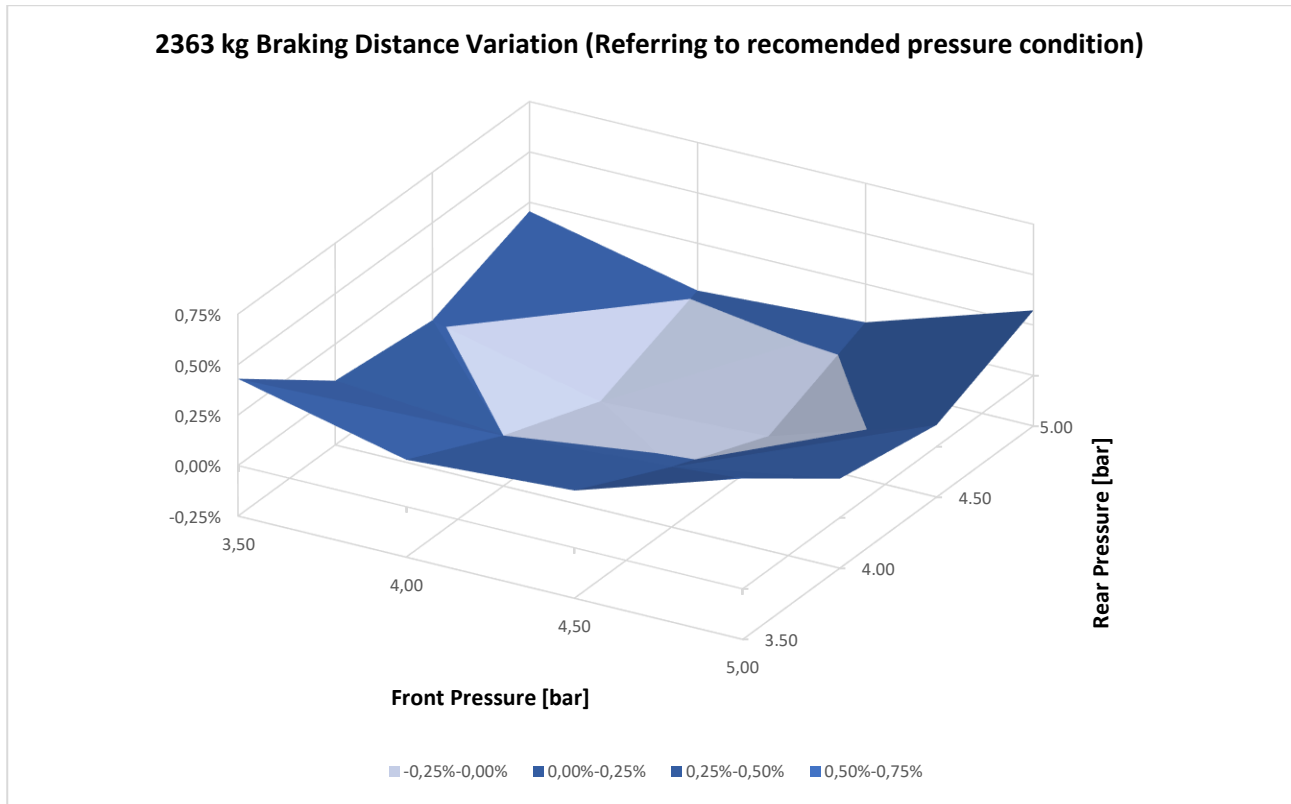


FIGURE 4.23 Braking distance variation compared to the condition at recommended inflation pressure (2363 kg IVECO Daily with 195/75 R16 Tires)

The braking distance has a minimum near the prescribed pressure and then increase again. The best configuration is with 4 bar on front tires and 4,5 bar on rear tires, allowing a reduction of only the 0.18%. The maximum increase of stopping distance occurs at 5 bar on front axle and 3,5 bar on rear (+0, 55%). The maximum pitch occurs at lower pressure on front and higher on rear axle (Fig 4.24).

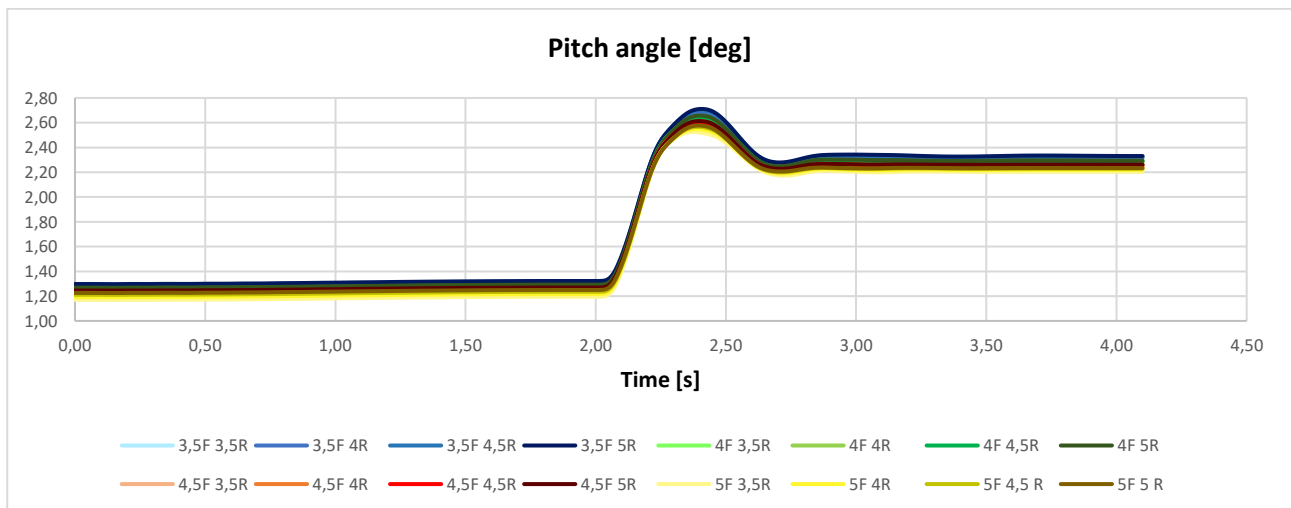


FIGURE 4.24 Pitch angle of the vehicle for different pressure conditions (2363 kg IVECO Daily with 195/75 R16 Tires)

The effect on stopping distance is bigger for the fully loaded vehicle and has a more linear behaviour (Fig 4.25). The best condition is obtained with the lower pressure on both axles, allowing a reduction of distance of the 0,7%. The worst condition is instead at 5 bar on front and 4,5 bar on rear axle (+1,03%).

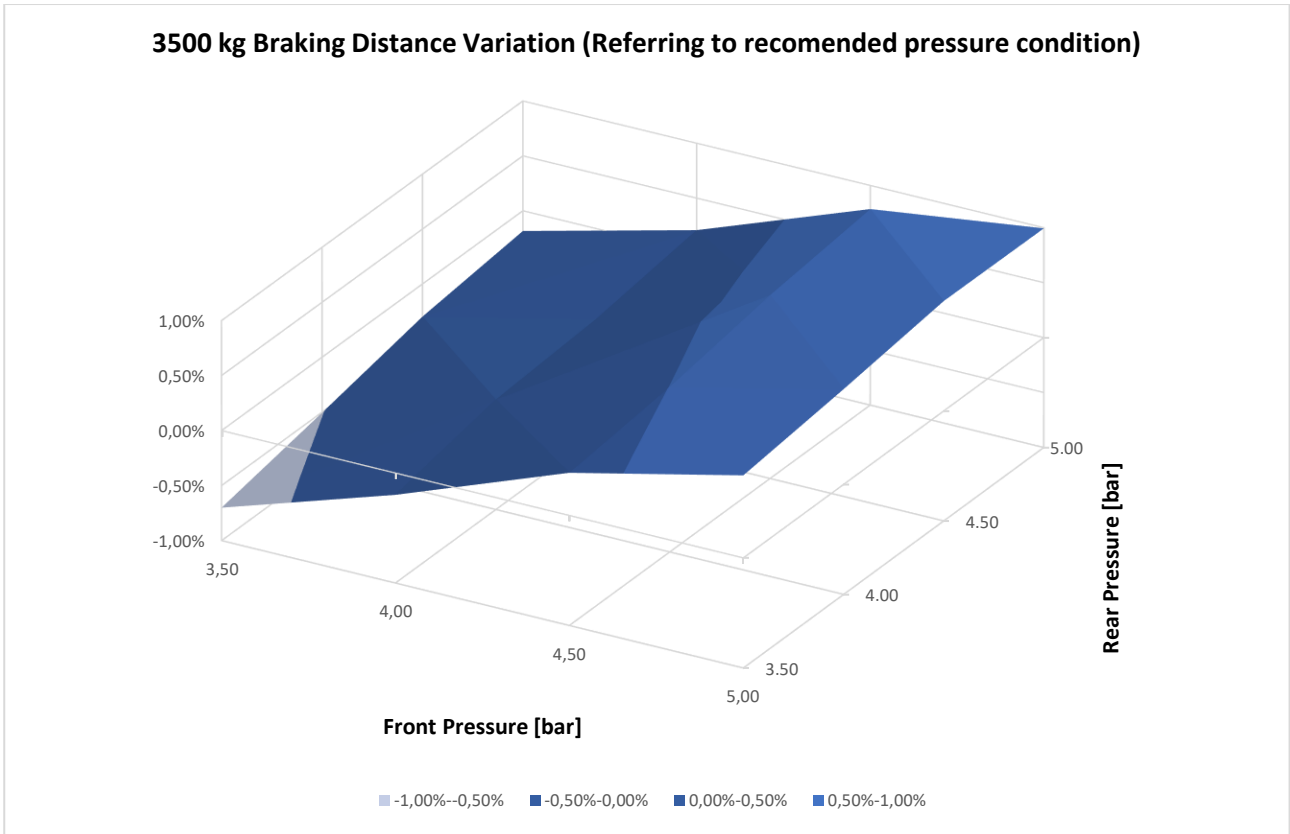


FIGURE 4.25 Braking distance variation compared to the condition at recommended inflation pressure (3500 kg IVECO Daily with 195/75 R16 Tires)

The pitch angle is smaller for the fully loaded vehicle, but the effect of pressure is the same (Fig 4.26).

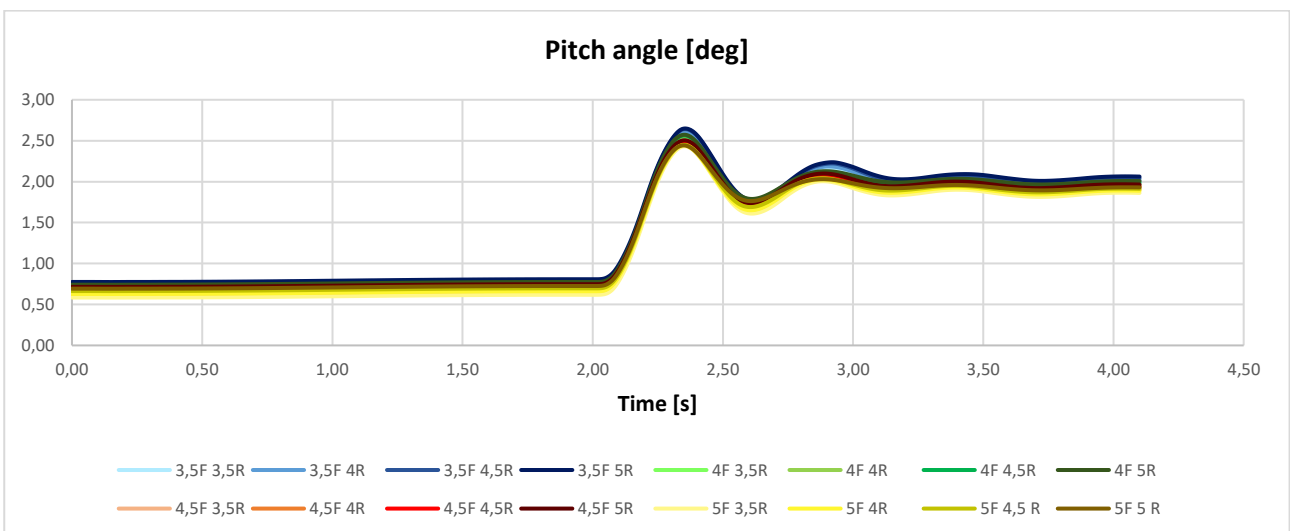


FIGURE 4.26 Pitch angle of the vehicle for different pressure conditions (3500 kg IVECO Daily with 195/75 R16 Tires)

4.2.3 Analysis of braking results and literature overview

The factors that influence braking distance are the actual adherence of the tire (that at high load decrease with the pressure) and the load transfer. For both used tires, at full load the vehicle has a smaller stopping distance for 3,5 bar inflation on both axles. At lower load the maximum adherence occurs for values slightly higher than the recommended pressure, on the other hand the pitch angle and the load transfer are bigger for a lower pressure on front tires. In the end the ideal condition for braking for the unladen vehicle is at higher pressure on rear axle and lower on front. The 195/75 R 16 tire was tested also at 5 bar but at that pressure the adherence becomes again lower.

The relatively low variation of the stopping distance encourages to pursuit strategies more addressed to the reduction of fuel consumption, being the braking distance in a safety margin in each case. An increase of pressure until 4,75 or 4,5 bar on rear wheels for the vehicle at full load could however achieve both the results of reducing braking distance and rolling resistance.

The simulations should be repeated with a model with an ABS system, however experimental tests by K. M. Marshek, J.F. Cuderman II and M. J. Johnson [17] registered an even lower influence of inflation pressure on braking distance for a vehicle provided with ABS, compared to the braking at locked wheels. Another simulation with the ADAMS model of the Punto for an emergency braking from 100 Km/h with and without ABS leads to the same results (Fig 4.27): the influence of pressure is bigger of approximately the 0,2% for the vehicle with no ABS.

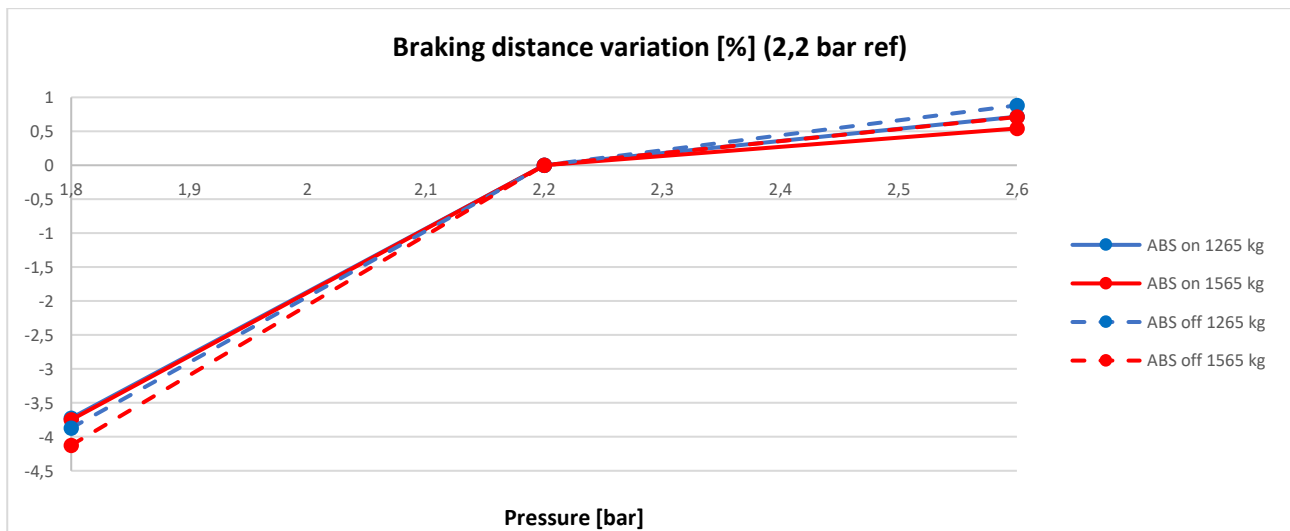


FIGURE 4.27 Influence of pressure on braking distance for the vehicle with (full lines) and without ABS (dashed lines) (Fiat Grande Punto)

4.2.4 Lateral dynamics (225/65 R16)

The simulations were performed for the two load conditions and with both type of tires. Here are presented the results for step steer and steering pad manoeuvres with tire 225/65 R16.

4.2.4.1 Step Steer

The steering angle is 15 deg and the initial speed is 70 km/h. On Fig 4.28 is indicated the load in each tire during the manoeuvre and the corresponding cornering stiffness.

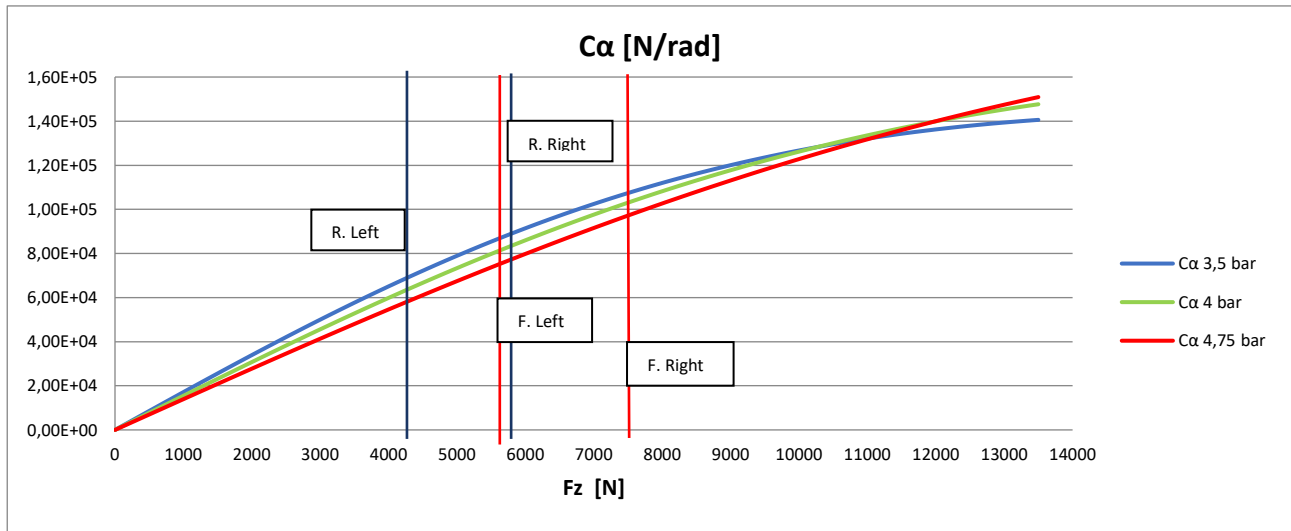


FIGURE 4.28 Cornering Stiffness in function of load for different pressures, the vertical load acting on the tires during a step steer manoeuvre is indicated (2356 kg Iveco Daily with 225/65 R16 tires)

For front and rear axles the pressure increase causes a decrease of cornering stiffness. In Fig 4.29 is plotted the effect on lateral acceleration.

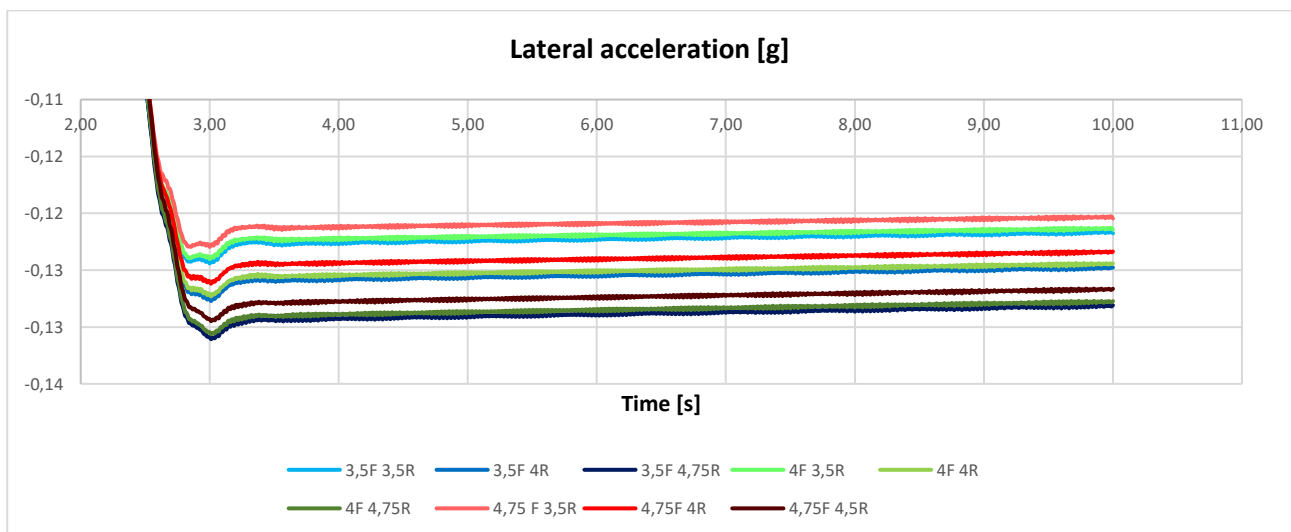


FIGURE 4.29 Lateral acceleration for different pressures (2356 kg Iveco Daily with 225/65 R16 tires)

The lateral acceleration, so the acceleration gain (Fig 4.30), increases increasing rear pressure (more oversteer) and decreasing front pressure in accordance with the effect on cornering stiffness.

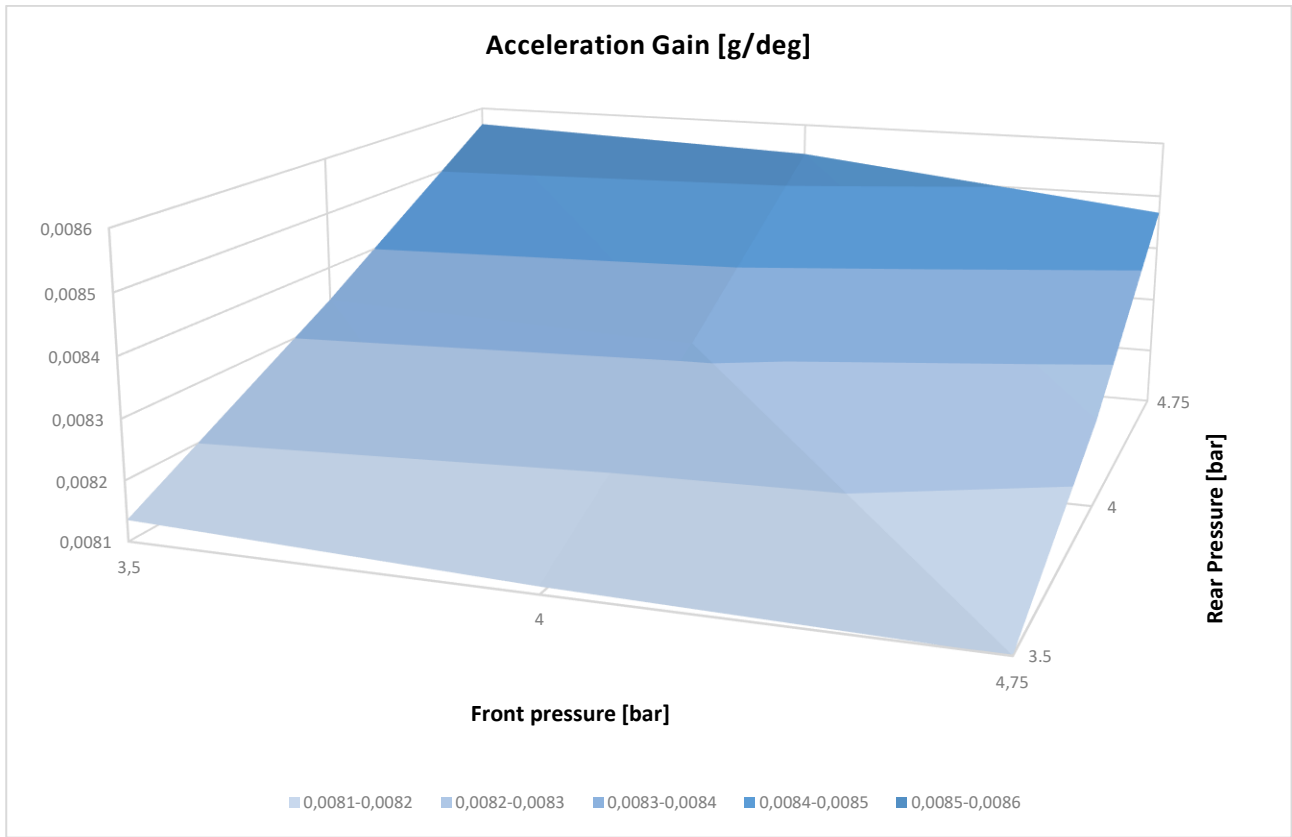


FIGURE 4.30 Acceleration Gain for different pressures (2356 kg Iveco Daily with 225/65 R16 tires)

For the vehicle in full load, the tires still work in the zone in which the cornering stiffness decrease with pressure except the rear right, for which the stiffness is almost the same for 3,5 and 4 bar (Fig 4.31). The load increase is mostly on rear axle.

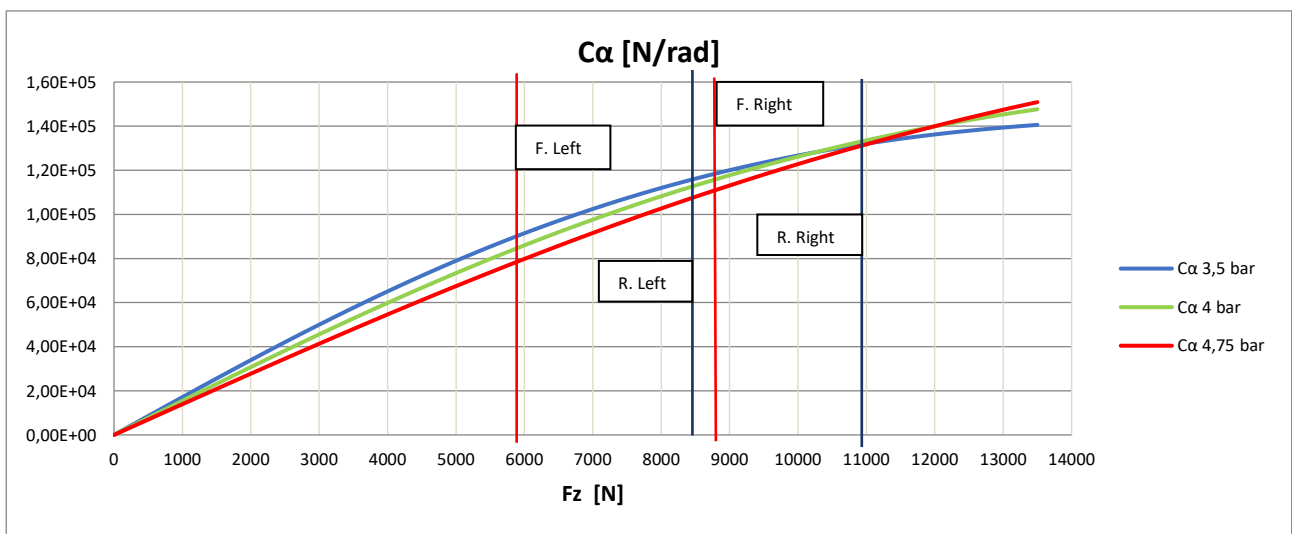


FIGURE 4.31 Cornering Stiffness in function of load for different pressures, the vertical load acting on the tires during a step steer manoeuvre is indicated (3500 kg Iveco Daily with 225/65 R16 tires)

Consequently, the effect on the acceleration (Fig 4.32) and on the acceleration gain (Fig 4.33) is the same as for the unladen vehicle, with a behaviour generally more oversteering. The effect of pressure change on rear axle is smaller and the curvature gain is almost the same for 3,5 and 4 bar.

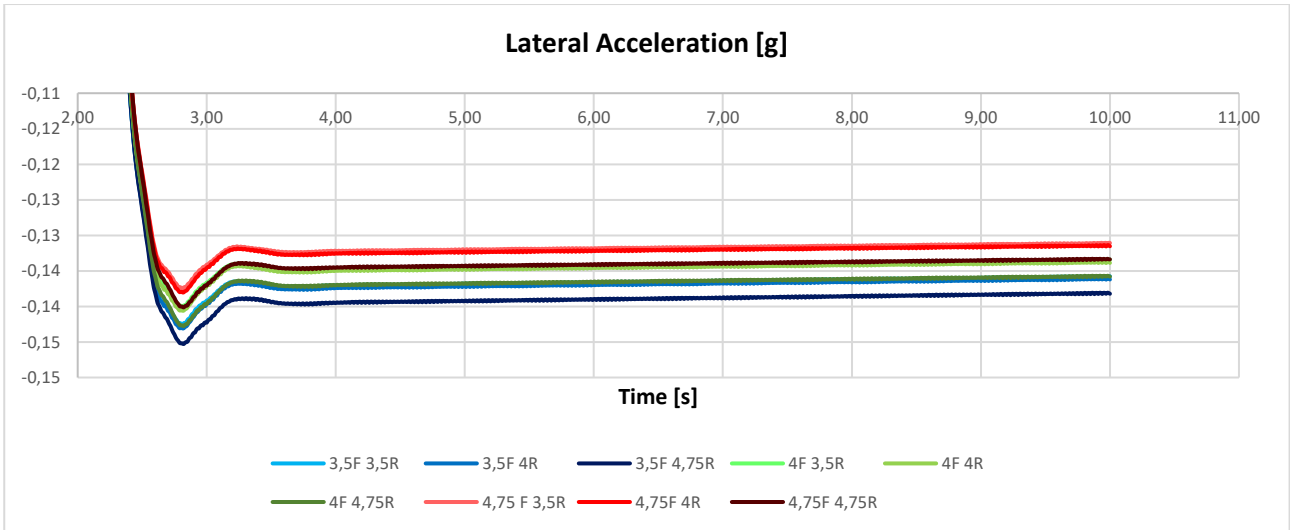


FIGURE 4.32 Lateral acceleration for different pressures (3500 kg Iveco Daily with 225/65 R16 tires)

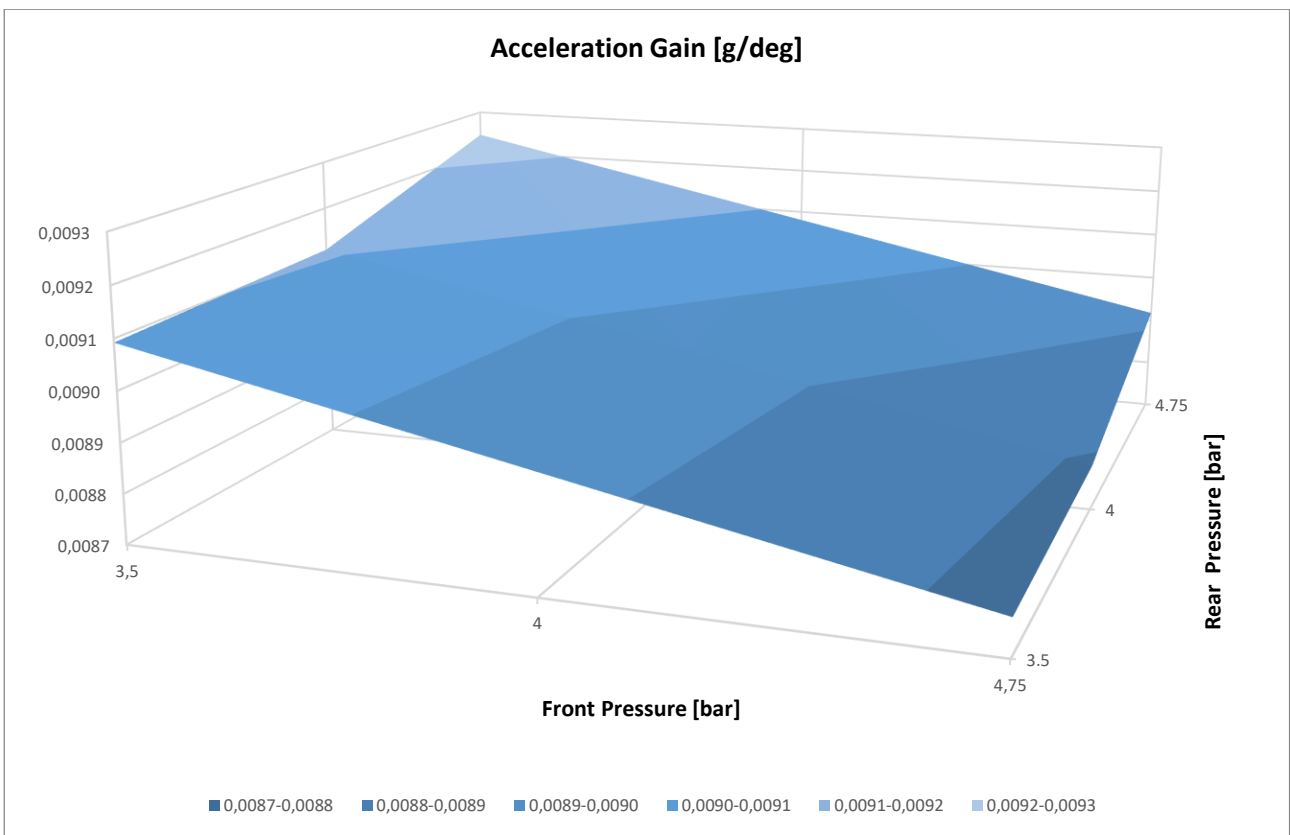


FIGURE 4.33 Acceleration Gain for different pressures (3500 kg Iveco Daily with 225/65 R16 tires)

4.2.4.2 Steering Pad

The curvature radius is 40m and the lateral acceleration increase from 0.1 to 0.7 g. The curvature gain is calculated in the same way as it was done for the Punto and confirms an increase of oversteer increasing rear pressure and decreasing front pressure for the unladen vehicle (Fig 4.34).

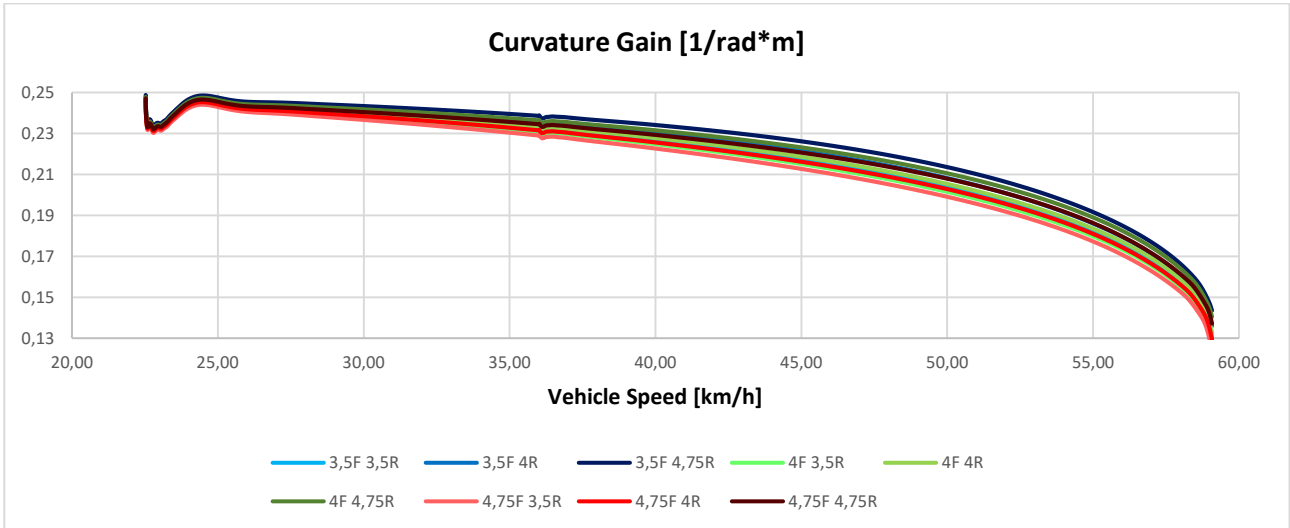


FIGURE 4.34 Curvature gain for different pressures (2356 kg Iveco Daily with 225/65 R16 tires)

At full load the vehicle is more oversteering at low speed and then understeers after 55 km/h. The effect of pressure is the same as the unladen vehicle but smaller (Fig 4.35).

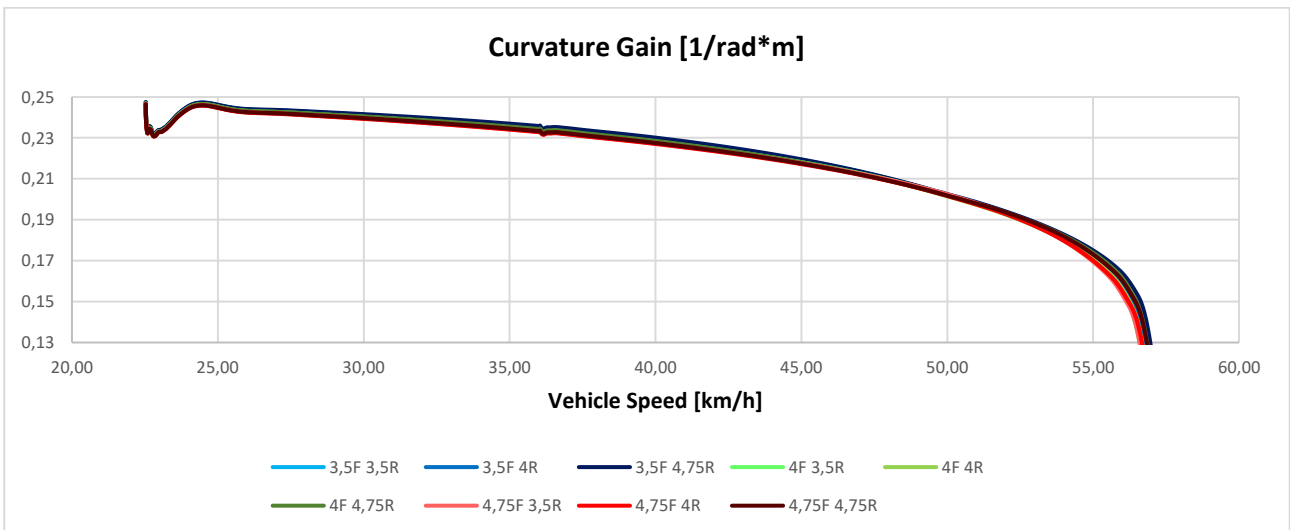


FIGURE 4.34 Curvature gain for different pressures (3500 kg Iveco Daily with 225/65 R16 tires)

4.2.5 Lateral dynamics (195/75 R16)

The same simulations were performed with the 195/75 R16 tire.

4.2.5.1 Step Steer

The tire cornering stiffness is more sensitive to load and the front right tire is near the crossing point of the curves. For the other tires a pressure increase causes a decrease of stiffness (Fig 4.36).

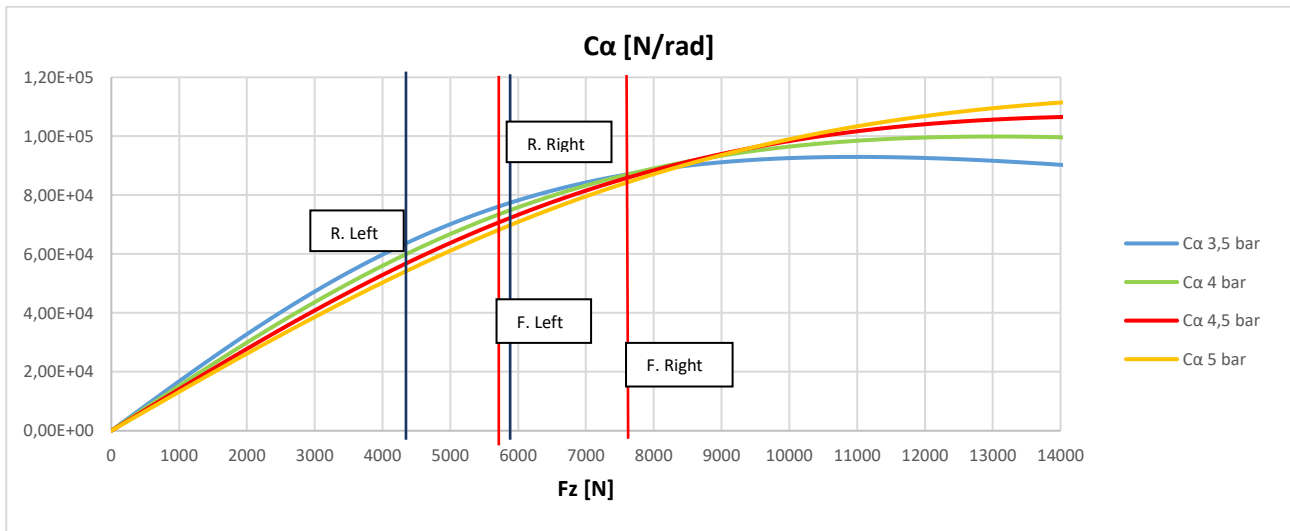


FIGURE 4.36 Cornering Stiffness in function of load for different pressures, the vertical load acting on the tires during a step steer manoeuvre is indicated (2356 kg Iveco Daily with 195/75 R16 tires)

In Fig 4.37 is plotted the effect on lateral acceleration.

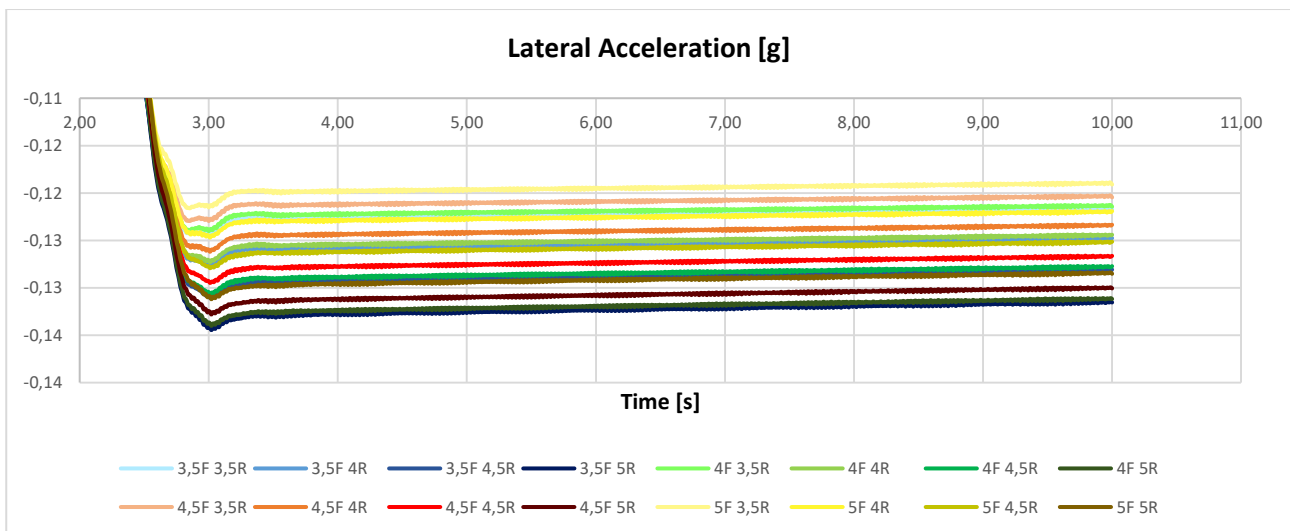


FIGURE 4.37 Lateral acceleration for different pressures (2356 kg Iveco Daily with 195/75 R16 tires)

The lateral acceleration and the acceleration gain (Fig 4.38), increase increasing rear pressure and decreasing front pressure.

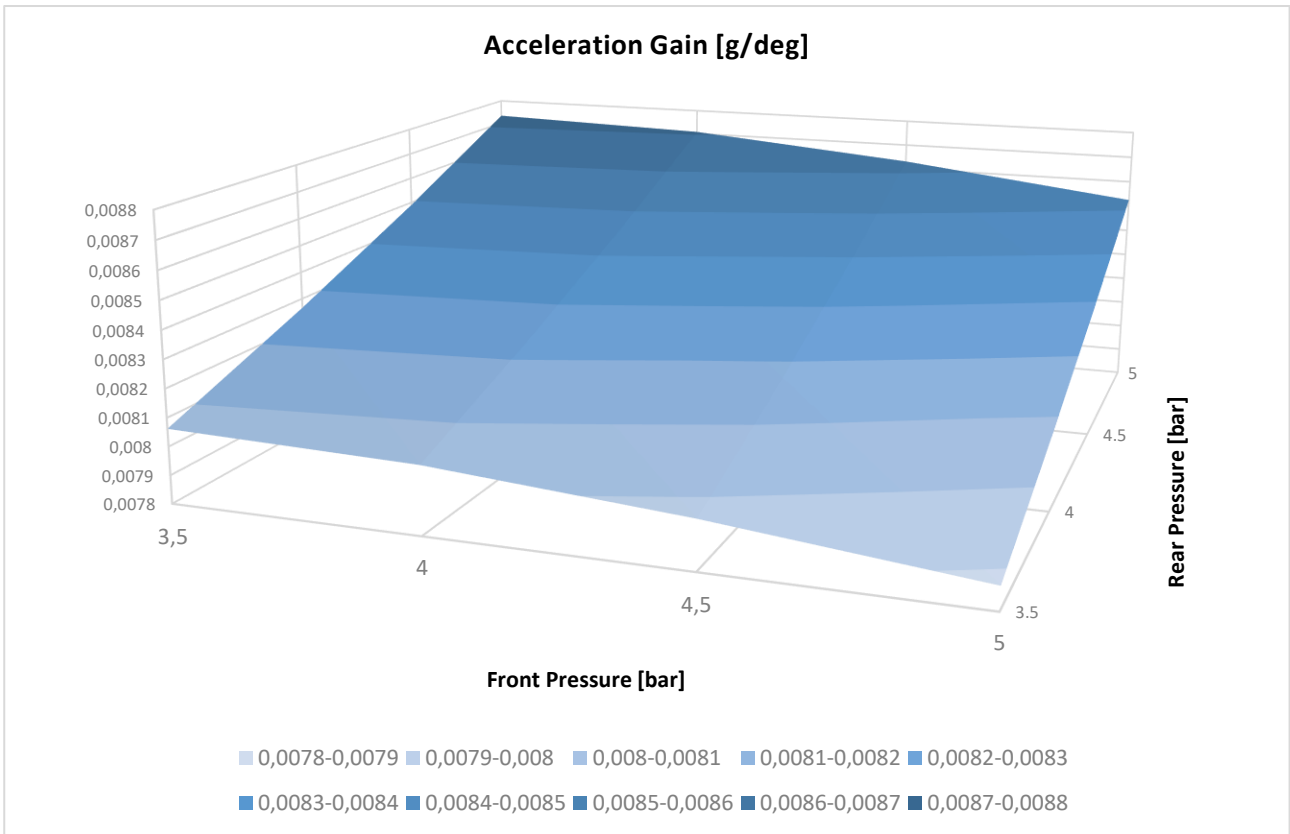


FIGURE 4.38 Acceleration Gain for different pressures (2356 kg Iveco Daily with 195/75 R16 tires)

For the vehicle in full load, the rear tires and the front right are in a load condition over the cross point for which an increase of pressure correspond to an increase of cornering stiffness. (Fig 4.39)

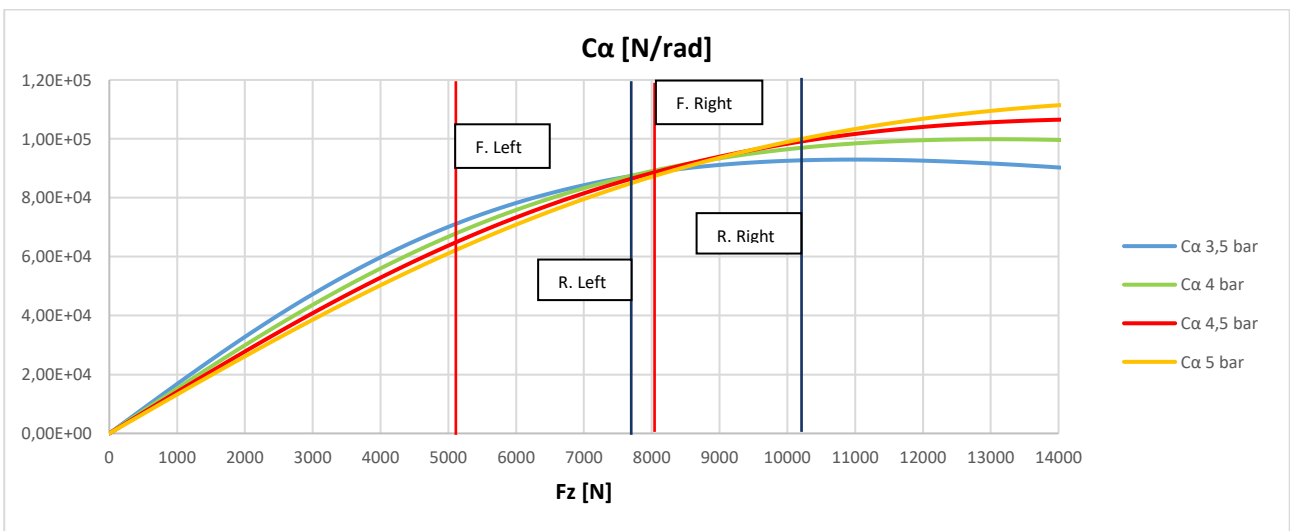


FIGURE 4.39 Cornering Stiffness in function of load for different pressures, the vertical load acting on the tires during a step steer manoeuvre is indicated (3500 kg Iveco Daily with 195/75 R16 tires)

The effect of pressure on acceleration (Fig 4.40) and acceleration gain (Fig 4.41) then is opposite to as it was for the unladen vehicle: an increase of front pressure causes oversteer, while on rear tires causes understeer.

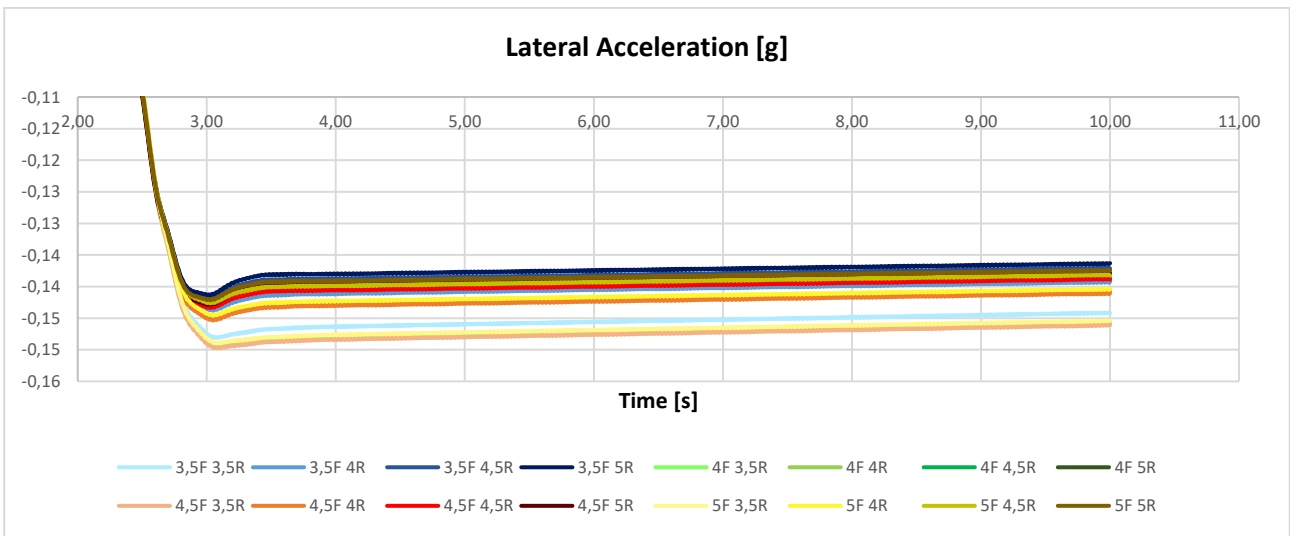


FIGURE 4.40 Lateral acceleration for different pressures (3500 kg Iveco Daily with 195/75 R16 tires)

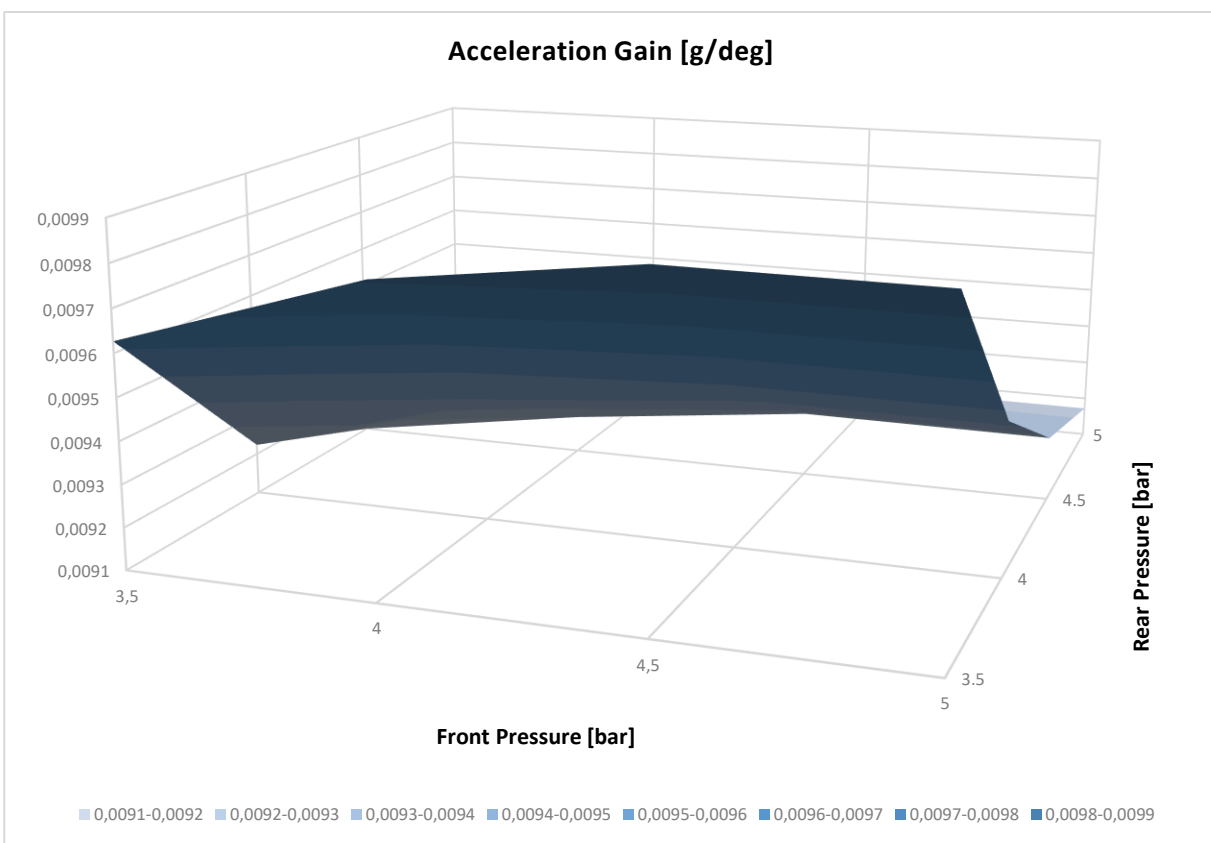


FIGURE 4.41 Acceleration Gain for different pressures (3500 kg Iveco Daily with 195/75 R16 tires)

4.2.5.2 Steering Pad

As for the step steer the front pressure change has a small effect on cornering behaviour. Increasing rear pressure instead the vehicle becomes more oversteer (Fig 4.42).

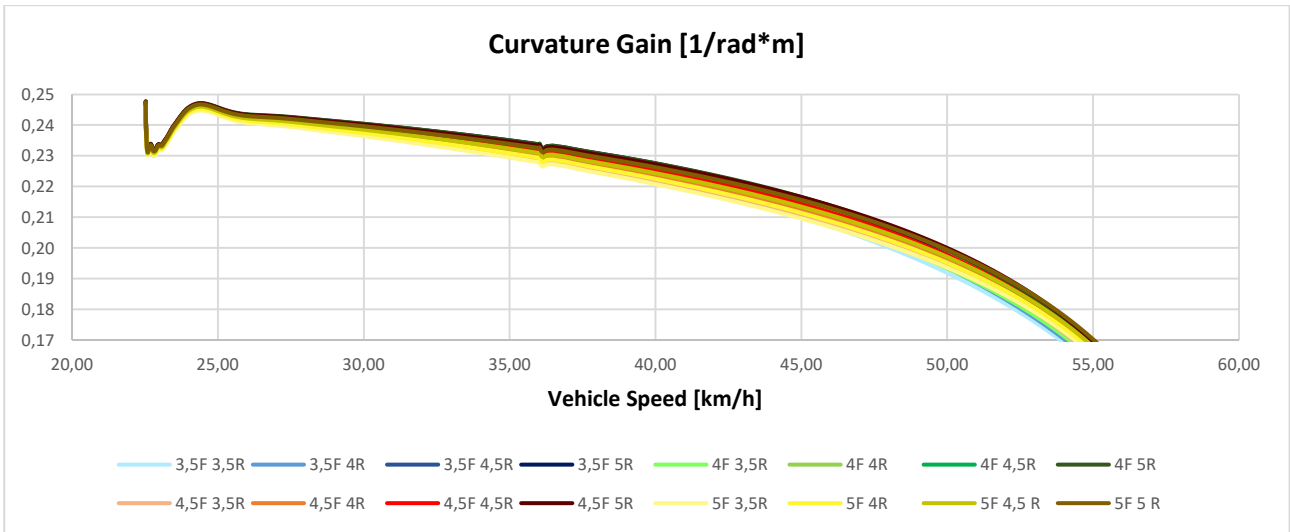


FIGURE 4.42 Curvature gain for different pressures (2356 kg Iveco Daily with 195/75 R16 tires)

At full load the understeer increase decreasing front pressure and increasing rear pressure. (Fig 4.43).

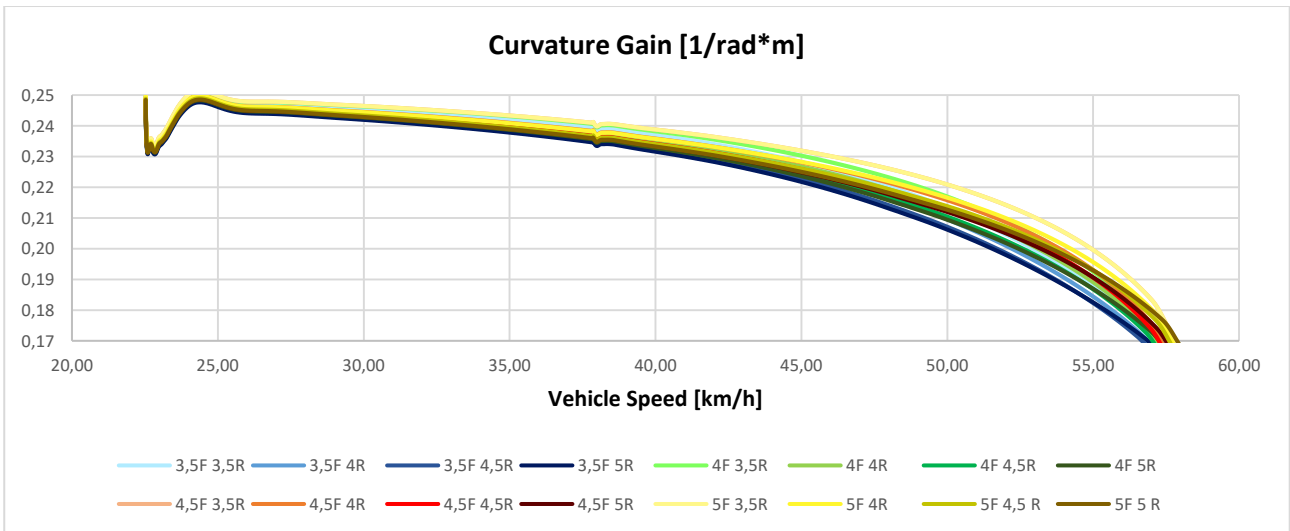


FIGURE 4.43 Curvature gain for different pressures (3500 kg Iveco Daily with 195/75 R16 tires)

4.2.6 Analysis of lateral dynamics results and literature overview

The effect of pressure on vehicle dynamics is bigger for the tire 195/75 R16, more sensitive to load changes. For this tire, the oversteering tendency of the vehicle at full loaded can be corrected decreasing front pressure and increasing rear pressure. The opposite occurs for the tire 225/65 R16 and in lower magnitude, evidencing that the effect of pressure can change in a quantitative

and qualitative way according to the tire typology. The results are consistent with the analysis through Pacejka MF that can be then used to predict the entity of the pressure effect.

For both tires no pressure combination results in dangerous oversteering conditions, allowing an integration with other strategies.

M K Al-Solihat, S Rakheja, and A K W Ahmed in [14] analysed the effect of tire pressure on the dynamics of an urban bus. The pressure change however was the same for front and rear wheels. The results showed an effect on understeer similar to the one observed for tire 195/75 R16 and an increase of yaw and roll rates at a lower pressure.

5 Vehicle Dynamics Strategies

In this section is made an overview of the possible strategies to control vehicle dynamics and their possible interaction.

5.1 Passenger Car (Grande Punto)

A pressure control can be used to optimize braking distance and to compensate the increased oversteer of the vehicle in full load.

5.1.1 Longitudinal dynamics

As it was seen in the previous chapters, a lower pressure can reduce stopping distance: the best condition is at 1,8 bar on both front and rear axle and allows a reduction of the 3,70% for the vehicle in standard B (1350 kg) and of the 3,73% for the vehicle at full load (1762 kg). The bigger stopping distance instead occurs at 2,6 bar on both axes, but the increase is of the 0,52% in standard B and 0,46% at full load.

In Fig 5.1 and 5.2 is visible the effect of pressure change for front and rear tires. The stopping distance is mainly influenced by front tires, because due to load transfer they contribute more to the total braking force. The difference is bigger for standard B load condition, due to the weight distribution that is more on the front axle. At full load the distribution is more even and limits the amount of load transfer.

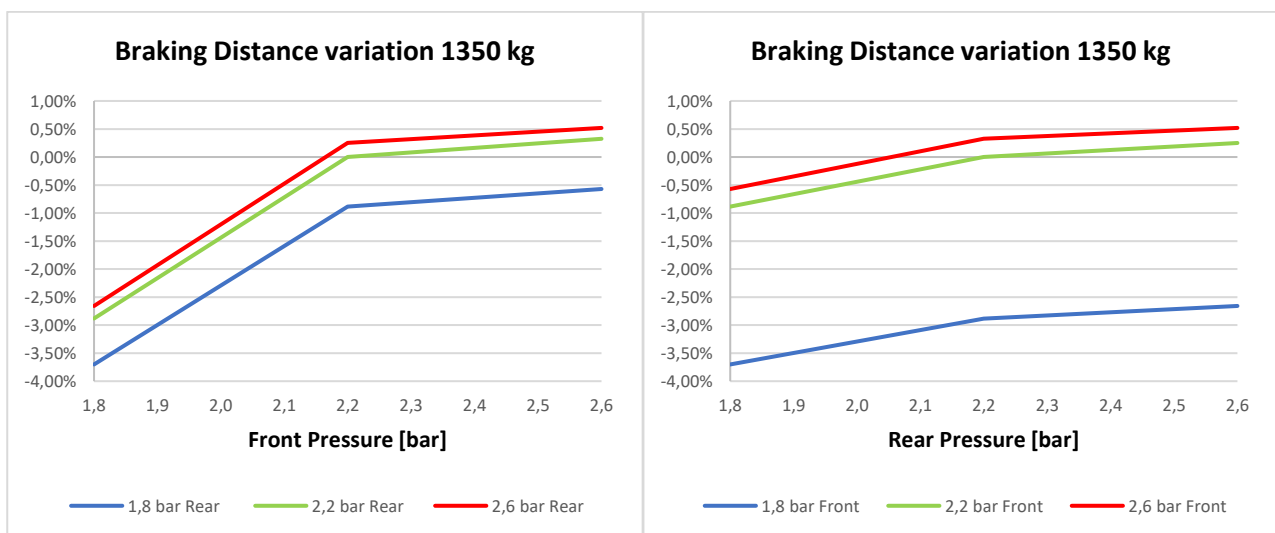


FIGURE 5.1 Braking distance variation changing front and rear tires pressure (1350 kg Grande Punto)

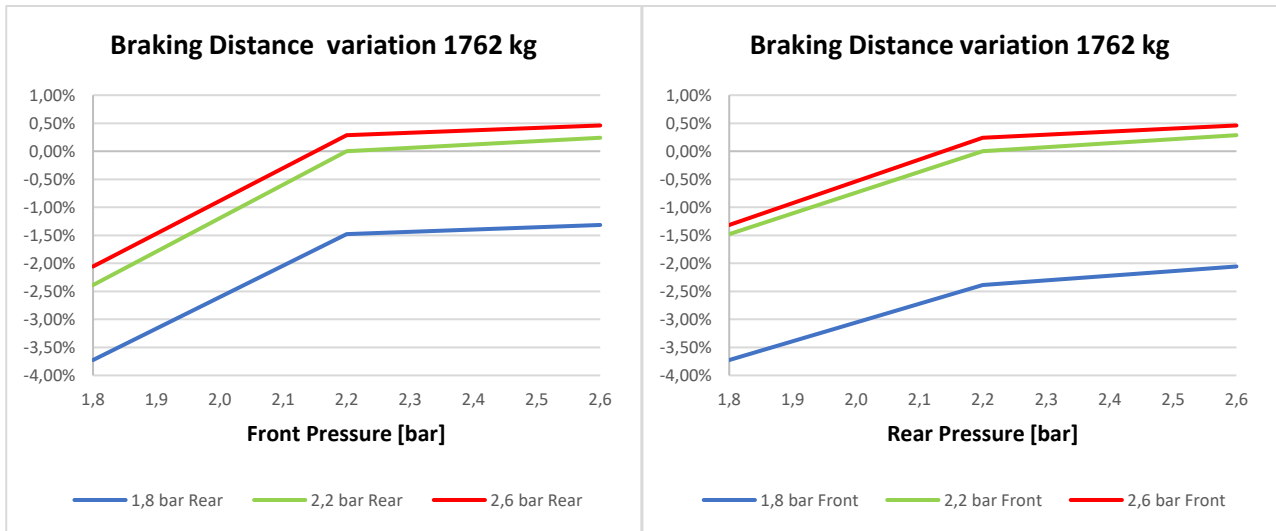


FIGURE 5.2 Braking distance variation changing front and rear tires pressure (1762 kg Grande Punto)

Inflation pressure however doesn't affect only the peak adherence, but also the correspondent slip ratio, limiting the efficiency of the ABS system. Guoxing Li, TieWang, Ruiliang Zhang, Fengshou Gu, Jinxian Shen proposed an improved slip ratio prediction that takes in account pressure change that led to improvements in the braking distance and braking time, compared to the traditional ABS controller [18] (Fig 5.3).

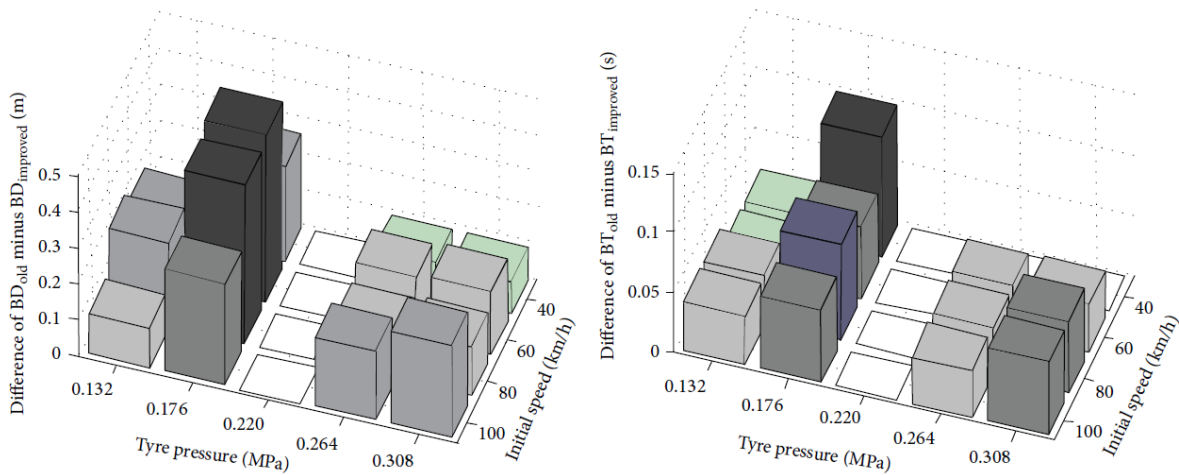


FIGURE 5.3 Improvement on braking distance (left) and braking time (right) using a slip ratio prediction that takes in account pressure change.

In conclusion, there is the opportunity of a non-negligible improvement on braking distance at lower inflation pressure and a limited worsening at higher pressures in the range considered.

5.1.2 Lateral dynamics

A tire pressure control can be used to change the steering behaviour of the vehicle. The ATPC team developed a tool capable to calculate and suggest the optimal pressure combination allowing the fully loaded vehicle to have a curvature gain as close as possible to the vehicle in standard B. The suggested pressures are 1,8 bar on front tires and 2,6 bar on rear tires (Fig 5.4). These pressures were used for steering pad manoeuvres during experimental tests in Balocco, that confirmed the trend (fig 5.5).

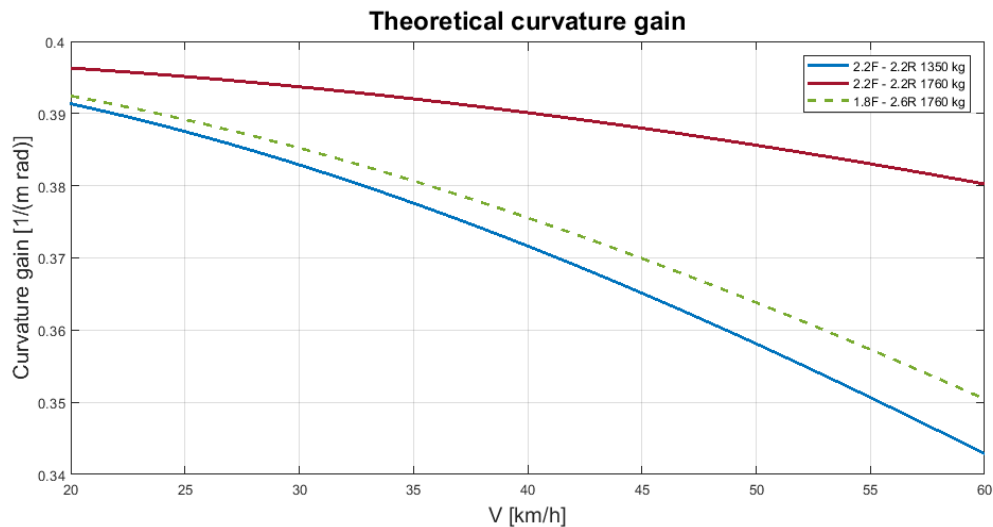


FIGURE 5.4 Theoretical curvature gain from ATPC tool for the vehicle in standard B (blue line), full load (red line) and full load changing tire pressure (green line).

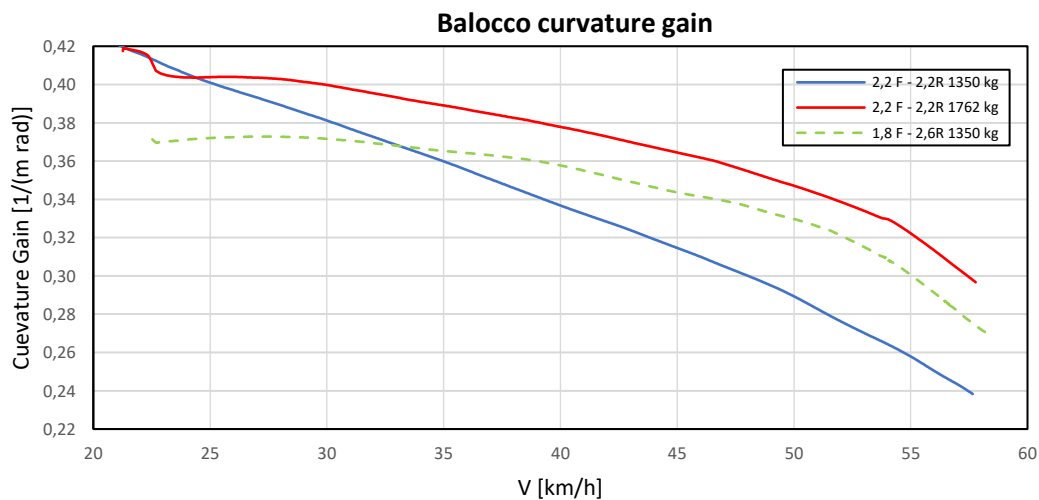


FIGURE 5.5 Experimental curvature gain for a steering pad manoeuvre for the vehicle in standard B (blue line), full load (red line) and full load changing tire pressure (green line).

The experimental tests were used to tune the simplified ADAMS model of the Punto, obtaining a steering behaviour closer to the one registered in Balocco (Fig 5.6) and increasing its validity.

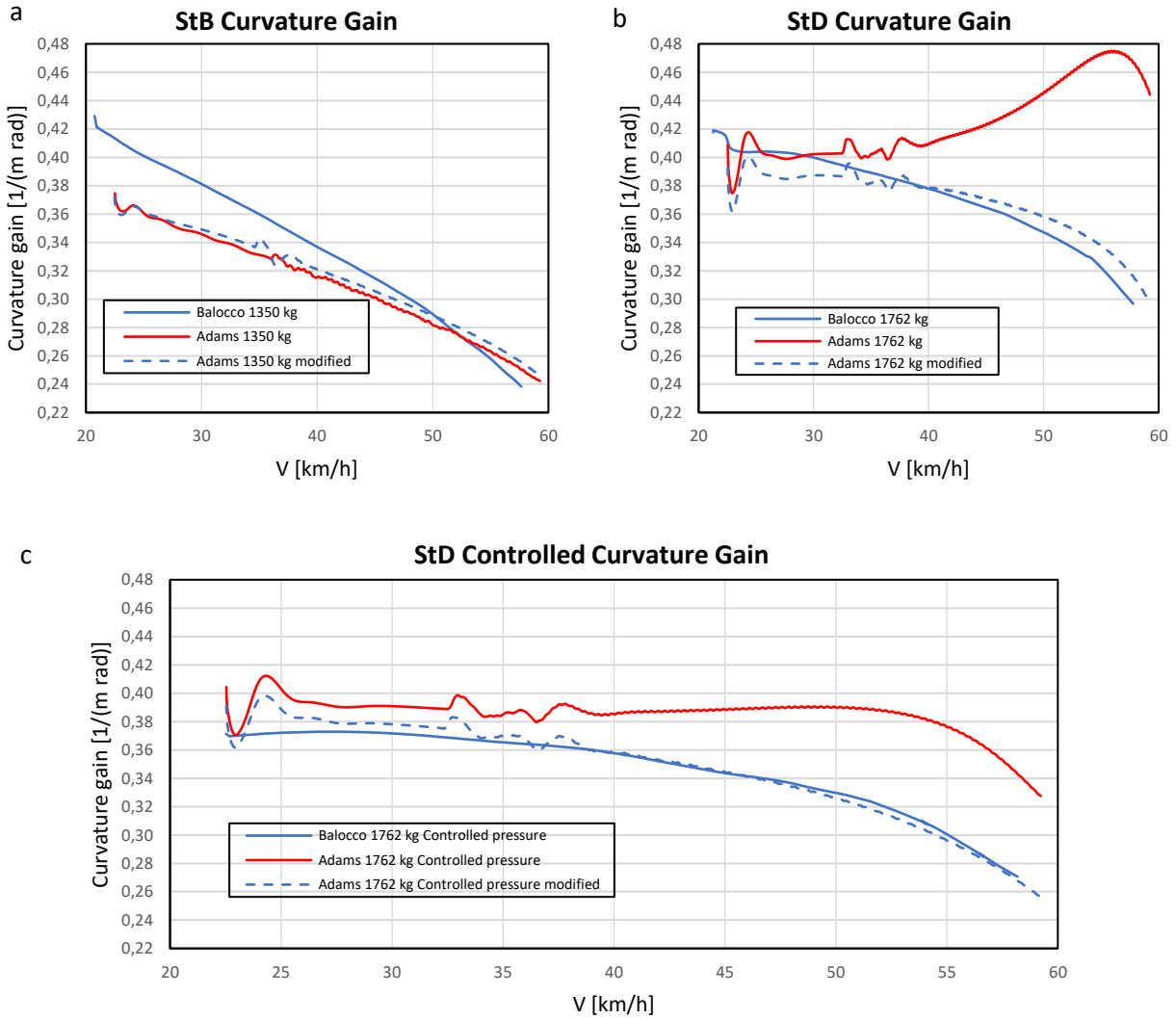


FIGURE 5.6 Curvature gain of the improved ADAMS model of the Punto for the vehicle in standard B (a), full load (b) and full load changing tire pressure (c).

The simulations with this latter model confirmed the pressures suggested by the tool. Analysing the steering pad studied in Chapter 4, the curve 1,8F 2,6R is the closest to the standard B gain.

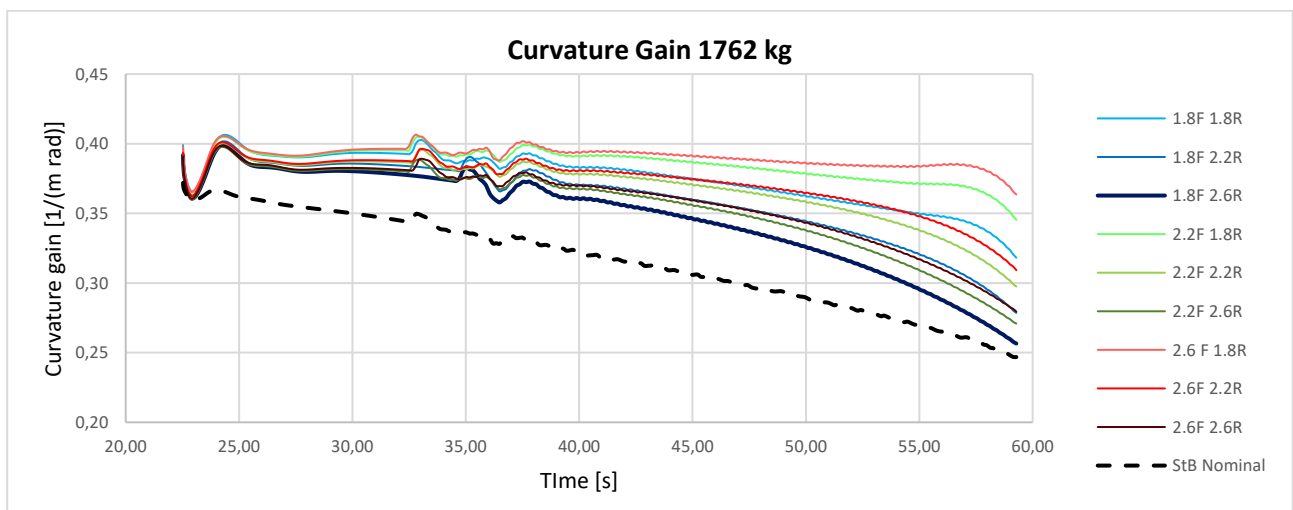


FIGURE 5.7 Curvature Gain for the Punto in full load (full lines) and in Standard B (dashed line).

In Fig 5.8 is plotted the effect of the suggested pressures for the steering pad and in Fig 5.9 for the step steer manoeuvres of chapter 4.

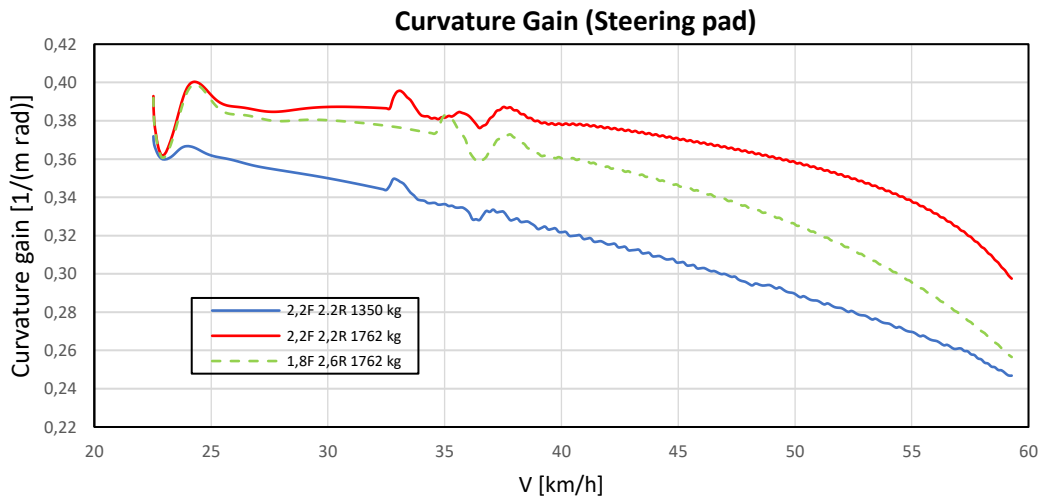


FIGURE 5.8 Curvature gain for a steering pad manoeuvre for the vehicle in standard B (blue line), full load (red line) and full load changing tire pressure (green line).

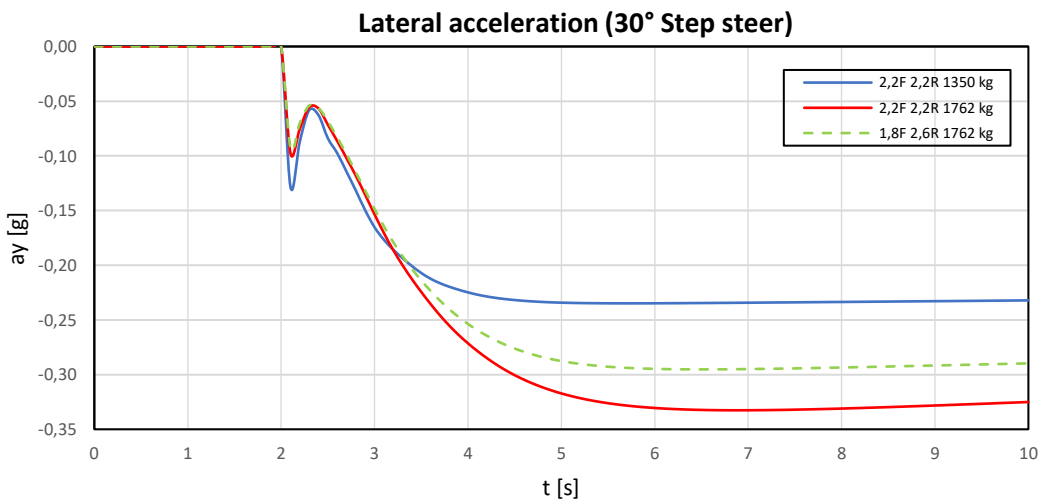


FIGURE 5.9 Lateral acceleration for a step steer manoeuvre for the vehicle in standard B (blue line), full load (red line) and full load changing tire pressure (green line).

5.1.3 Interaction between strategies

On Table 5.1 and 5.2 is indicated the effect on braking distance as variation from the performance of the vehicle at the recommended pressure of some possible strategies.

| Strategies (1350 kg) | Braking distance variation |
|-----------------------------------|----------------------------|
| Standard pressure (2,2F 2,2R) | - |
| Best braking distance (1,8F 1,8R) | -3,70% |
| Best Consumptions (2,6F 2,6R) | +0,52% |

TABLE 5.1 Effect of different strategies on braking distance for the vehicle in standard B

| Strategies (1762 kg) | Braking distance variation |
|-----------------------------------|----------------------------|
| Standard pressure (2,2F 2,2R) | - |
| Best braking distance (1,8F 1,8R) | -3,73% |
| Best Cornering (1,8F 2,6R) | -2,06% |
| Best Consumptions (2,6F 2,6R) | +0,46% |

TABLE 5.2 Effect of different strategies on braking distance for the vehicle in full load

The “cornering strategy” suggested by the tool allows also a reduction of the braking distance that is not negligible, on the other hand the use of a higher pressure to reduce rolling resistance doesn’t bring to a significant worsening of braking performance for both the load conditions.

In Fig 5.10 and 5.11 is visible the effect of the strategies on cornering performance, evidencing a not dangerous change of behaviour. At full load, the condition allowing minimum braking distance results a bit more oversteering, while the high-pressure configuration being more understeering gets closer to the condition suggested by the tool.

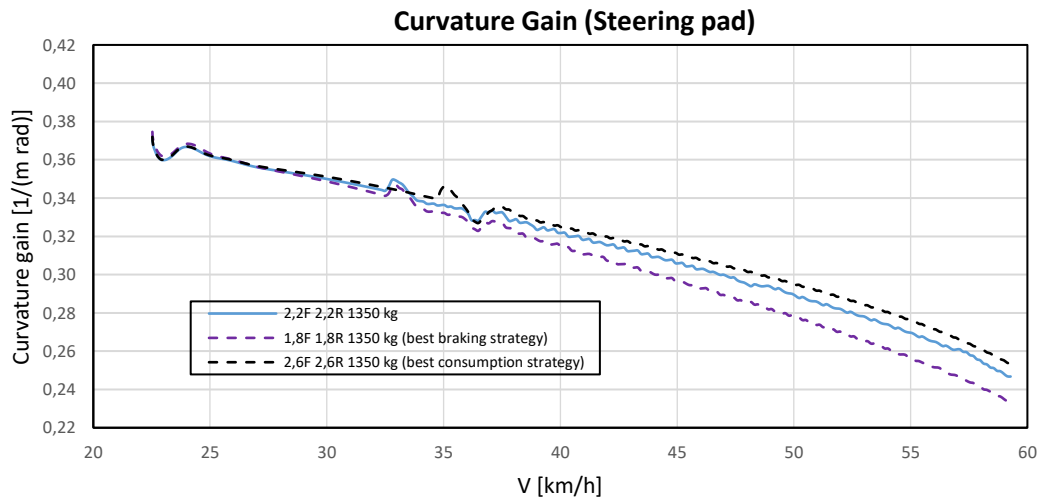


FIGURE 5.10 Curvature gain for a steering pad manoeuvre using different strategies

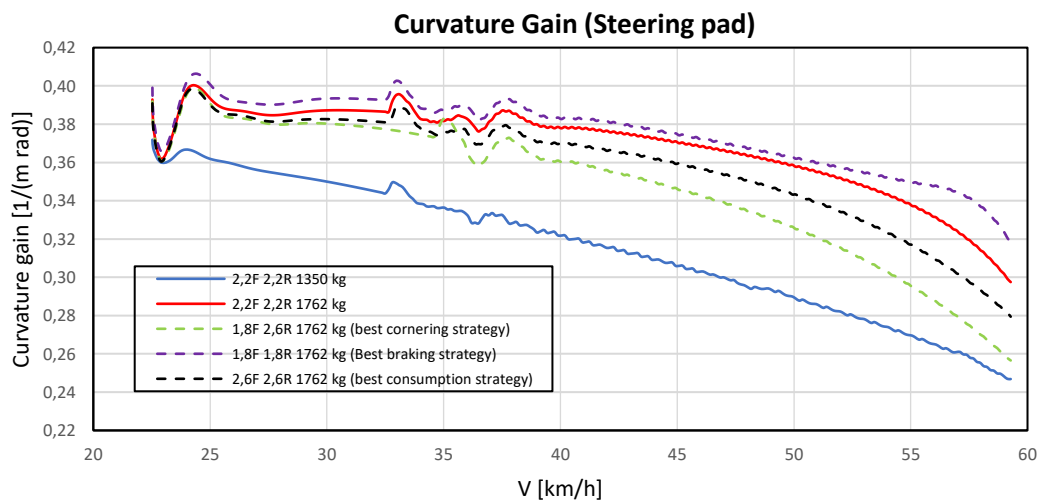


FIGURE 5.11 Curvature gain for a steering pad manoeuvre using different strategies

5.2 Light duty vehicle with 225/65 R16 tires (Daily)

5.2.1 Longitudinal dynamics

For the unladen vehicle the configuration that allows the minimum stopping distance is 3,5 bar on front axle and 4,75 on rear, allowing a reduction of the 1.01% compared to the braking at nominal inflation pressure, while at full load the optimal condition is 3,5 on all wheels with a reduction of distance of the 0.56%. In the worst condition the distance grows of the 1.11% for the unladen vehicle (4,75F 3,5R) and 0,93% at full load (4,75F 4,75R). The effect of pressure at full load is the same for both axles, while at low load is opposite for front and rear tires (Fig 5.12, Fig 5.13).

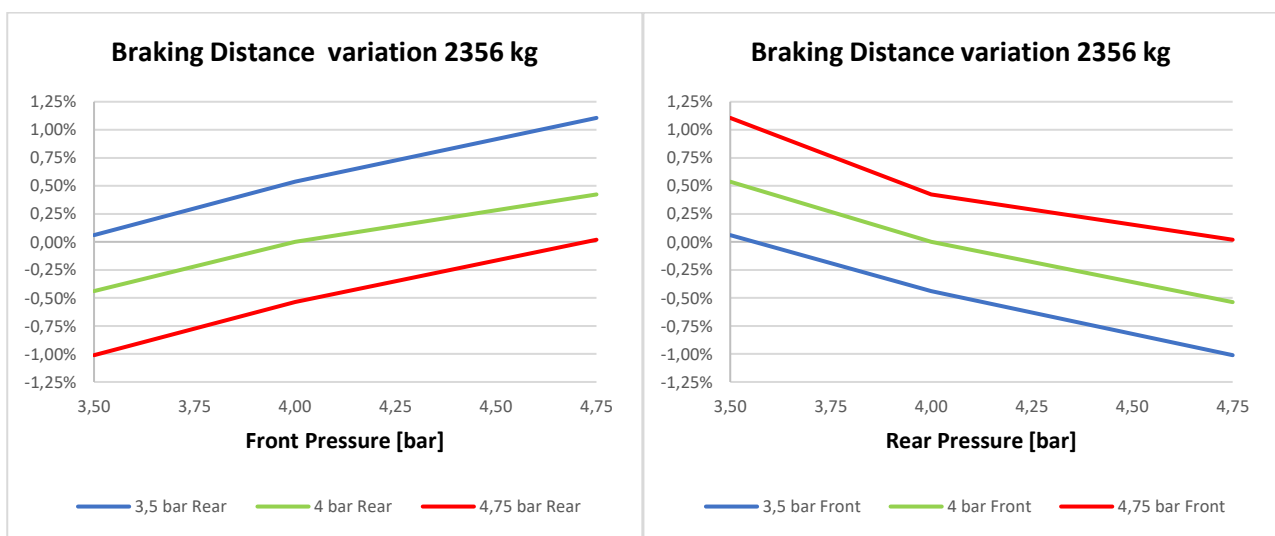


FIGURE 5.12 Braking distance variation changing front and rear tires pressure (2356 kg Daily)

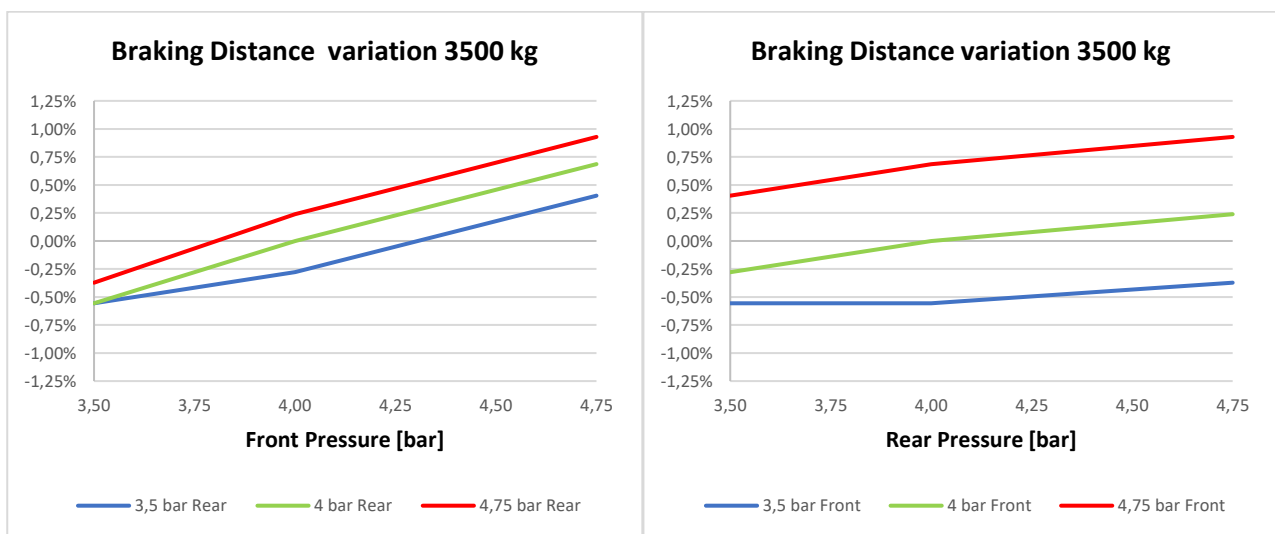


FIGURE 5.13 Braking distance variation changing front and rear tires pressure (3500 kg Daily)

5.2.2 Lateral dynamics

The tool suggests a 4,7 bar inflation pressure on front tires and 3.8 bar on rear to compensate the oversteering behaviour of the vehicle in full load (Fig 5.14). The curvature gain calculated from the steering pad manoeuvre using pressure close to the suggested shows that the vehicle in full load reaches a highly understeer condition and a low effect of pressure (Fig 5.15). The high load transfer in the manoeuvre makes tires work with a vertical force for which the cornering stiffness is not sensitive to pressure changes.

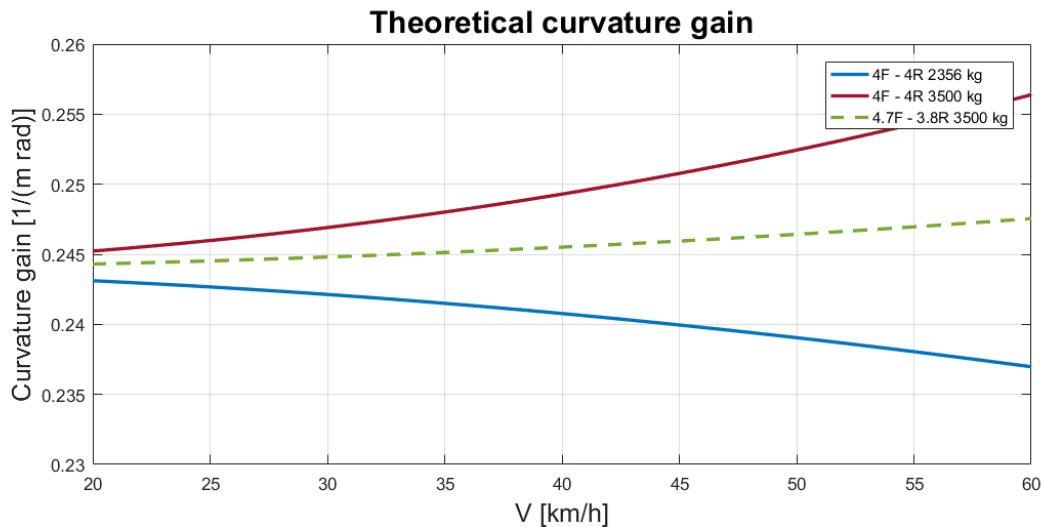


FIGURE 5.14 Theoretical curvature gain from ATPC tool for the unladen vehicle (blue line), full load (red line) and full load changing tire pressure (green line).

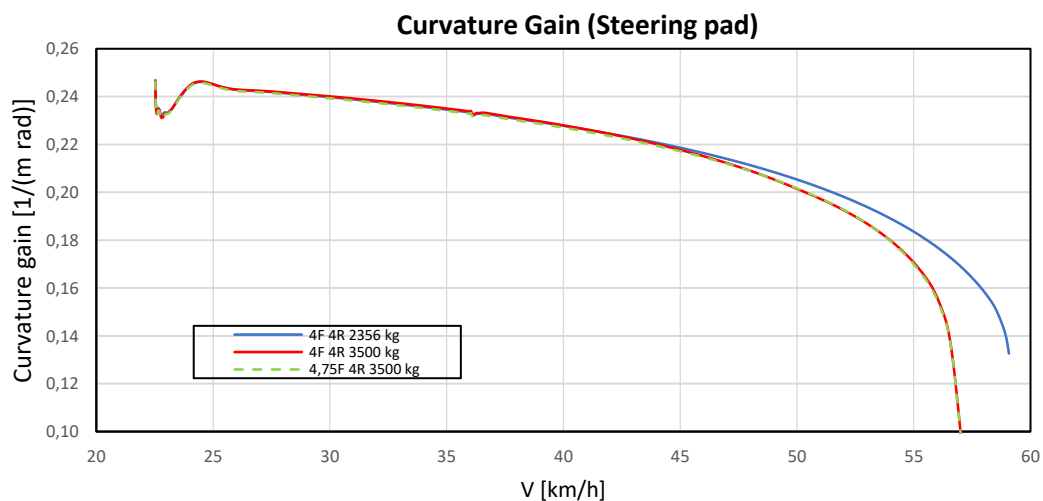


FIGURE 5.15 Curvature gain for a steering pad manoeuvre for the unladen vehicle (blue line), full load (red line) and full load changing tire pressure (green line).

Considering a step steer (15 deg), the vehicle doesn't reach that level of understeer and the results match more the ATPC tool suggestion (Fig 5.16): a more oversteer full loaded vehicle (bigger acceleration at same steering angle) that becomes more understeer with 4,75 bar on front tires. The tool suggested 3,8 bar on rear tires: the curve at 3,5 bar is really close to the 4 bar but actually results the more effective.

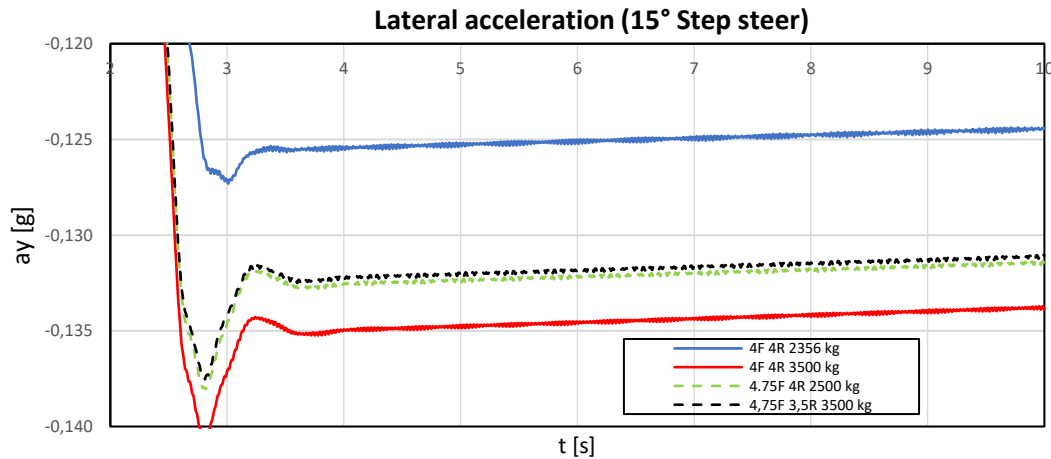


FIGURE 5.16 Lateral acceleration for a step steer manoeuvre for the vehicle in standard B (blue line), full load (red line) and full load changing tire pressure (dashed lines).

5.2.3 Interaction between strategies

The relative impact on braking distance is less than on the Punto, this is good for low consumption strategies that see a braking distance increase that is absolutely negligible for the unladen vehicle (Table 5.3) and safe in full load (Table 5.4). The cornering strategy causes also a contained distance increase.

| Strategies 2356 kg | Braking distance variation |
|------------------------------------|----------------------------|
| Standard pressure (4F 4R) | - |
| Best braking distance (3,5F 4,75R) | -1,01% |
| Best Consumptions (4,75F 4,75R) | +0,02% |

TABLE 5.3 Effect of different strategies on braking distance for the unladen vehicle

| Strategies 3500 kg | Braking distance variation |
|-----------------------------------|----------------------------|
| Standard pressure (4F 4R) | - |
| Best braking distance (3,5F 3,5R) | -0,56% |
| Best Cornering (4,75F 3,5R) | +0,40% |
| Best Consumptions (4,75F 4,75R) | +0,93% |

TABLE 5.4 Effect of different strategies on braking distance for the vehicle in full load

The braking and consumption strategies cause an increase of oversteer for the unladen vehicle remaining however in safety (Fig 5.17).

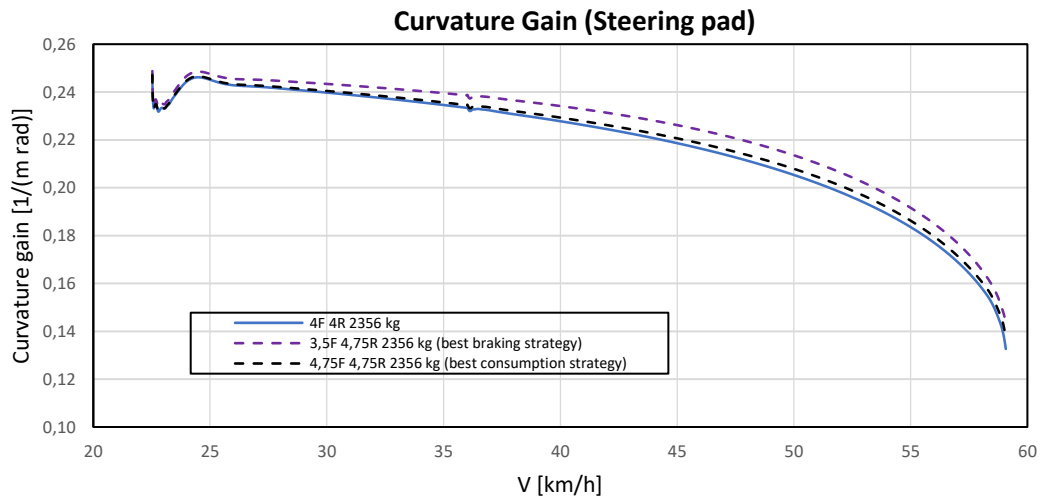


FIGURE 5.17 Curvature gain for a steering pad manoeuvre using different strategies

The effect at full load is clearer observing a less demanding manoeuvre like the step steer on Fig 5.18. As it was observed on the Punto, the optimal braking strategy causes an increase of oversteer, while the high pressure configuration reduces it (even if it is of a small quantity).

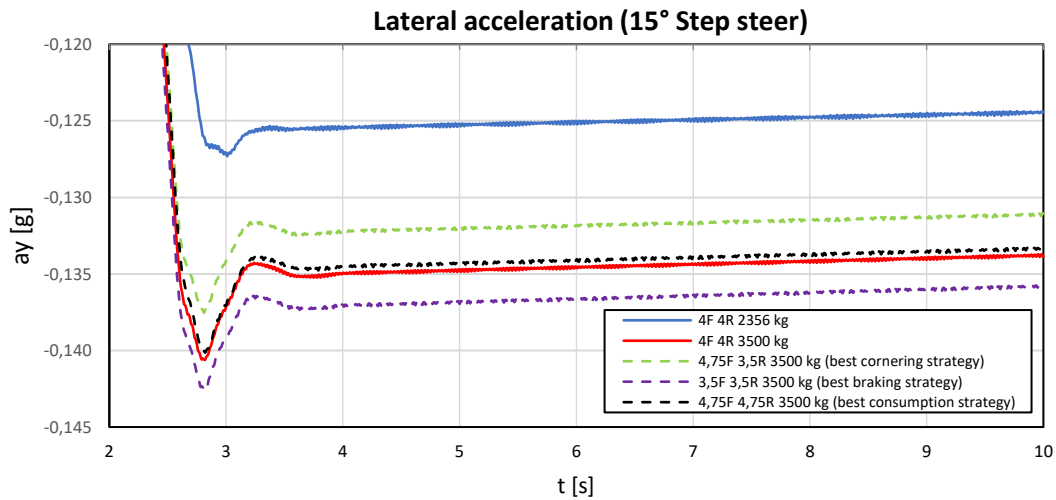


FIGURE 5.18 Lateral acceleration for a step steer manoeuvre using different strategies

5.3 Light duty vehicle with 195/75 R16 tires (Daily)

5.3.1 Longitudinal dynamics

The configuration that allows the minimum stopping distance is 4 bar on front axle and 4,5 on rear for the unladen vehicle: the distance is however reduced of the 0,18%. At full load instead, the optimal condition is 3,5 on all wheels like it was for the 225/65 R16 tire: the distance reduction is of the 0,70%. In the worst condition the distance grows of the 0,55% for the unladen vehicle (5F 3,5R) and 1,03% at full load (5F 4,5R). The effect of pressure is bigger at full load, especially for the front tires (Fig 5.19, Fig 5.20).

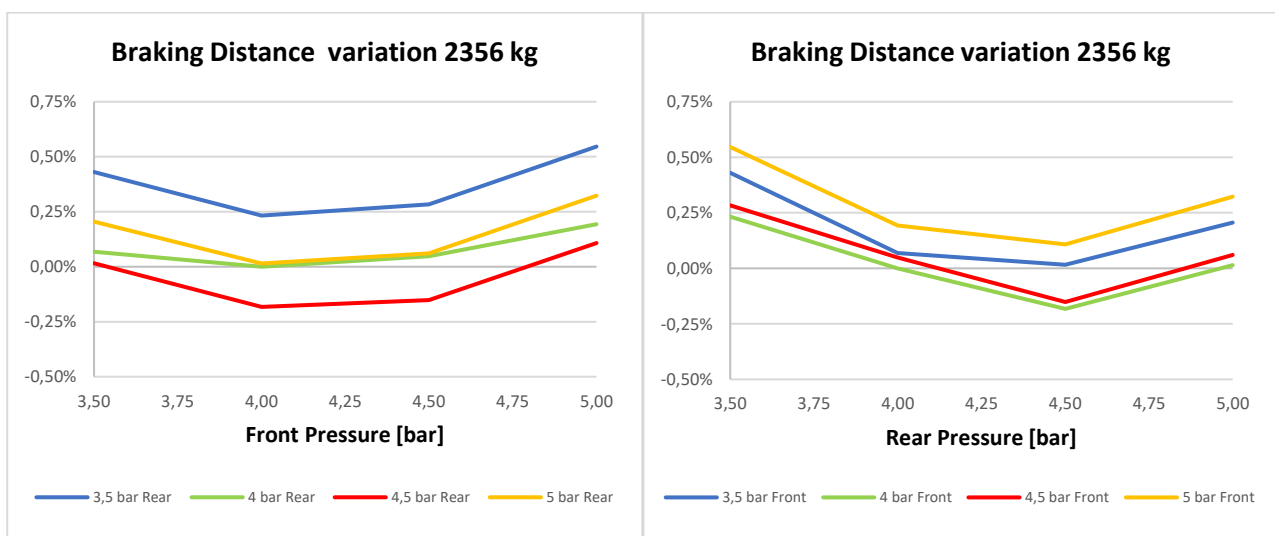


FIGURE 5.19 Braking distance variation changing front and rear tires pressure (2356 kg Daily)

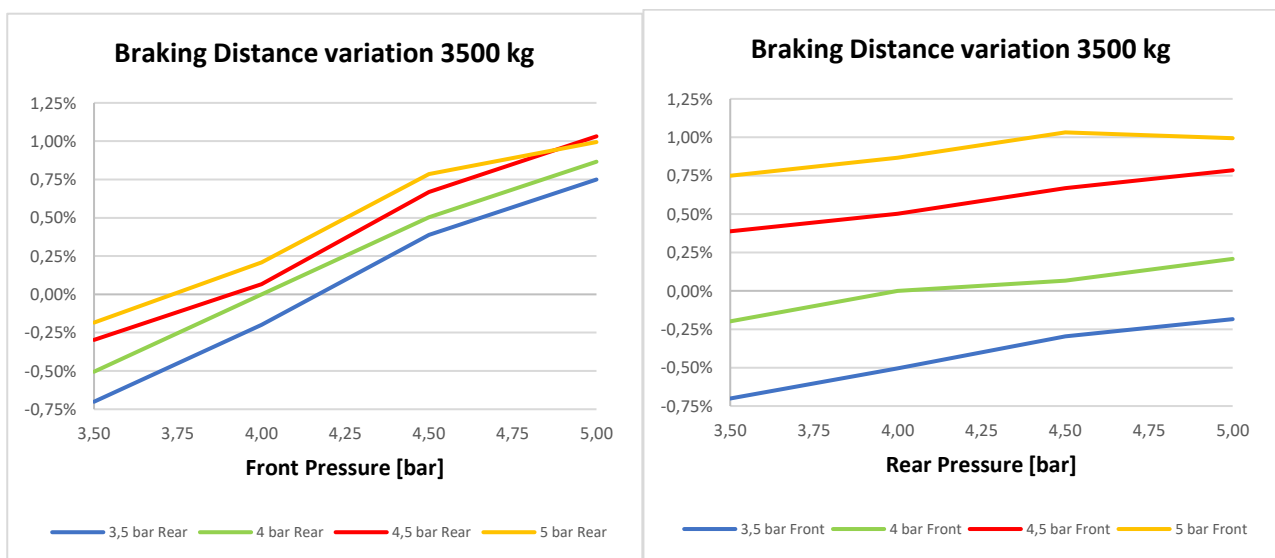


FIGURE 5.20 Braking distance variation changing front and rear tires pressure (3500 kg Daily)

5.3.2 Lateral dynamics

The pressure configuration suggested by the tool is 5 bar for all tires (Fig 5.21). The curvature gain calculated from the steering pad manoeuvre instead shows a better behaviour at 3,5 bar on front tires and 5 on rear (Fig 5.22).

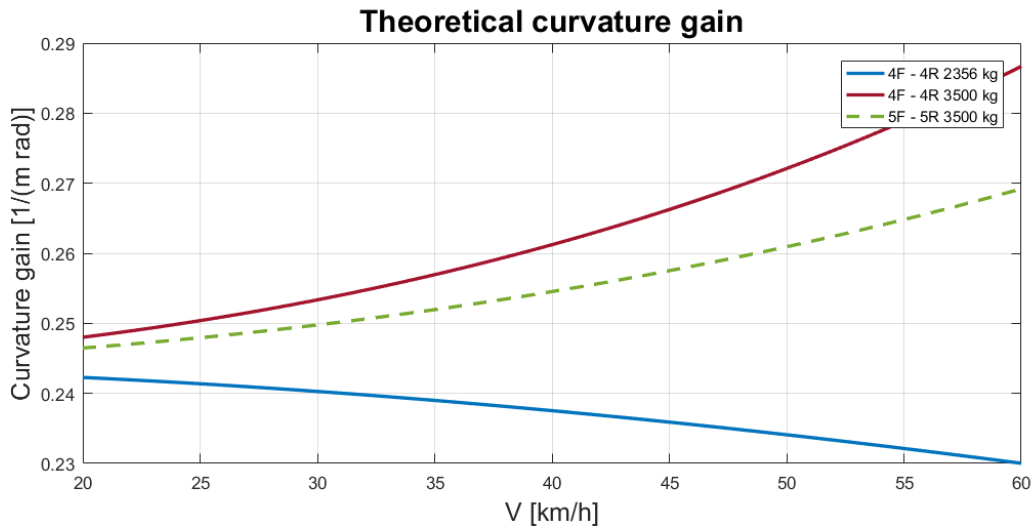


FIGURE 5.21 Theoretical curvature gain from ATPC tool for the unladen vehicle (blue line), full load (red line) and full load changing tire pressure (green line).

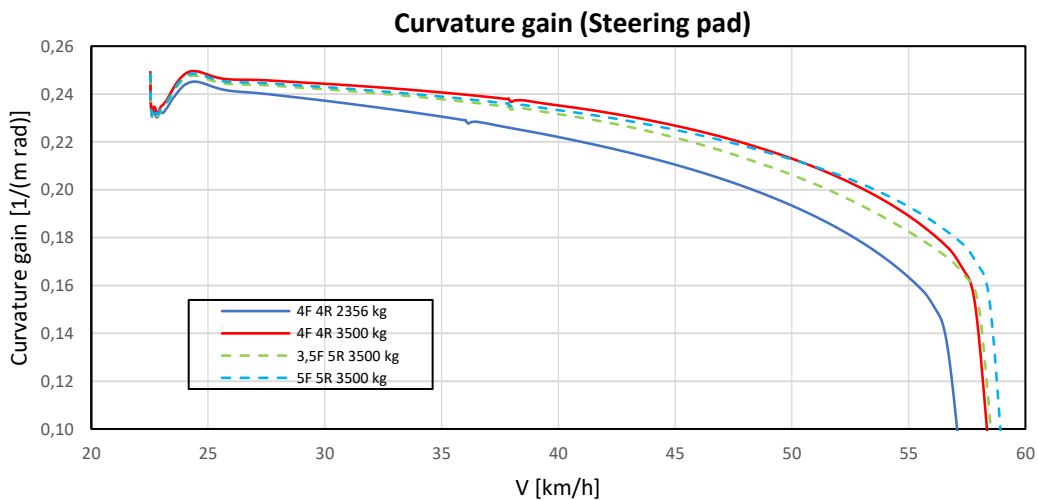


FIGURE 5.22 Curvature gain for a steering pad manoeuvre for the unladen vehicle (blue line), full load (red line) and full load changing tire pressure (dashed lines).

The previous trend is confirmed also for the step steer (Fig 5.23): the 3,5F 5R configuration is the most understeer and permits to get closer to the behaviour of the unladen vehicle. The model used in the tool doesn't consider the presence of suspensions and their contribution to the load transfer: in this case a more complex model is needed to predict the behaviour of the vehicle.

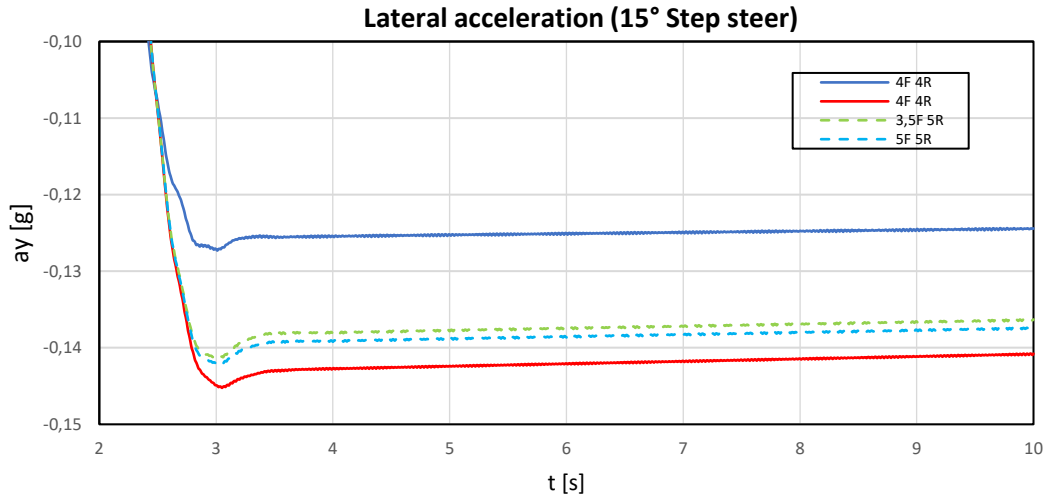


FIGURE 5.23 Lateral acceleration for a step steer manoeuvre for the vehicle in standard B (blue line), full load (red line) and full load changing tire pressure (dashed lines).

5.3.3 Interaction between strategies

As for the 225/65 R16 tire, the distance variation is quite low, for the unladen vehicle, the reduction that can be obtained doesn't justify the use of a strategy aimed to braking performance. Higher pressures instead, besides reducing rolling resistance, allow a small distance increase (5 bar) or even a reduction (4,5 bar) (Table 5.5).

| Strategies 2356 kg | Braking distance variation |
|---------------------------------|----------------------------|
| Standard pressure (4F 4R) | - |
| Best braking distance (4F 4,5R) | -0,18% |
| Lower Consumptions (4,5F 4,5R) | -0,15% |
| Best Consumptions (5F 5R) | +0,32% |

TABLE 5.5 Effect of different strategies on braking distance for the unladen vehicle

In full load, the variations are bigger but not so much to create dangerous conditions. The cornering strategy allows also a reduction of braking distance.

| Strategies 3500 kg | Braking distance variation |
|-----------------------------------|----------------------------|
| Standard pressure (4F 4R) | - |
| Best braking distance (3,5F 3,5R) | -0,70% |
| Best Cornering (3,5F 5R) | -0,18% |
| Lower Consumptions (4,5F 4,5R) | +0,67% |
| Best Consumptions (5F 5R) | +0,99 |

TABLE 5.6 Effect of different strategies on braking distance for the vehicle in full load

As it was observed with the first tire, the use of the considered strategies causes a small increase of oversteer for the unladen vehicle (Fig 5.24, Fig 5.25).

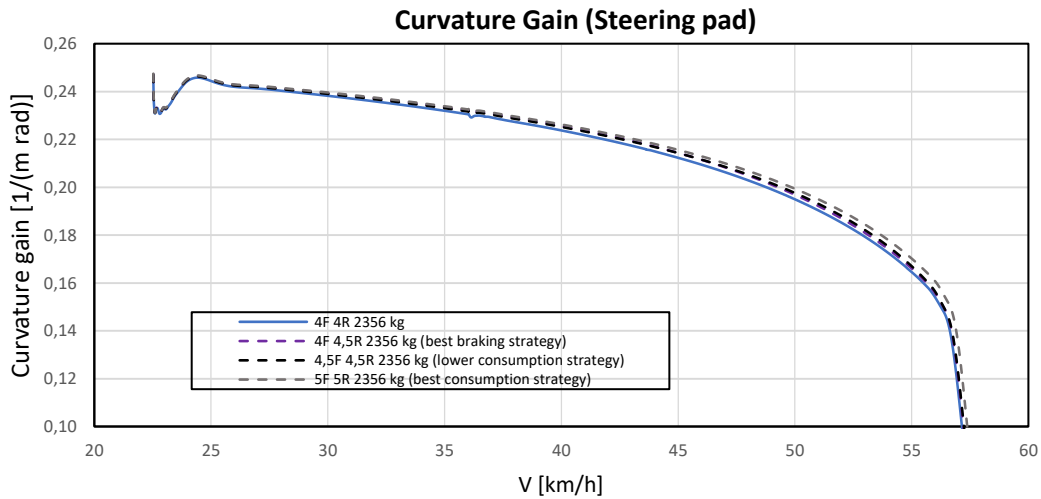


FIGURE 5.24 Curvature gain for a steering pad manoeuvre using different strategies

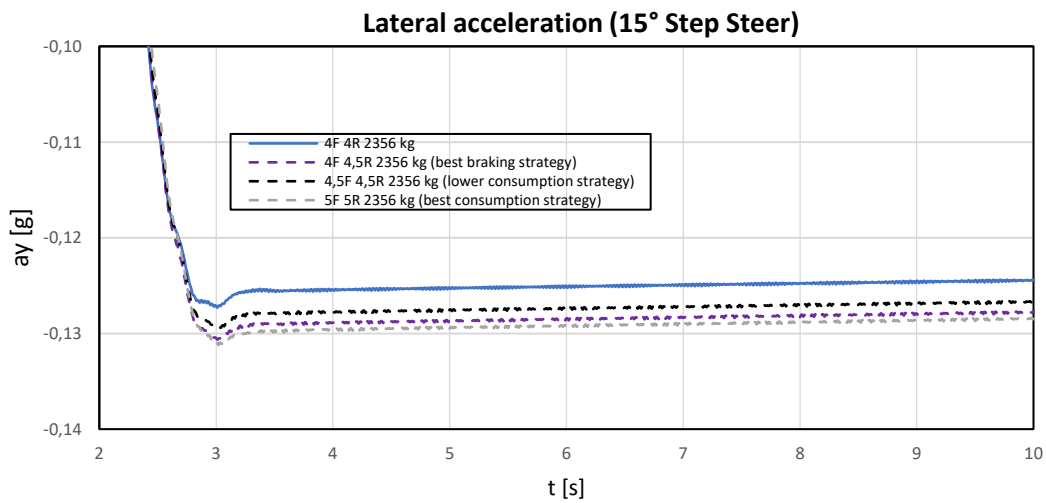


FIGURE 5.25 Lateral acceleration for a step steer manoeuvre using different strategies

For the vehicle in full load instead, the braking and consumption strategies reduces oversteer, that instead increase for the optimal braking strategy (Fig 5.27).

As it is visible from Fig 5.26 the steering pad manoeuvre is too demanding for any of the strategy chosen and the vehicle understeers losing front axle traction. However, at 5 bar this occurs at a slightly higher speed.

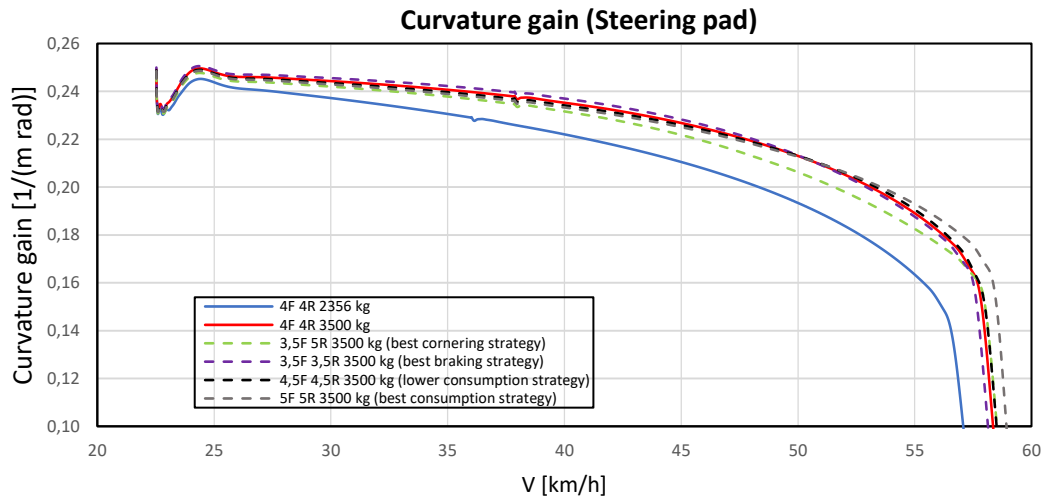


FIGURE 5.26 Curvature gain for a steering pad manoeuvre using different strategies

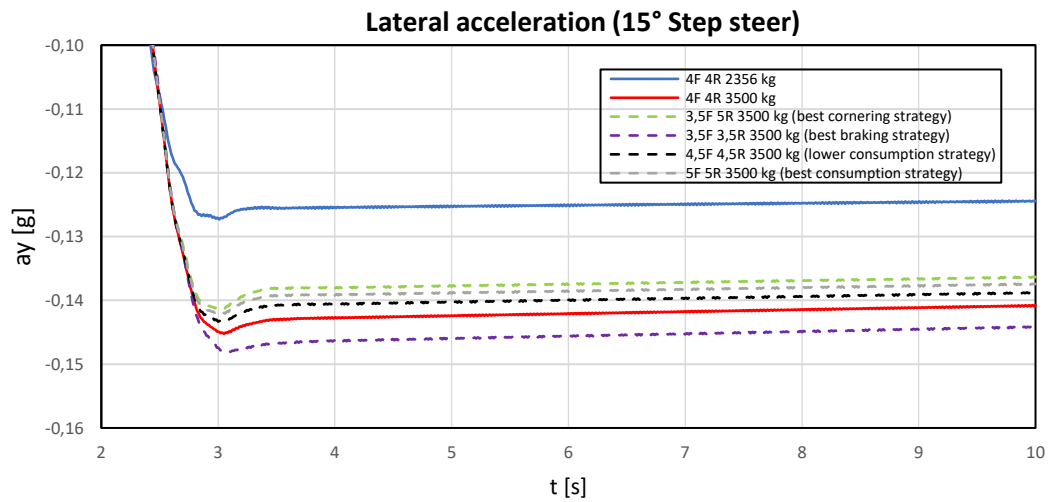


FIGURE 5.27 Lateral acceleration for a step steer manoeuvre using different strategies

6 Conclusions

Inflation pressure has an impact on the performance of the tire, in particular on adherence (allowing to choose pressure configurations to reduce the braking distance of the vehicle) and cornering stiffness, that recalling the definition of understeer factor ($K_{us} = \frac{mg}{l^2} \left(\frac{b}{c_1} - \frac{a}{c_2} \right)$), permit to act on cornering behaviour, compensating the variations caused by increased load.

In the range considered no pressure configuration caused dangerous conditions: the increase of braking distance is always below the 1% while about cornering behaviour deviations from the nominal condition are registered but without an excessive increase of oversteer or understeer even for demanding manoeuvres. On the contrary for the Punto, stopping distance can be reduced of almost 4%.

The effect of pressure change however depends on the characteristics of the single tire: mainly to their sensitivity to load change. For this reason, to have predictable results, a previous characterization of the tire is needed. A step further could be the determination of Pacejka parameters directly from on road data [19], that could allow an adaptation of the ATPC control to different tires. The use of the version 6 of the magic formula could allow a more complete spectrum of the effects of pressure and eliminate the need to have a set of parameters for each inflation condition. Moreover a FTire model could take also in account stresses and dissipations in the contact patch.

A tool based on a rigid model of the vehicle permits to calculate the ideal pressure configuration after load change (determined by a mass estimation model developed by the team). The model is effective for the Grande Punto, while overestimate the oversteering behaviour of the Daily. It must be considered in fact that the curvature gain is calculated in steady state and that the effect of suspension is neglected. So a more complex model is needed at the expense of increased computational power, in addition it should be integrated to an actual manoeuvre simulation (e.g. a step steer) to overcome the limitations of the steady state computation of the curvature gain.

7 Bibliography

- [1] NHTSA, Research Note – “Tire Pressure Special Study” - Washington, D.C., August 2001.
- [2] Michelin, Kwik Fit - “Four in 10 motorists using “dangerous” or “very dangerous” tyres” - Michelin - Kwik fit, 2018.
- [3] Stefano D’Ambrosio, Roberto Vitolo – “Potential impact of active tire pressure management on fuel consumption reduction in passenger vehicles” – Proc IMechE Part D: J Automobile Engineering 1–15 - 2018.
- [4] G. Genta, L. Morello – “The Automotive Chassis, Volume 1: Components Design”–Springer, 2009.
- [5] Edward M. Kasprzak, Kemper E. Lewis, Douglas L. Milliken - “Inflation Pressure Effects in the Nondimensional Tire Model” - Society of Automotive Engineers, Inc 2006.
- [6] R. A. Douglas, W. D. Woodward, A. Woodside – “Road contact stresses and forces under tires with low inflation pressure” - Article in Canadian Journal of Civil Engineering · February 2011.
- [7] Pallavi Pant, Roy M. Harrison - “Estimation of the contribution of road traffic emissions to particulate matter concentrations from field measurements: A review”- Elsevier Ltd 2013.
- [8] Adachi, K., Tainosho, Y. - “Characterization of heavy metal particles embedded in tire dust” - Environment International 30 (8) 2004.
- [9] J. Reimpell H. Stoll, J. W. Betzler – “The Automotive Chassis: Engineering Principles” - Elsevier Science 2001.
- [10] H. B. Pacejka – “Tyre And Vehicle Dynamics” – Elsevier,2006.
- [11] I. J.M. Besselink , A. J.C. Schmeitz & H. B. Pacejka – “An improved Magic Formula/Swift tyre model that can handle inflation pressure changes”, - Vehicle System Dynamics, 48:S1, 337-352, DOI: 10.1080/00423111003748088, 2010.
- [12] G. Genta, L. Morello – “The Automotive Chassis, Volume 2: System Design” – Springer, 2009.
- [13] Fancher, P. S. (Ed.) “Descriptive parameters used in analysing the braking and handling of heavy trucks”– measurements of the longitudinal and lateral traction properties of truck tyres, vol. 3, Data volume III (Notebook III). Final report UM-HSRI-81-19-3-4, University of Michigan, Highway Safety Research Institute, 1981, pp. 357–373.
- [14] M K Al-Solihat, S Rakheja, and A K W Ahmed – “Influence of tyre pressure on an urban bus transient and steady state handling performance” - Proceedings of the Institution of Mechanical Engineers, Part D: Journal of Automobile Engineering, vol. 224, no. 7, pp. 893-908, 2010.
- [15] Vladimír Rievaj, Ján Vrábek, Anton Hudák – “Tire Inflation Pressure Influence on a Vehicle Stopping Distances” - International Journal of Traffic and Transportation Engineering 2013.

- [16] D. Hadryś, T. Węgrzyn, and M. Miros, “The influence of various pressures in pneumatic tyre on braking process of car with anti-lock braking system,” *Transport problems*, vol. 3, pp. 85-94, 2008.
- [17] Kurt M. Marshek and Jerry F. Cuderman II Mark J. Johnson - “Performance of Anti-Lock Braking System Equipped Passenger Vehicles – Part III: Braking as a Function of Tire Inflation Pressure” - Society of Automotive Engineers, Inc 2002.
- [18] Guoxing Li, TieWang, Ruiliang Zhang, Fengshou Gu, Jinxian Shen - “An Improved Optimal Slip Ratio Prediction considering Tyre Inflation Pressure Changes” - Hindawi Publishing Corporation *Journal of Control Science and Engineering*, 2015.
- [19] Van Gennip, M.D. and McPhee, J., “Parameter Identification for Combined Slip Tire Models using Vehicle Measurement System,” *SAE Technical Paper 2018-01-1339*, 2018, doi:10.4271/2018-01-1339

8 List of figures

| | |
|--------------------------------------------------------------------------------------------------------------------------------------------------------------------------------------------------------------------------------------------------------------------------------------------------------------------------------------------------------------------------------------------------------------------|---|
| FIGURE 1.1. Electro-pneumatic layout of the ATPC system with air compressor (1); ejector (9); central electro-valves: one on the compressor line (7) and one on the vacuum line (8); vent valve (2); four pipelines for the connection of the tires to the central part (10), including a solenoid valve (3), pressure transducer (11), rotating pneumatic joint (6), and an on-wheel valve or valve unit (4)..... | 1 |
| FIGURE 1.2. (a) Rolling tire on a deformable surface: ground deformation and spring back. (b) Forces F_z and F_r and contact pressure σ_z in a rolling tire..... | 2 |
| FIGURE 1.3. (a)Effect of inflation pressure on $f(V)$. (b) Rolling resistance for different values of load and pressure..... | 3 |
| FIGURE 1.4 Percentage of fuel consumption referring to the reference pressure of the tire for the different driving cycles..... | 3 |
| FIGURE 1.5 Percentage of fuel consumption for baseline and variable pressure strategy changing the load of the vehicle..... | 4 |
| FIGURE 1.6. Three-dimensional vertical contact load plots for (a) 4.6 kN tire load, inflation pressure 690 kN/m ² ; (b) 4.6 kN tire load, inflation pressure 100 kN/m ² ; (c) 19.6 kN tire load, inflation pressure 690 kN/m ² ; and (d) 19.6 kN tire load, inflation pressure 100 kN/m ² | 5 |
| FIGURE 1.7 Effect of inflation pressure on tire life (©2011 Michelin North America Inc.)..... | 6 |

| | |
|---------------------------------------------------------------------------------------------------------------------------------------------------------------------------------------------------------------------------------------------------|----|
| FIGURE 1.8 Effect of tread wear on peak longitudinal adherence..... | 6 |
| FIGURE 1.9 (a) Hydrodynamic lift of the wheel (aquaplaning) (b) adherence in function of speed on a wet road for a tire with tread (curve A) and without tread (curve B)..... | 7 |
| FIGURE 2.1. Section of a wheel including rim and tire and their main dimensions..... | 8 |
| FIGURE 2.2. Left: substructure of a radial tire, right: substructure of a cross ply..... | 9 |
| FIGURE 2.3. Radial tire structure: 1 running tread; 2 steel belt; 3 edge protection for the belt, in rayon or nylon; 4 sidewall; 5 two layers substructure ; 6 cap; 7 inner lining; 8 flipper; 9 bead profile; 10 core profile; 11 bead core..... | 9 |
| FIGURE 2.4. Standardized table for load index..... | 10 |
| FIGURE 2.5. Standardized table for speed class..... | 11 |
| FIGURE 2.6 Reference system used to study the forces exchanged between tire and ground..... | 11 |
| FIGURE 2.7. Contact pressure distribution for a braking (a) and driving (b) wheel..... | 12 |
| FIGURE 2.8. (a) Centre of instantaneous rotation and slip speed for a braking wheel. (b) Instantaneous centre of rotation by pure rotation C, by braking C' and by traction C'' | 13 |
| FIGURE 2.9. (a) Slipping area for different values of slip σ . (b) Qualitative diagram of μ_x in function of the longitudinal slip σ | 13 |
| FIGURE 2.10. Wheel-road contact in presence of sideslip. (a) path of a point on the tread on the equator plane; (b) contact zone and slip zone for different values of α (not in scale)..... | 14 |
| FIGURE 2.11. Lateral deformation, distribution of the pressures σ_z e τ_y , slip and lateral speed for a cornering tire..... | 14 |
| FIGURE 2.12. Lateral force F_y and self-aligning moment M_z for different tires subjected to the same load, with same size and inflation pressure..... | 15 |
| FIGURE 2.13 Curve produced by the magic formula. With meaning of curve parameters..... | 16 |
| FIGURE 2.14. Curves $F_y(\alpha)$ and $M_z(\alpha)$ obtained with the magic formula..... | 17 |
| FIGURE 2.15. Tire pressure effects for a passenger car tyre; left: cornering stiffness and right: self-aligning moment..... | 17 |
| FIGURE 2.16. Forces acting on a vehicle moving on an inclined road..... | 19 |
| FIGURE 2.17. Kinematic steering for a four-wheeled and for a two-wheeled vehicle..... | 21 |
| FIGURE 2.18 Simplified model for dynamic steering..... | 23 |
| FIGURE 2.19 Mono-track model to study the handling of a two axle vehicle..... | 26 |
| FIGURE 2.20 Reference frame to study of the motion of a rigid vehicle..... | 28 |
| FIGURE 2.21 Position and velocity of the centre P_i of the contact area of the i-th wheel..... | 29 |

| | |
|----------------------------------------------------------------------------------------------------------------------------------------------------------------------------------------------------------------------------------------|----|
| FIGURE 2.22 Steady state response to a steering input. Path curvature gain as a function of speed (a) and handling diagram (b) for an oversteer, an understeer and a neutral steer vehicle..... | 32 |
| FIGURE 2.23 Geometrical definition of steering behaviour of a single axle steering vehicle..... | 33 |
| FIGURE 2.24 Steady state response to a steering input. Plot of the path curvature gain as a function of speed (a) and handling diagram (b) for a vehicle that at low speed is oversteer and then becomes understeer at high speed..... | 34 |
| FIGURE 3.1 Longitudinal adherence in function of slip for different levels of pressure and load (Tire 185/65 R 15)..... | 36 |
| FIGURE 3.2 Effect of pressure and load on the peak value of adherence (Tire 185/65 R 15)..... | 36 |
| FIGURE 3.3 Effect of pressure and load on longitudinal slip stiffness (Tire 185/65 R 15)..... | 36 |
| FIGURE 3.4 Lateral adherence in function of sideslip for different levels of pressure and load (Tire 185/65 R 15)..... | 37 |
| FIGURE 3.5 Effect of pressure and load on peak lateral adherence (Tire 185/65 R 15)..... | 37 |
| FIGURE 3.6 Cornering stiffness in function of pressure for the two load conditions (Tire 185/65 R 15)..... | 38 |
| FIGURE 3.7 Effect of pressure and load on cornering stiffness (Tire 185/65 R 15)..... | 38 |
| FIGURE 3.8 Self aligning-moment in function of sideslip for different values of inflation pressure and load (Tire 185/65 R 15)..... | 39 |
| FIGURE 3.9 Effect of pressure and load on self-aligning moment stiffness (Tire 185/65 R 15)..... | 39 |
| FIGURE 3.10 Longitudinal adherence in function of slip for different levels of pressure and load (Tire 225/65 R 16)..... | 40 |
| FIGURE 3.11 Effect of pressure and load on peak longitudinal adherence (Tire 225/65 R 16)..... | 41 |
| FIGURE 3.12 Effect of pressure and load on longitudinal slip stiffness (Tire 225/65 R 16)..... | 41 |
| FIGURE 3.13 Lateral adherence in function of sideslip angle for different levels of pressure and load (Tire 225/65 R 16)..... | 42 |
| FIGURE 3.14 Effect of pressure and load on peak lateral adherence (Tire 225/65 R 16)..... | 42 |
| FIGURE 3.15 Effect of pressure and load on cornering stiffness (Tire 225/65 R 16)..... | 42 |
| FIGURE 3.16 Effect of pressure and load on cornering stiffness (Tire 225/65 R 16)..... | 43 |
| FIGURE 3.17 Self aligning-moment in function of sideslip for different values of inflation pressure and load (Tire 225/65 R 16)..... | 43 |
| FIGURE 3.18 Effect of pressure and load on self-aligning moment stiffness (Tire 185/65 R 15)..... | 44 |
| FIGURE 3.19 Longitudinal adherence in function of slip for different levels of pressure and load (Tire 195/75 R 16) | 45 |

| | |
|-------------------------------------------------------------------------------------------------------------------------------------------------------------------------------------------|----|
| FIGURE 3.20 Effect of pressure and load on peak longitudinal adherence (Tire 195/75 R 16)..... | 45 |
| FIGURE 3.21 Effect of pressure and load on longitudinal slip stiffness (Tire 195/75 R 16)..... | 46 |
| FIGURE 3.22 Lateral adherence in function of sideslip angle for different levels of pressure and load (Tire 195/75 R 16)..... | 46 |
| FIGURE 3.23 Effect of pressure and load on peak lateral adherence (Tire 195/75 R 16)..... | 47 |
| FIGURE 3.24 Effect of pressure and load on cornering stiffness (Tire 195/75 R 16)..... | 47 |
| FIGURE 3.25 Effect of pressure and load on cornering stiffness (Tire 195/75 R 16)..... | 47 |
| FIGURE 3.26 Self aligning-moment in function of sideslip for different values of inflation pressure and load (Tire 195/75 R 16)..... | 48 |
| FIGURE 3.27 Effect of pressure and load on self-aligning moment stiffness (Tire 195/75 R 16)..... | 48 |
| FIGURE 4.1 Brake demand (Grande Punto)..... | 50 |
| FIGURE 4.2 Braking distance variation compared to the condition at recommended inflation pressure (1350 kg Grande Punto)..... | 51 |
| FIGURE 4.3 Pitch angle of the vehicle for different pressure conditions (1350 kg Grande Punto).... | 51 |
| FIGURE 4.4 Braking distance variation compared to the condition at recommended inflation pressure (1762 kg Grande Punto)..... | 52 |
| FIGURE 4.5 Pitch angle of the vehicle for different pressure conditions (1762 kg Grande Punto)... | 52 |
| FIGURE 4.6 Braking distance variation compared to the unladen condition at recommended inflation pressure (1763 kg Grande Punto)..... | 53 |
| FIGURE 4.7 Influence of pressure on braking performance..... | 54 |
| FIGURE 4.8 Influence of front tires pressure on braking distance..... | 54 |
| FIGURE 4.9 Cornering Stiffness in function of load for different pressures, the vertical load acting on the tires during a step steer manoeuvre is indicated (1350 kg Grande Punto)..... | 55 |
| FIGURE 4.10 Lateral acceleration for different pressures (1350 kg Grande Punto)..... | 55 |
| FIGURE 4.11 Acceleration Gain for different pressures (1350 kg Grande Punto)..... | 56 |
| FIGURE 4.12 Cornering Stiffness in function of load for different pressures, the vertical load acting on the tires during a step steer manoeuvre is indicated (1762 kg Grande Punto)..... | 57 |
| FIGURE 4.13 Lateral acceleration for different pressures (1762 kg Grande Punto)..... | 57 |
| FIGURE 4.14 Acceleration Gain for different pressures (1762 kg Grande Punto)..... | 58 |
| FIGURE 4.15 Steering wheel angle for different pressures (1350 kg Grande Punto)..... | 58 |
| FIGURE 4.16 Curvature gain for different pressures (1350 kg Grande Punto)..... | 59 |
| FIGURE 4.17 Steering wheel angle for different pressures (1762 kg Grande Punto)..... | 59 |

| | |
|----------------------------------------------------------------------------------------------------------------------------------------------------------------------------------------------------------------|----|
| FIGURE 4.18 Curvature gain for different pressures (1762 kg Grande Punto)..... | 60 |
| FIGURE 4.19 Braking distance variation compared to the condition at recommended inflation pressure (2363 kg IVECO Daily with 225/65 R16 Tires)..... | 61 |
| FIGURE 4.20 Pitch angle of the vehicle for different pressure conditions (2363 kg IVECO Daily with 225/65 R16 Tires)..... | 61 |
| FIGURE 4.21 Braking distance variation compared to the condition at recommended inflation pressure (3500 kg IVECO Daily with 225/65 R16 Tires)..... | 62 |
| FIGURE 4.22 Pitch angle of the vehicle for different pressure conditions (3500 kg IVECO Daily with 225/65 R16 Tires)..... | 62 |
| FIGURE 4.23 Braking distance variation compared to the condition at recommended inflation pressure (2363 kg IVECO Daily with 195/75 R16 Tires)..... | 63 |
| FIGURE 4.24 Pitch angle of the vehicle for different pressure conditions (2363 kg IVECO Daily with 195/75 R16 Tires)..... | 63 |
| FIGURE 4.25 Braking distance variation compared to the condition at recommended inflation pressure (3500 kg IVECO Daily with 195/75 R16 Tires)..... | 64 |
| FIGURE 4.26 Pitch angle of the vehicle for different pressure conditions (3500 kg IVECO Daily with 195/75 R16 Tires)..... | 64 |
| FIGURE 4.27 Influence of pressure on braking distance for the vehicle with (full lines) and without ABS (dashed lines) (Fiat Grande Punto)..... | 65 |
| FIGURE 4.28 Cornering Stiffness in function of load for different pressures, the vertical load acting on the tires during a step steer manoeuvre is indicated (2356 kg Iveco Daily with 225/65 R16 tires)..... | 66 |
| FIGURE 4.29 Lateral acceleration for different pressures (2356 kg Iveco Daily with 225/65 R16 tires)..... | 66 |
| FIGURE 4.30 Acceleration Gain for different pressures (2356 kg Iveco Daily with 225/65 R16 tires)..... | 67 |
| FIGURE 4.31 Cornering Stiffness in function of load for different pressures, the vertical load acting on the tires during a step steer manoeuvre is indicated (3500 kg Iveco Daily with 225/65 R16 tires)..... | 67 |
| FIGURE 4.32 Lateral acceleration for different pressures (3500 kg Iveco Daily with 225/65 R16 tires)..... | 68 |
| FIGURE 4.34 Curvature gain for different pressures (2356 kg Iveco Daily with 225/65 R16 tires)..... | 69 |
| FIGURE 4.34 Curvature gain for different pressures (3500 kg Iveco Daily with 225/65 R16 tires)..... | 69 |

| | |
|----------------------------------------------------------------------------------------------------------------------------------------------------------------------------------------------------------------|----|
| FIGURE 4.36 Cornering Stiffness in function of load for different pressures, the vertical load acting on the tires during a step steer manoeuvre is indicated (2356 kg Iveco Daily with 195/75 R16 tires)..... | 70 |
| FIGURE 4.37 Lateral acceleration for different pressures (2356 kg Iveco Daily with 195/75 R16 tires)..... | 70 |
| FIGURE 4.38 Acceleration Gain for different pressures (2356 kg Iveco Daily with 195/75 R16 tires)..... | 71 |
| FIGURE 4.39 Cornering Stiffness in function of load for different pressures, the vertical load acting on the tires during a step steer manoeuvre is indicated (3500 kg Iveco Daily with 195/75 R16 tires)..... | 71 |
| FIGURE 4.40 Lateral acceleration for different pressures (3500 kg Iveco Daily with 195/75 R16 tires)..... | 72 |
| FIGURE 4.41 Acceleration Gain for different pressures (3500 kg Iveco Daily with 195/75 R16 tires)..... | 72 |
| FIGURE 4.42 Curvature gain for different pressures (2356 kg Iveco Daily with 195/75 R16 tires)..... | 73 |
| FIGURE 4.43 Curvature gain for different pressures (3500 kg Iveco Daily with 195/75 R16 tires)..... | 73 |
| FIGURE 5.1 Braking distance variation changing front and rear tires pressure (1350 kg Grande Punto)..... | 75 |
| FIGURE 5.2 Braking distance variation changing front and rear tires pressure (1762 kg Grande Punto)..... | 76 |
| FIGURE 5.3 Improvement on braking distance (left) and braking time (right) using a slip ratio prediction that takes in account pressure change..... | 76 |
| FIGURE 5.4 Theoretical curvature gain from ATPC tool for the vehicle in standard B (blue line), full load (red line) and full load changing tire pressure (green line)..... | 77 |
| FIGURE 5.5 Experimental curvature gain for a steering pad manoeuvre for the vehicle in standard B (blue line), full load (red line) and full load changing tire pressure (green line)..... | 77 |
| FIGURE 5.6 Curvature gain of the improved ADAMS model of the Punto for the vehicle in standard B (a), full load (b) and full load changing tire pressure (c)..... | 78 |
| FIGURE 5.7 Curvature Gain for the Punto in full load (full lines) and in Standard B (dashed line).... | 78 |
| FIGURE 5.8 Curvature gain for a steering pad manoeuvre for the vehicle in standard B (blue line), full load (red line) and full load changing tire pressure (green line)..... | 79 |
| FIGURE 5.9 Lateral acceleration for a step steer manoeuvre for the vehicle in standard B (blue line), full load (red line) and full load changing tire pressure (green line)..... | 79 |
| FIGURE 5.10 Curvature gain for a steering pad manoeuvre using different strategies..... | 80 |

| | |
|--------------------------------------------------------------------------------------------------------------------------------------------------------------------------------------|----|
| FIGURE 5.11 Curvature gain for a steering pad manoeuvre using different strategies..... | 80 |
| FIGURE 5.12 Braking distance variation changing front and rear tires pressure (2356 kg Daily)..... | 81 |
| FIGURE 5.13 Braking distance variation changing front and rear tires pressure (3500 kg Daily)..... | 81 |
| FIGURE 5.14 Theoretical curvature gain from ATPC tool for the unladen vehicle (blue line), full load (red line) and full load changing tire pressure (green line)..... | 82 |
| FIGURE 5.15 Curvature gain for a steering pad manoeuvre for the unladen vehicle (blue line), full load (red line) and full load changing tire pressure (green line)..... | 82 |
| FIGURE 5.16 Lateral acceleration for a step steer manoeuvre for the vehicle in standard B (blue line), full load (red line) and full load changing tire pressure (dashed lines)..... | 83 |
| FIGURE 5.17 Curvature gain for a steering pad manoeuvre using different strategies..... | 84 |
| FIGURE 5.18 Lateral acceleration for a step steer manoeuvre using different strategies..... | 84 |
| FIGURE 5.19 Braking distance variation changing front and rear tires pressure (2356 kg Daily)..... | 85 |
| FIGURE 5.20 Braking distance variation changing front and rear tires pressure (3500 kg Daily)..... | 85 |
| FIGURE 5.21 Theoretical curvature gain from ATPC tool for the unladen vehicle (blue line), full load (red line) and full load changing tire pressure (green line)..... | 86 |
| FIGURE 5.22 Curvature gain for a steering pad manoeuvre for the unladen vehicle (blue line), full load (red line) and full load changing tire pressure (dashed lines)..... | 86 |
| FIGURE 5.23 Lateral acceleration for a step steer manoeuvre for the vehicle in standard B (blue line), full load (red line) and full load changing tire pressure (dashed lines)..... | 87 |
| FIGURE 5.24 Curvature gain for a steering pad manoeuvre using different strategies..... | 88 |
| FIGURE 5.25 Lateral acceleration for a step steer manoeuvre using different strategies..... | 88 |
| FIGURE 5.26 Curvature gain for a steering pad manoeuvre using different strategies..... | 89 |

9 List of Tables

| | |
|----------------------------------------------------------------------------------------------------------------|----|
| TABLE 3.1 Tire models provided by Michelin (The nominal pressure for each tire is highlighted in red)..... | 35 |
| TABLE 3.2 Distribution on the wheels for the two load conditions examined (Grande Punto)..... | 35 |
| TABLE 3.3 Effect of inflation pressure on main tire parameters for two load conditions (Tire 185/65 R15)..... | 39 |
| TABLE 3.4 Distribution on the wheels for the two load conditions examined (Iveco Daily)..... | 40 |
| TABLE 3.5 Effect of inflation pressure on main tire parameters for two load conditions (Tire 225/65 R 16)..... | 44 |
| TABLE 3.6 Effect of inflation pressure on main tire parameters for two load conditions (Tire 195/75 R 16)..... | 49 |
| TABLE 5.1 Effect of different strategies on braking distance for the vehicle in standard B..... | 79 |
| TABLE 5.2 Effect of different strategies on braking distance for the vehicle in full load..... | 80 |
| TABLE 5.3 Effect of different strategies on braking distance for the unladen vehicle..... | 83 |
| TABLE 5.4 Effect of different strategies on braking distance for the vehicle in full load..... | 83 |
| TABLE 5.5 Effect of different strategies on braking distance for the unladen vehicle..... | 87 |
| TABLE 5.6 Effect of different strategies on braking distance for the vehicle in full load..... | 87 |